HE
18.5
.A37
no.
DOT-
TSC-
UMTA-
82-54.1

MTA-MA-06-0100-82-1
OT-TSC-UMTA-82-54, 1

DEVELOPMENT OF A DESIGN TECHNOLOGY FOR GROUND SUPPORT FOR TUNNELS IN SOIL

Volume I: Time-Dependent Response Due to Consolidation in Clays

DEPARTMENT OF
TRANSPORTATION
JUL - 1983
LIBRARY

Paul R. Johnston
G. Wayne Clough

Stanford University
Department of Civil Engineering
Stanford CA 94305

February 1983
Final Report

This document is available to the public through the National Technical Information Service, Springfield, Virginia 22161.

U.S. Department of Transportation
Urban Mass Transportation Administration

Office of Technical Assistance
Office of Systems Engineering
Washington DC 20590

NOTICE

This document is disseminated under the sponsorship of the Department of Transportation in the interest of information exchange. The United States Government assumes no liability for its contents or use thereof.

NOTICE

The United States Government does not endorse products or manufacturers. Trade or manufacturers' names appear herein solely because they are considered essential to the object of this report.

HE 18.5 .A37 no. DOT-TSC-UMTA-82-54, 1

Technical Report Documentation Page

1. Report No. UMTA-MA-06-0100-82-1	2. Government Accession No.	3. Recipient's Catalog No.
4. Title and Subtitle Development of a Design Technology for Ground Support for Tunnels in Soil - Vol. I - Time Dependent Response Due to Consolidation in Clays		5. Report Date February 1983
		6. Performing Organization Code TSC/DOT-75
7. Author(s) Paul R. Johnston and G. Wayne Clough		8. Performing Organization Report No. DOT-TSC-UMTA-82-54, 1
9. Performing Organization Name and Address Stanford University* Department of Civil Engineering Stanford, California 94305		10. Work Unit No. (TRAIS) UM248/R2650
		11. Contract or Grant No. DOT-TSC-1726
12. Sponsoring Agency Name and Address U. S. Department of Transportation Urban Mass Transportation Administration Office of Technical Assistance Office of Systems Engineering Washington, D. C. 20590		13. Type of Report and Period Covered Final Report August 1979 to January 1982
		14. Sponsoring Agency Code URT-10

15. Supplementary Notes *Under Contract to: U.S. Department of Transportation Research and Special Programs Administration Transportation Systems Center Cambridge, Massachusetts 02142

DEPARTMENT OF TRANSPORTATION JUL - 1983 LIBRARY

DEPARTMENT OF TRANSPORTATION JUL - 1983 LIBRARY

16. Abstract

Ground movements caused by construction of shallow soil tunnels are a major problem since overlying streets, utilities and buildings are potentially affected. One of the least understood contributors to tunnel related movements are the long term components due to consolidation in clayey or silty soils as a result of dissipation of excess pore pressures induced during construction. This report presents an investigation of this phenomenon. A review of field data showing time dependent movements and liner load changes is provided. Subsequently, a finite element procedure is described to simulate this behavior and parametric study results are discussed. It is shown that consolidation related effects lead to long term ground and liner movements and changes in liner loading patterns. Consolidation influences are largest in cases with flexible liners or shield with large tail voids. Increasing the size of a tail void or the flexibility of a liner leads to greater shearing of the soil, and hence more excess pore pressure. In some instances, ground settlements can be doubled by consolidation effects. This points to the need for ground control during tunneling in clays or silts to avoid increasing long term movements.

Advanced pressurized face shields are shown to be capable of reducing long term consolidation movements. These machines can be operated so as to reduce shear stress levels in soils prior to the increases caused by soil movements into the tail void. Use of this technology would appear advisable in soft ground tunneling.

17. Key Words Tunnels, Soft Ground, Consolidation, Movements, Liner Loads, Finite Element		18. Distribution Statement DOCUMENT IS AVAILABLE TO THE PUBLIC THROUGH THE NATIONAL TECHNICAL INFORMATION SERVICE, SPRINGFIELD, VIRGINIA 22161	
19. Security Classif. (of this report) Unclassified	20. Security Classif. (of this page) Unclassified	21. No. of Pages 232	22. Price

Form DOT F 1700.7 (8-72) Reproduction of completed page authorized

PREFACE

This report is the first in a series dealing with ground control for tunnels constructed by shield techniques in soil. It addresses the issue of the contribution of time-dependent dissipation of excess pore pressures to the long-term behavior of the ground around a tunnel and the liner support system. Because most tunnel monitoring to date has concerned only short-term response, this work uses primarily analytical methods to generate the necessary data. However, the available field information is also reviewed.

Other reports to be issued in the series associated with this one focus exclusively on ground control obtained by using advanced shield tunneling, a subject also briefly addressed herein. The research sponsorship for all of the work was provided by the U.S. Department of Transportation, Urban Mass Transportation Administration (UMTA) and the Transportation Systems Center (TSC) of Cambridge, Massachusetts. Mr. Philip A. Mattson of TSC served as contract monitor and provided valuable assistance throughout. Mr. Gilbert L. Butler of UMTA helped in development of the original ideas for the project.

METRIC CONVERSION FACTORS

Approximate Conversions to Metric Measures

Symbol	When You Know	Multiply by	To Find	Symbol
		LENGTH		
in	inches	*2.5	centimeters	cm
ft	feet	30	centimeters	cm
yd	yards	0.9	meters	m
mi	miles	1.6	kilometers	km
		AREA		
in^2	square inches	6.5	square centimeters	cm^2
ft^2	square feet	0.09	square meters	m^2
yd^2	square yards	0.8	square meters	m^2
mi^2	square miles	2.6	square kilometers	km^2
	acres	0.4	hectares	ha
		MASS (weight)		
oz	ounces	28	grams	g
lb	pounds	0.45	kilogrems	kg
	short tons (2000 lb)	0.9	tonnes	t
		VOLUME		
tsp	teaspoons	5	milliliters	ml
Tbsp	tablespoons	15	milliliters	ml
fl oz	fluid ounces	30	milliliters	ml
c	cups	0.24	liters	l
pt	pints	0.47	liters	l
qt	quarts	0.95	liters	l
gal	gallons	3.8	liters	l
ft^3	cubic feet	0.03	cubic meters	m^3
yd^3	cubic yards	0.76	cubic meters	m^3
		TEMPERATURE (exact)		
°F	Fahrenheit temperature	5/9 (after subtracting 32)	Celsius temperature	°C

*1 in = 2.54 (exactly). For other exact conversions and more detailed tables, see NBS Misc. Publ. 286, Units of Weights and Measures, Price $2.25, SD Catalog No. C13.10:286.

Approximate Conversions from Metric Measures

Symbol	When You Know	Multiply by	To Find	Symbol
		LENGTH		
mm	millimeters	0.04	inches	in
cm	centimeters	0.4	inches	in
m	meters	3.3	feet	ft
m	meters	1.1	yards	yd
km	kilometers	0.6	miles	mi
		AREA		
cm^2	square centimeters	0.16	squere inches	in^2
m^2	square meters	1.2	square yards	yd^2
km^2	square kilometers	0.4	square miles	mi^2
ha	hectares (10,000 m^2)	2.5	acres	
		MASS (weight)		
g	grams	0.035	ounces	oz
kg	kilograms	2.2	pounds	lb
t	tonnes (1000 kg)	1.1	short tons	
		VOLUME		
ml	milliliters	0.03	fluid ounces	fl oz
l	liters	2.1	pints	pt
l	liters	1.06	quarts	qt
l	liters	0.26	gallons	gal
m^3	cubic meters	35	cubic feet	ft^3
m^3	cubic meters	1.3	cubic yards	yd^3
		TEMPERATURE (exact)		
°C	Celsius temperature	9/5 (then add 32)	Fahrenheit temperature	°F

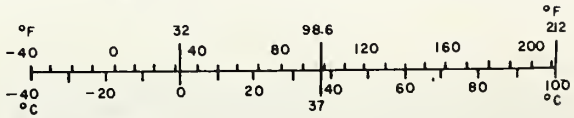

CONTENTS

Chapter		page
1.	INTRODUCTION	1
2.	TIME-DEPENDENT BEHAVIOR OF SHIELD DRIVEN TUNNELS	6
	2.1 Introduction	6
	2.2 Review of Shield Tunneling	6
	2.3 Causes of Time-dependent Behavior	11
	2.4 Observed Time Effects Due to Pore Pressure Dissipation	13
	2.4.1 Settlements	13
	2.4.2 Liner Loads and Shapes	21
	2.4.3 Summary	23
	2.5 Finite Element Modelling of the Construction Procedure	23
	2.5.1 Plane Strain Assumption	24
	2.5.2 Tunnel Excavation	24
	2.5.3 Liner Installation	25
	2.5.4 Soil Model	25
	2.5.5 Consolidation	26
	2.5.6 Summary	26
3.	DEVELOPMENT OF THE CAM CLAY SOIL MODEL FOR USE IN A FINITE ELEMENT CODE	28
	3.1 Introduction	28
	3.2 The Cam Clay Model	30
	3.2.1 Introduction	30
	3.2.2 Yield Surface	30
	3.2.3 Failure Envelope	31
	3.2.4 Flow Rule	32
	3.2.5 Hardening Rule	34
	3.3 Elastic Effective Stress-Strain Behavior	34
	3.4 Elasto-Plastic Effective Stress-Strain Behavior	37
	3.4.1 Derivation of the Stress-Strain Matrix	37
	3.4.2 Calculation of the Derivatives	38
	3.5 Material Parameters Required	41
	3.6 Reduction to One- and Two-Dimensional Problems	43
	3.6.1 Axisymmetric	44
	3.6.2 Plane Strain	44
	3.6.3 One Dimension	45

3.7 Fully Drained and Undrained Behavior 45
3.8 Finite Element Algorithms 46

3.8.1 Introduction 46
3.8.2 Stress-Strain Matrix 47
3.8.3 Stress Updating 47

3.9 Comparison of the Finite Element Results with Test Data . 47

4. EXTENDING THE MODEL TO INCLUDE CONSOLIDATION 51

4.1 Introduction 51
4.2 Governing Equations 52
4.3 Finite Element Formulation 54
4.4 Material Parameters Required 57
4.5 Reduction to One- and Two-Dimensional Problems 57
4.6 Finite Element Algorithms 58
4.7 Verification of One-Dimensional Seepage 63

4.7.1 Vertical Drainage 63
4.7.2 Radial Drainage 64

4.8 Verification of One-Dimensional Consolidation 67
4.9 Consolidation of a Clay Layer under a Uniform Strip Load . 72
4.10 Effect of Element Choice on Solution Accuracy 73
4.11 Effect of Integration Rule on Solution Accuracy 78

5. FINITE ELEMENT FORMULATION FOR LARGE DEFORMATIONS 81

5.1 Introduction 81
5.2 Choosing a Reference Frame 81
5.3 Choosing Appropriate Measures of Stress and Strain 82
5.4 Initial Stress Stiffness Matrix 83
5.5 Updating Stresses and Displacements 86
5.6 Residual Load Correction 87
5.7 Verification of Stress Correction Due to Rotations 88
5.8 Large Deformation One-Dimensional Consolidation 88
5.9 Summary 90

6. CONSOLIDATION ANALYSES OF TUNNELS 92

6.1 Introduction 92
6.2 Problem Definition 93

6.2.1 Geometry 93
6.2.2 Soil Conditions 93
6.2.3 Boundary and Initial Conditions 97
6.2.4 Liner Properties 98
6.2.5 Construction Performance 99
6.2.6 Summary 100

6.3 Behavior of a Typical Tunnel 100

6.3.1 Settlements 102
6.3.2 Excess Pore Pressures 106
6.3.3 Soil Pressures Acting on the Liner 111
6.3.4 Soil Stresses 117

6.4 Effect of the Liner Stiffness 121

6.4.1 Settlements 122
6.4.2 Liner Stresses 124
6.4.3 Excess Pore Pressures and Soil Stresses 124
6.4.4 Summary 127

6.5 Effect of the Tail Void Size 130

6.5.1 Settlements 130
6.5.2 Soil Pressures Acting on the Liner 131
6.5.3 Excess Pore Pressures and Soil Stresses 132

6.6 Effect of Soil Strength 132

6.6.1 Settlements 136
6.6.2 Soil Stresses Acting on Liner 139
6.6.3 Excess Pore Pressures and Soil Stresses 139

6.7 Effect of Soil Permeability 143
6.8 Effect of Initial Excess Pore Pressures 143

7. SUMMARY AND CONCLUSIONS 153

Appendix page

A. PEPCO USER'S MANUAL 158

A.1 Introduction 158
A.2 Program Capabilities 158
A.3 Program Overview 159
A.4 Element Library 162
A.5 Material Library 170
A.6 Input 173

A.6.1 Control Block 175
A.6.2 Mesh Block 182
A.6.3 Initial Stress Block 186
A.6.4 Load Block 189

A.7 Sample Input 194

B. SUBROUTINE LISTINGS 196
C. TUNNEL INPUT DECK FOR PEPCO 202
D. REPORT OF NEW TECHNOLOGY 212

REFERENCES 213

LIST OF FIGURES

Figure		page
2.1.	Settlement Mechanisms for an On-line Shield	7
2.2.	Pitching of Shield Produces Extra Settlement Potential	7
2.3.	Typical Earth Pressure Balance Shield	10
2.4.	Observed Settlement Versus Time for Tunnels in Clay and Silts in Chicago and Osaka	14
2.5.	Observed Settlement Versus Time for a Tunnel in Clay	17
2.6.	Observed Ground Movements, Versus Time For An Earth Balance Shield in San Francisco (After Clough, et al., 1982)	20
2.7.	Variation of Radial Load on the Liner with Time	22
2.8.	Variation of Horizontal Diameter with Time	22
2.9.	Procedure for Simulation of Tunnel Construction	27
3.1.	Cam Clay Yield Model	33
3.2.	Cam Clay Hardening Model	36
3.3.	Finite Element Mesh for Triaxial Tests	49
3.4.	Drained Triaxial Compression Tests on Weald Clay	50
4.1.	Schematic of the Element Equations	60
4.2.	Element L3P2	61
4.3.	Pore Pressure Distribution for Vertical Drainage	65
4.4.	Pore Pressure Distribution for Radial Drainage	66
4.5.	Finite Element Mesh for One-Dimensional Consolidation	69
4.6.	Excess Pore Pressures for One-Dimensional Consolidation	70
4.7.	Settlement Versus Time for One-Dimensional Consolidation	71
4.8.	Finite Element Mesh for Strip Load on a Clay Layer	74

4.9. Settlement Versus Time for Strip Load on a Clay Layer 75

4.10. Oscillations in Space for the Q8P8 Element 77

4.11. Oscillations in Time for the Q4P4 Element 79

4.12. Effect of Integration Rule on Solution Accuracy 80

5.1. Effect of Large Strains on One-Dimensional Consolidation . . . 91

6.1. Finite Element Mesh for Tunnel Analyses 94

6.2. Shear Strength Versus Depth 96

6.3. Typical Surface Settlement Profiles 104

6.4. Surface Settlements Plotted as an Error Function 104

6.5. Displaced Mesh Plots for a Typical Tunnel 107

6.6. Degree of Consolidation Versus Time for a Typical Tunnel . . 108

6.7. Maximum Surface Settlement Versus Time 108

6.8. Excess Pore Pressure Contours for a Typical Tunnel 109

6.9. Soil Stresses Acting on a Typical Liner 112

6.10. Bending Component of Pressure on a Liner Versus Time 115

6.11. Typical Liner Spreading as a Function of Time 116

6.12. Typical Effective Stress Paths for Soil Close to the Liner . 118

6.13. Percentage of Critical State Contours for a Typical Tunnel . 119

6.14. Principal Stresses for a Typical Tunnel 120

6.15. Effect of Liner Stiffness on Surface Settlement 125

6.16. Effect of Liner Stiffness on Liner Stresses 126

6.17. Effect of Liner Stiffness on Excess Pore Pressures 128

6.18. Effect of Liner Stiffness on Percent of Critical State . . . 129

6.19. Surface Settlement Profiles for a Tail Void of 2 inches . . 133

6.20. Error Function Plot for a Tail Void of 2 inches 133

6.21. Effect of Tail Void Size on Excess Pore Pressures 134

6.22. Effect of Tail Void Size on Remolded Zone 135

6.23. Surface Settlement Profiles for OCR = 2 137

6.24. Error Function Plot for OCR = 2 137

6.25. Excess Pore Pressure Contours for OCR = 2 140

6.26. Remolded Zone for OCR = 2 141

6.27. Principal Stresses for OCR = 2 142

6.28. Settlement Versus Time for Different Soil Permeabilities . . 144

6.29. Liner Spreading Versus Time for Different Permeabilities . . 144

6.30. Outward Tunnel Displacements Designed to Induce Initial Pore Pressure 146

6.31. Excess Pore Pressures for Case of Initial Outward Movements 148

6.32. Contours of Percent Critical State Mobilized 149

6.33. Surface Settlement Profiles for Case of Initial Outward Movements 151

A.1. Program Structure 160

A.2. Q4 Element Type 1 163

A.3. Q4P4 Element Type 2 163

A.4. Q8 Element Type 3 165

A.5. Q8P4 Element Type 4 165

A.6. Q8P8 Element Type 5 167

A.7. BM2D Element Type 6 167

A.8. L3P2 Element Type 7 169

A.9. L2P2 Element Type 8 169

A.10. Input Data Blocks 174

LIST OF TABLES

Table		page
3.1.	Weald Clay Material Parameters	48
5.1.	Rotation of Stresses	88
5.2.	Final Settlements Computed by Different Methods	90
6.1.	OCR Dependent Parameters	97
6.2.	Boston Blue Clay Parameters for Cam Clay Model	97
6.3.	Parameters Used in Finite Element Tunnel Analyses	100
6.4.	Excess Pore Pressures Near Tunnel	110
6.5.	Variation of Settlements with Liner Stiffness	122
6.6.	Effect of Liner Stiffness on Vertical Diameter Shortening	123
6.7.	Effect of Liner Stiffness on Liner Pressures	124
6.8.	Effect of Liner Stiffness on Maximum Excess Pore Pressure	127
6.9.	Effect of Tail Void on Maximum Surface Settlements	131
6.10.	Effect of Tail Void on Liner Pressures	132
6.11.	Effect of OCR on Maximum Surface Settlement	136
6.12.	Effect of OCR on Settlement Trough	138
6.13.	Effect of Initial Outward Displacement Caused By Pressurized Face Shield	152
A.1.	Parameters for Material Type 1, EL2D	171
A.2.	Parameters for Material Type 2, CC2D	172
A.3.	Parameters for Material Type 3, BM2D	173

EXECUTIVE SUMMARY

A major technical challenge with shallow tunneling in urban areas is to limit settlements of the ground surface which may cause damage to buildings. The question of how much settlement will occur has largely been studied empirically in the past. However, as refinements in settlement control and construction techniques are developed it becomes more important to understand the mechanisms of these problems.

One particular aspect of ground response to tunneling which is only poorly understood is the effect of mobilization and dissipation of excess pore pressures in cohesive soil. Based on a limited amount of field data, it would appear that the delayed settlements which are related to pore pressure dissipation can be larger than those which occur immediately after the shield passes. The available data suggests that time-dependent settlements can be a problem for both conventional as well as advanced shields. Time-dependent movements are also noted to be strongest where the shield procedures lead to formation of a large tail void or otherwise cause significant remolding of the soil. In the case of advanced shields using a pressurized face, consolidation effects may be influenced by initial outward heaving of the soil at the face.

In addition to time-dependent settlements, a number of field measurements have shown that long term changes in liner diameter and load distribution on the liner occur. The observations suggest that the

radial load and horizontal liner diameter increase approximately linearally with the logarithm of elapsed time after construction. This behavior has important implications for liner design as well for repair on construction alteration work undertaken some years after the original tunnel construction is completed.

This investigation was undertaken to study those aspects of the time dependent tunnel response which are due to dissipation of excess pore pressures generated in the ground during tunneling. For this purpose, a finite element code is developed which simulates tunneling in soil, explicitly taking into account pore pressure mobilization and dissipation in time. The program provides a means of investigating time dependent effects on tunneling settlements, and liner loads as related to consolidation in the soil around the tunnel.

The program incorporates an elasto-plastic soil model and large strain effects in order to reasonably simulate the behavior of the soil as it flows plastically to fill the tail void around the tunnel. Other aspects of the tunneling problem are simulated as realistically as possible. Provisions are made for modelling gravity stress profiles, soil properties varying with depth, and liner installation after mobilization of a user specified degree of soil closure into the tunnel.

Parametric studies on tunnel construction in clay are performed into the effects of soil strength, tunnel liner stiffness, size of the tail void, initial soil heave and permeability of the soil. The results indicate that time-related consolidation effects around tunnels in cohesive soil can be of great importance. Surface settlements and liner

loads generally increase with time until the consolidation process is completed. The increase in settlements is observed to be large when flexible liners are used, soft soils are present, or the tail void is large. Small degrees of initial outward heave due to a pressurized face shield seem to have beneficial effects since settlements are reduced relative to cases where only inward movement occurs.

The result of the parametric studies also show that liner loads, load distribution and diameter change with time. Typically the predicted trends are similar to those observed in the field during the consolidation process. With time, the load distribution tends to accentuate the bending stresses in the liner and the total loads increase slightly. The increases in stresses in the liner vary approximately linearally with the logarithm of time until the excess pore pressures are dissipated. A similar variation is observed for the lengthening of the horizontal diameter with time. These results in part explain the heretofore little understood changes which have been observed in the field.

Chapter 1

INTRODUCTION

Underground construction in urban areas is needed for rapid transit, water supply and sewage disposal. In the past, underground construction in the United States was usually performed using cut and cover techniques. Today, however, tunneling is becoming more popular because of recent advances in shield tunneling technology and because it causes less environmental disruption.

One major technical challenge with shallow tunneling in urban areas is to limit settlements of the ground surface which may cause damage to buildings. The question of how much settlement will occur has largely been studied empirically in the past. However, as refinements in settlement control and construction techniques are developed it becomes more important to understand the mechanisms of these problems.

One particular aspect of ground response to tunneling and related activities which is only poorly understood is the effect of mobilization and dissipation of excess pore pressures in cohesive soils. In his excellent state-of-the-art paper, Peck (1969) noted, "Delayed settlements due to long-time consolidation of the clay around the tunnel should not be overlooked. These may spread much more widely than those due to the tunneling operations themselves." This behavior has become even more significant where advanced shield techniques are used, since

there is field evidence that the soil in this case is heaved aside as the shield moves forward (Clough, et al., 1982). The soil around the shield is thus remolded, and time dependent movements are observed due to consolidation.

Probably the main reason for a lack of study of the consolidation problem is that it is complex and difficult to characterize analytically. Also few field data are available, since most actual field measurements are made only during or immediately after construction, and pore pressures, per se, are rarely monitored at all.

This report presents to the knowledge of the authors the first comprehensive investigation of time-dependent effects due to the dissipation of excess pore pressures around tunnels. In particular, the following items are addressed:

1. Available field documentation on time effects.

2. Development of a finite element code which allows simulation of tunneling in cohesive soil, explicitly taking into account pore pressure mobilization and dissipation in time.

3. The mechanism of excess pore pressure development and dissipation around tunnels in cohesive soil and its effects on time-dependent settlements and liner loads.

4. The mechanism of excess pore pressure development and dissipation in cohesive soil during advanced shield tunneling with a pressurized face.

From the results of these studies an assessment is developed of the significance of time-related consolidation effects around tunnels in cohesive soil.

In order to set the stage for the analytical studies, Chapter II presents a review of the existing literature on time-dependent tunnel behavior. Also, a technique for realistically simulating the construction procedure of a tunnel using the finite element method is introduced. This includes modelling in plane strain the excavation of the soil, the installation of a liner and the closing of a non-uniform tail void gap.

The finite element method is used because it allows the coupled equations of elasticity and fluid flow to be solved for complicated boundary and soil conditions. Closed form analytical solutions to such problems are impossible. The finite element method is particularly useful for performing parametric studies which may be used to identify the most important factors contributing to the time-dependent behavior of surface settlements and liner loads.

An elasto-plastic soil model is needed to provide a good representation of the stress-strain behavior of the clay, since it undergoes yielding as it moves into the tail void. The Cam clay soil model, an elasto-plastic strain hardening model is used herein. This model was developed at Cambridge University, where it has been used in both experimental and analytical tunnel modelling. A method for implementing it in a two- or three-dimensional code is presented in Chapter III.

A theory for elasto-plastic consolidation is outlined in Chapter IV. This theory allows the equations governing the ground movement to be coupled with those governing the flow of water through the soil voids in order to calculate the excess pore pressures. A pore pressure degree of freedom is added to some of the nodal points. In order to incorporate this theory into the finite element code, a numerical stability study was used to choose a suitable finite element and integration rule for the time domain. Using this method, the development and dissipation of pore pressures in time may be modelled for the case of a tunnel in a saturated cohesive soil typical of many urban areas.

Large strains occur near the tail void as it is closed. Since this closing is the major cause of the surface settlements, it is important that a large strain formulation be used. A simple approach is demonstrated in Chapter V, which gives accurate solutions even when displacements are large. The method is efficient since the symmetry of the stiffness matrix is maintained.

The final finite element code which incorporates all of the options offers a tool which will accurately simulate the construction of a tunnel including predictions of surface settlements, liner stresses and excess pore pressures. Results of parametric studies on tunnel construction in clay are given in Chapter VI. The effects of varying soil strength, tunnel liner stiffness, size of the shield tail void, and permeability of the soil are considered. Also, the influence of an initial outward movement of the soil is examined. This effect is modelled since heaving can occur during advanced shield tunneling.

Finally, comparisons are made between finite element behavior and existing field data.

The final chapter provides a summary of the work done, and conclusions and recommendations are given. Following this chapter three appendices are included which describe the computer code and present a User's Guide for it.

Chapter 2

TIME-DEPENDENT BEHAVIOR OF SHIELD DRIVEN TUNNELS

2.1 INTRODUCTION

In this chapter both existing field data and theoretical studies on the time-dependent behavior of tunnels are reviewed. A method for modelling the construction procedure and subsequent time-dependent behavior of shield driven tunnels using finite elements is given. First, current technology in shield tunneling methods is outlined.

2.2 REVIEW OF SHIELD TUNNELING

Tunnels in soft clay are usually constructed with the aid of a shield. The shield is basically a steel cylinder which provides temporary support for the soil while excavation proceeds at the tunnel face, as shown in Figure 2.1. Liner segments are erected in the tail of the shield. The tunnel is advanced by jacking the shield ahead while thrusting against the in-place liner.

A tail void is created between the liner and the soil. The tail void size is determined by the thickness of the shield plus the tolerance gap between the outside of the liner and the inside of the shield. The tail void is further increased when overcutters are used to aid steering. Plowing occurs when proper alignment with grade is not maintained and this can add dramatically to the size of the tail void, as shown in Figure 2.2.

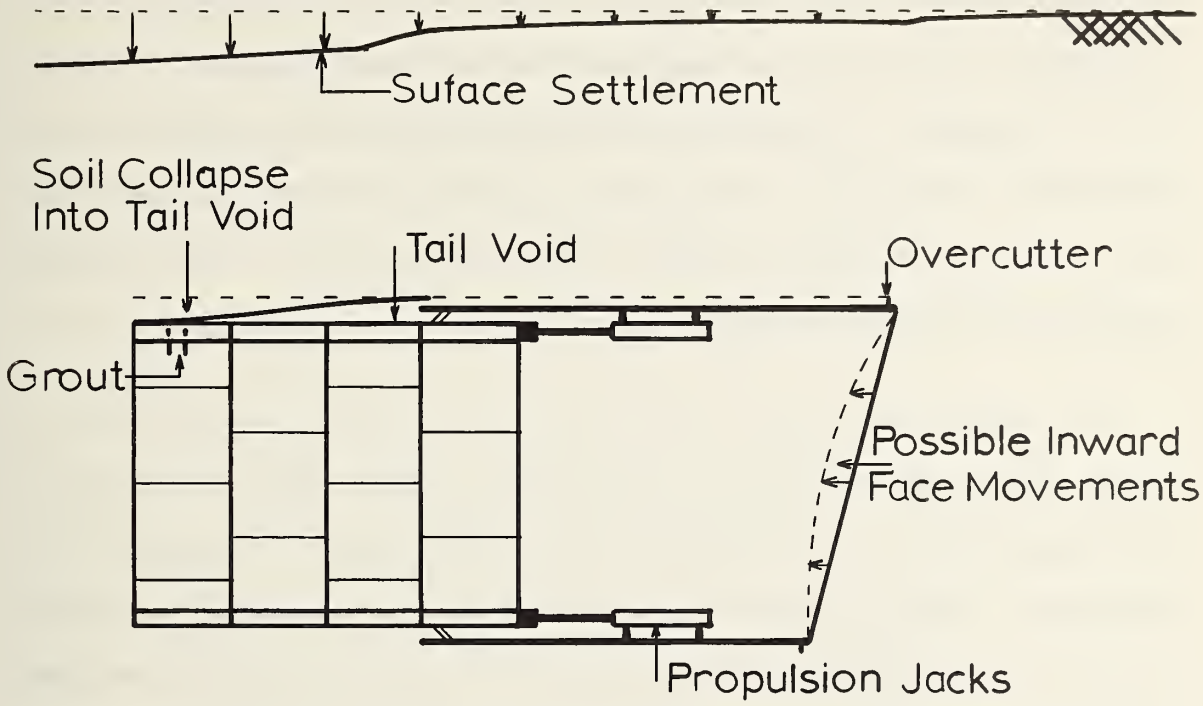

Figure 2.1: Settlement Mechanisms for an On-line Shield

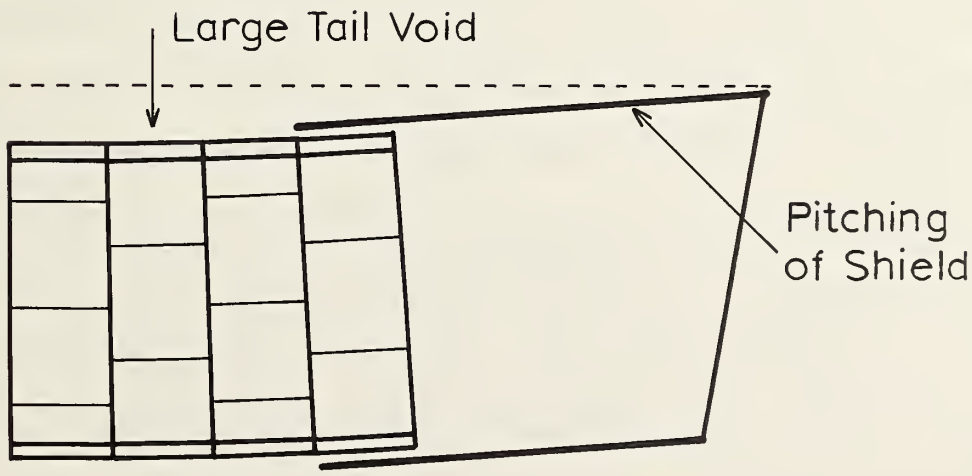

Figure 2.2: Pitching of Shield Produces Extra Settlement Potential

Attempts are usually made to fill the tail void by pumping some form of grout or pea gravel through holes in the liner segments. In weak soils, however, this void usually closes before any material can be injected. When grout is being injected, the gap between the shield and the liner must be large enough to house grout seals. This may also increase the size of the tail void.

In weak cohesive soil the face of the tunnel usually must be supported during the excavation procedure. Many different techniques for support exist, and in poor soil combinations of these may be required. Richardson and Mayo (1975) provide a useful review of conventional procedures for this purpose. The most prominent technique in the U.S. in the past involves the application of compressed air in the tunnel. Insurance costs have risen dramatically when compressed air is used however, and alternative techniques, particularly advanced closed face shields are becoming more attractive. Predecesors to the advanced shields were developed for use on the Bart system (Peterson and Frobenius, 1971); this type of shield had a closed face with a rotating cutter wheel. The cutter wheel had provisions for windows or doors which were opened to bring the soil in. However, where zones of running or flowing ground are encountered within the cohesive soil, compressed air has to be used to keep soil from moving freely through the cutter wheel openings. This essentially negates the advantages of such a machine.

To overcome the problems with compressed air, a new technology has been introduced where the tunnel face is supported either by a slurry

under pressure or by a combination of earth and water pressure. Clough (1980, 1981) has provided a general description of these shields. A typical earth pressure balance shield, is shown in Figure 2.3. The first application of this shield in the U.S. took place in 1981 in San Francisco for a sewer tunnel. The performance for this project is described in a companion volume for this research project (Clough, et al., 1982).

In spite of the innovations in shield technology for control of the soil at the face of the tunnel, a key problem remains: the tail void and the soil closure into it. Also excessive initial heaving and subsequent settlement can occur if the shield is not operated properly.

Surface settlements for shield tunneling may be divided into four stages, (Cording and Hansmire, 1975). They develop

1. ahead of the face.
2. over the shield.
3. during the erection of the lining at the tail of the shield.
4. with time and further advance of the tunnel, as the lining deflects.

The first three stages of surface settlement are shown schematically in Figure 2.1. If an advanced shield is being used, settlements ahead of the face should be small since the in-situ stresses at the face will be balanced. The settlement over the shield is somewhat larger, but the settlement is most noticeable on the surface as the tail of the shield passes.

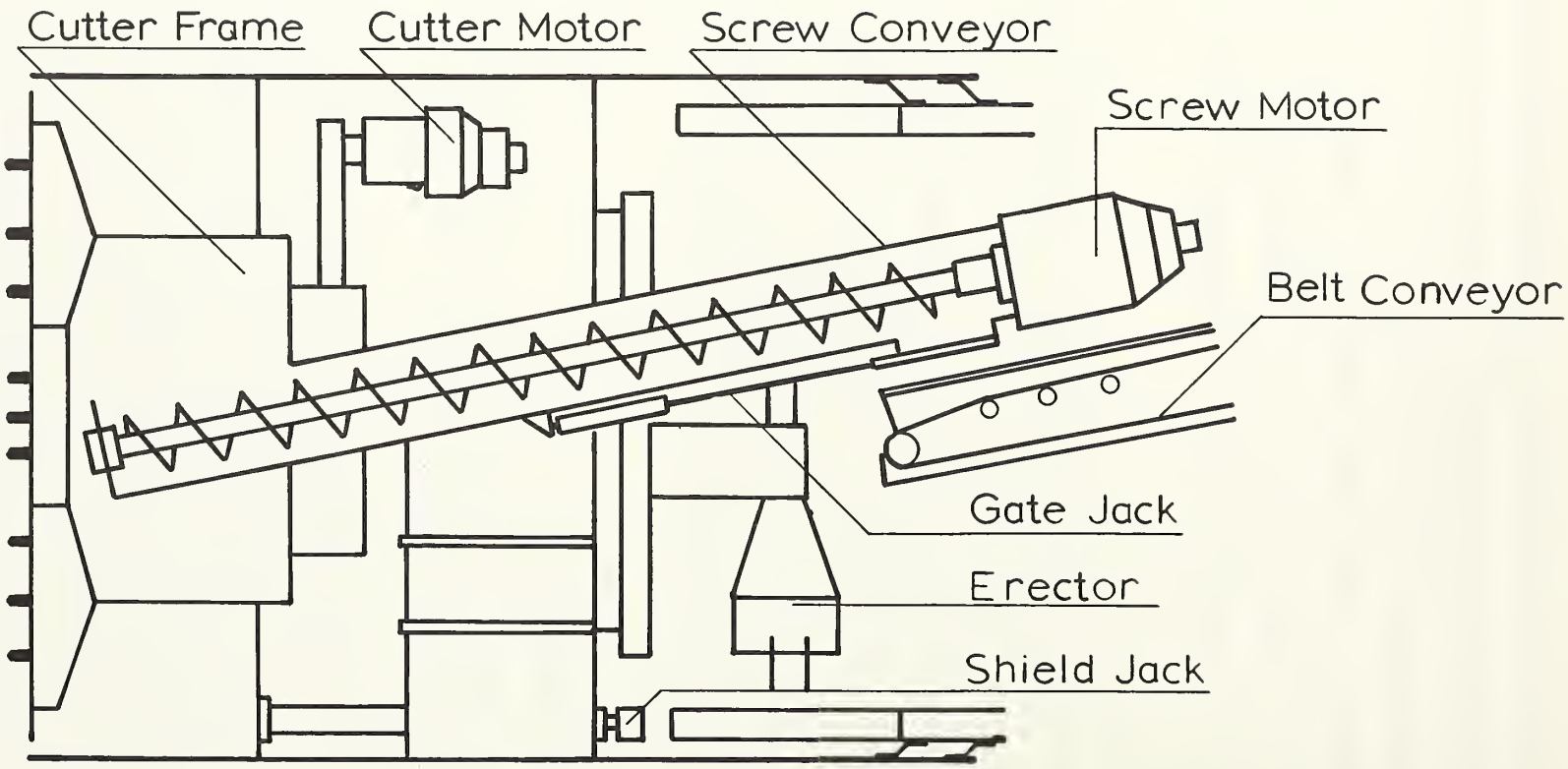

Figure 2.3: Typical Earth Pressure Balance Shield

Thus, surface settlements are highly dependent on the details of the shield design and the experience of the operators.

2.3 CAUSES OF TIME-DEPENDENT BEHAVIOR

Tunnel behavior in clay has been found to be time-dependent. Both surface settlements and liner stresses generally increase with time. There are four major causes of this time-dependent behavior.

First, a tunnel is constructed by advancing a heading. A three-dimensional state of stress exists near the heading, while away from the heading the state of stress may be assumed to be plane strain with zero strain in a direction parallel to the axis of the tunnel. As the heading advances with time away from a fixed point, the three-dimensional effect at this point diminishes.

Finite element techniques have been used to investigate this type of time-dependent behavior. Ghaboussi and Gioda (1977) studied the time-dependent effect of advancing tunnels using axisymmetric conditions. This assumption leads to an approximate solution which may give useful results for deep tunnels. Sakurai (1978) also investigated this problem, reducing it to plane strain by introducing the 'equivalent initial stress'. While this method appears to give some useful results, it remains an approximation to the true three dimensional behavior. The first full three-dimensional analysis of advancing shield tunnels is described in a report for this research project (Kasali and Clough, 1982).

A second cause of time-dependent behavior is due to the effect of soil creeping or undergoing secondary compression. Finite element techniques have been used to investigate this phenomenon using visco-elastic models by Ghaboussi and Gioda (1977), Sakurai (1978), and Tan and Clough (1980). This effect was found to be of particular importance where chemical grouting techniques are used.

For tunnels located below the water table there is a third cause of time-dependent behavior. In the long term, the tunnel may act as a pore water sink. As the water drains into the tunnel, the water table may be lowered, producing further settlements. Tunnel liners are usually water-proofed in order to prevent this effect. Nevertheless, it is difficult to make tunnel liners totally impervious. Fitzpatrick et al. (1981) used the finite element method to investigate the effect of liner leakage. An elastic soil model was used and the construction process itself was not modelled. The final settlement due to liner leakage was found to be proportional to the depth of the tunnel and the tunnel diameter. They also found that the flow of water into the tunnel was negligible when the liner permeability was two orders of magnitude greater than that of the soil.

The fourth cause of time-dependent behavior is due to consolidation of the remolded layer around the tunnel, the behavior which is the subject of this report. During the construction procedure there is a redistribution of stress in the neighborhood of the tunnel. This stress redistribution sets up excess pore pressures in the clay. Further settlements and changes in liner loads take place as these excess pore pressures dissipate.

2.4 OBSERVED TIME EFFECTS DUE TO PORE PRESSURE DISSIPATION

2.4.1 Settlements

One of the first documented case histories of shield tunneling in clay produced evidence of significant consolidation effects. The tunnel was constructed in Chicago in the early 1940's, and the performance has been described by Terzaghi (1942). The shield technique used was somewhat unusual in that it involved shoving a closed face shield through the clay with small doors in the face which were opened to allow the clay to squeeze through during the advance. The clay was generally soft to medium along the tunnel alignment with compressive strengths ranging from 600 to 1400 psf, (28.8 to 67.1 kN/m^2).

It was observed that as the shield moved through the soil, a pronounced heave surface occurred initially with movements, of one to four inches (2.5-10 cm). This apparently was caused by the fact that the volume of the soil entering the shield through the face doors was less than the advance volume occupied by the shield. Subsequent to the passage of the shield, and for many days thereafter, the ground surface settled. Figure 2.4 depicts the time dependent nature of the surface settlements. At this particular location time-dependent settlements were observed up to a period of 150 days, reaching values of eight to 10 inches (20-25.4 cm). Terzaghi (1942) attributed the initial subsidence effects after shield passage to a partial collapse of the clay onto the liner plate. But the significant subsequent time-dependent movements he felt were due to consolidation effects.

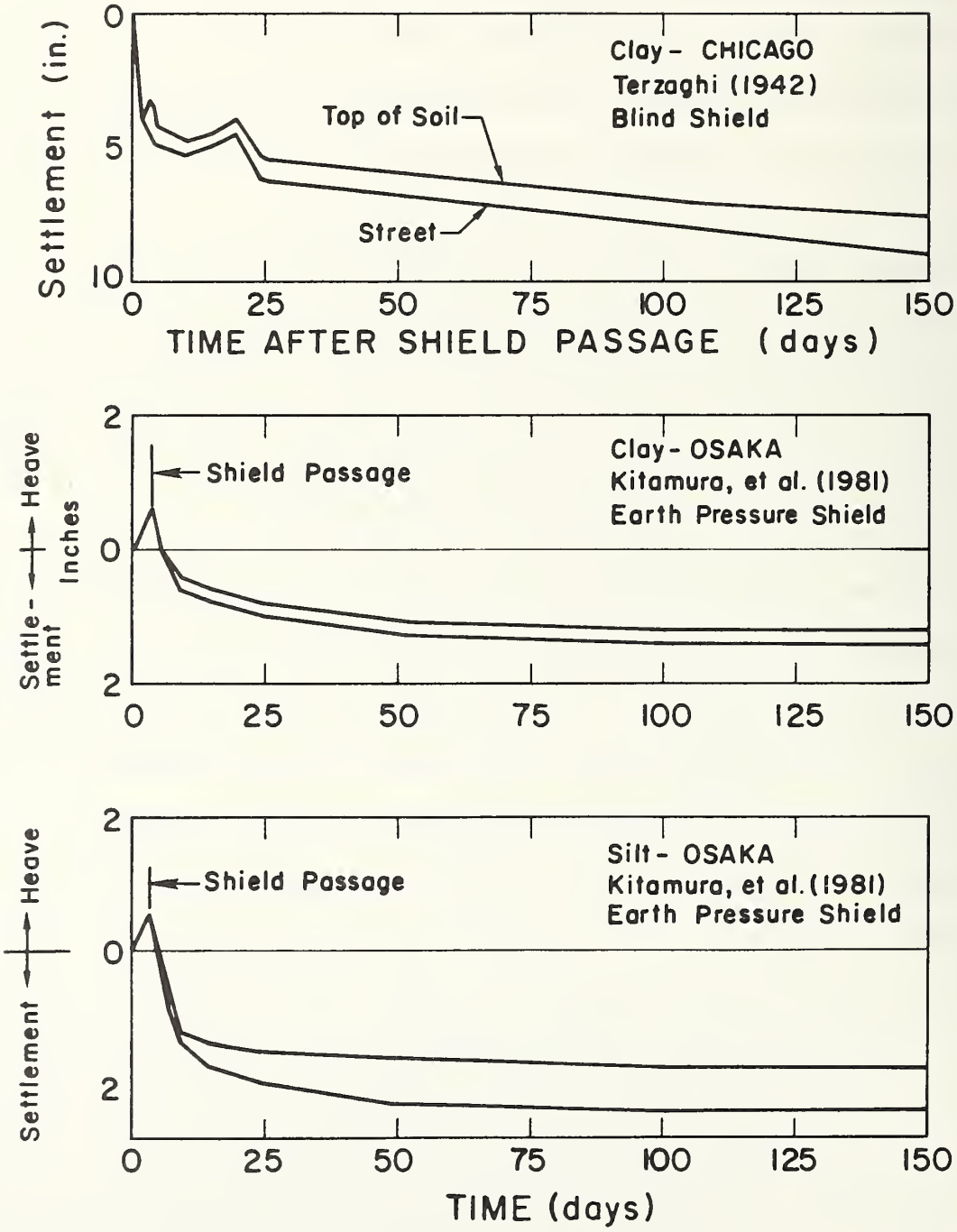

Figure 2.4: Observed Settlement Versus Time for Tunnels in Clay and Silts in Chicago and Osaka

Terzaghi (1942) explained the consolidation phenomenon as occurring because of excess pore pressures set up in a remolded zone in the clay around the tunnel, created as a result of the heaving of the soil during a shove. He noted that the pore pressures likely drained into the sand layer which was backfilled behind the liner plate after the liner segments emerged from the tail of the shield. It is significant that the settlements which ultimately occurred were always greater than the initial observed heave values.

Because of the significant ground movements induced by the shoving process discussed by Terzaghi (1942), this technique has been largely avoided in recent times. Open-face shields were preferred and largely used until the recent advent of the rotating cutter head machines with pressurized faces. In soft soils, compressed air has been conventionally used with open-face shields to control free stability. Few instances of time dependent movements have been reported for conventional or advanced shields, until the last few years.

Time-dependent settlement above a sewer tunnel in Thunder Bay, Ontario has been described by Belshaw and Palmer (1978) and Palmer and Belshaw (1980). A rotating cutterhead machine was used with a segmented concrete liner erected within the tail of the shield. The excavated diameter of the shield was 8.1 feet (2.47 m) at a depth of 31 feet (9.5 m) to the crown. The tunnel was constructed in a soft clay with a shear strengh of 730 psf (35 kN/m^2) at the tunnel springline. This clay extended from a depth of about 20 feet (6 m) to the bedrock at a depth of 80 feet (25 m). A layer of silt lay above the soft clay and the

water table was located at a depth of 5 feet (1.5 m). The surface settlement above the tunnel centerline was monitored at a test section, and was found to increase rapidly as the tail of the shield passed the test section. After about 12 days the settlement appeared to stop increasing. The settlement then began to increase again and was monitored for one year. This settlement is plotted versus time in Figure 2.5. After one year the settlement had increased by 100 percent, a behavior attributed to consolidation effects as the excess pore pressures in the region of remolded clay dissipated. Little to no drainage occurred into the tunnel since a clay seal was grouted in around it and only a minor drawdown was noted in piezometers located near the tunnel. It may be noted also that there is a strong similarity between the form of the results in Figure 2.5 and those reported by Terzaghi (1942) for the tunnel in Chicago.

The behavior of a later section of the tunnel in Thunder Bay was also monitored. Here the settlement was found to increase by only 15 percent during a similar time period as observed at the first test section. The difference in behavior was attributed to the greater clay cover in the earlier section and to shield alignment difficulties during the early driving stages at the first test section. Where the problems with shield steering occurred, presumably a greater zone of remolded clay was produced, giving rise to large future settlements. This is an important finding and suggests that quality of construction procedures has a large effect on the amount of consolidation after shield passage.

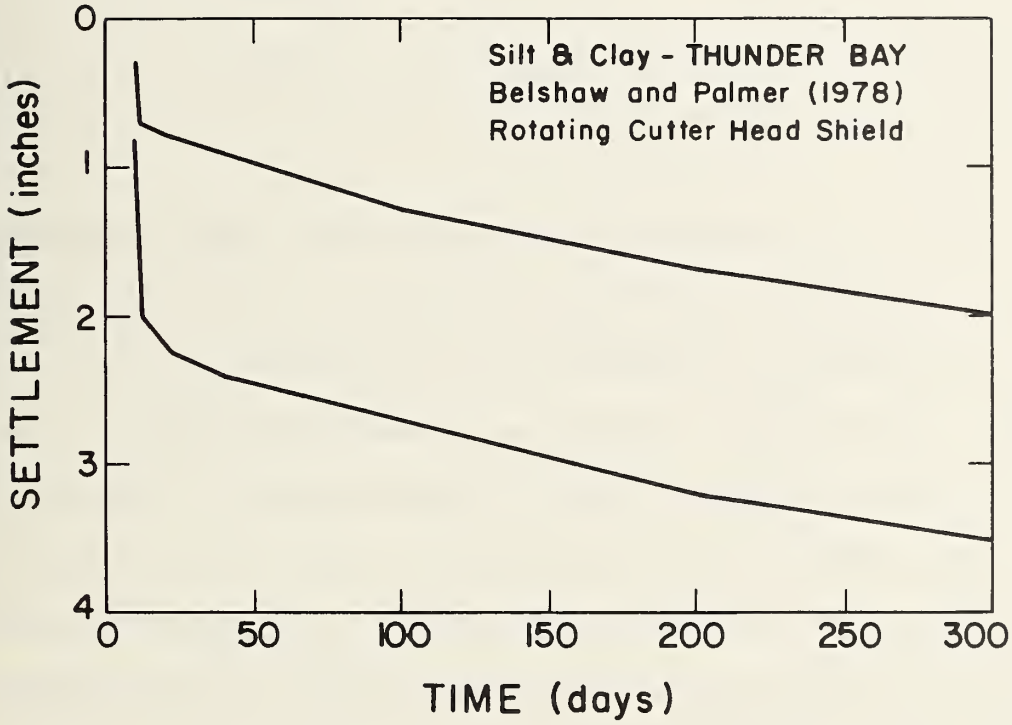

Figure 2.5: Observed Settlement Versus Time for a Tunnel in Clay

The most recent incidents of time dependent ground movements reported in the literature have been for earth balance shield projects. Kitamura, et al., (1981) described the observed surface movements, which occurred for a 22.1 ft. (6.7 m) diameter shield tunneling in silts and clays at a depth of 15-22 ft., (4.5-12.7 m). The movements are shown in Figure 2.4; as the shield approached the instrumentation station, a heave of 0.5 in (1.3 cm) was measured. As the shield passed the instrumentation line, settlements began to occur, and they continued for a period of 150 days (see Figure 2.4).

The initial rapid settlements immediately after shield passage are likely due to the tail void effect. However, there is an extended delayed settlement which eventually leads to a doubling of the initial movements. Importantly, the form of the settlement pattern is very similar to that described previously for the projects in Chicago and Thunder Bay. The delayed movements would appear to be related to consolidation of the soils around the tunnel. Presumably excess pore pressures were set up by the heaving effect in front of the shield and the inward movement toward the tail void.

The second earth pressure balance shield project where long-term settlements occurred was instrumented and monitored in 1981 by a team at Stanford University as a companion effort to the work reported herein. Details of the results are given elsewhere by Clough et al. (1982), and only the time-dependent response is described for this work. The tunnel, 12 ft. (3.6 m) in diameter and at a depth of about 30 ft. (9.1 m), is located in San Francisco. Along the alignment the soil profile

consists of about 20 ft. (6.1 m) of rubble fill underlain by soft silts and clays. The watertable is at a depth of about 10 ft (3 m).

Both vertical and lateral movements were measured during and following shield passage at three instrumentation stations. The data showed that most of the movements were concentrated in a zone around the shield and in primarily the soft soils. The rubble fill apparently acted as a structural element and smoothed the deflections over a broader area. The lateral movement devices showed very clearly that the shield initially heaved the soil aside and away from the face. While very little initial movement was observed at the surface, up to three inches (7.6 cm) of outward displacement occurred in the soft soil around the shield during each shove. Following shield passage, the soil began to move inwards towards the tunnel, and this trend has continued to the time of this writing (December 1981). Figure 2.6 shows a plot of measured surface movements versus time at one instrumentation station. As was the case with the earth balance shield behavior reported by Kitamura, et al. (1981), there is an initial heave during shield passage. This is followed by settlement which occurs over a period of 150 days. Small levels of continuing movements are continuing to be observed in the instrumentation at this site as of this date (December, 1981) and it is intended to continuing the monitoring process for at least one year.

In summary, the review of observed ground movements has shown that significant time dependent effects are common. This is true for both conventional and advanced shields.

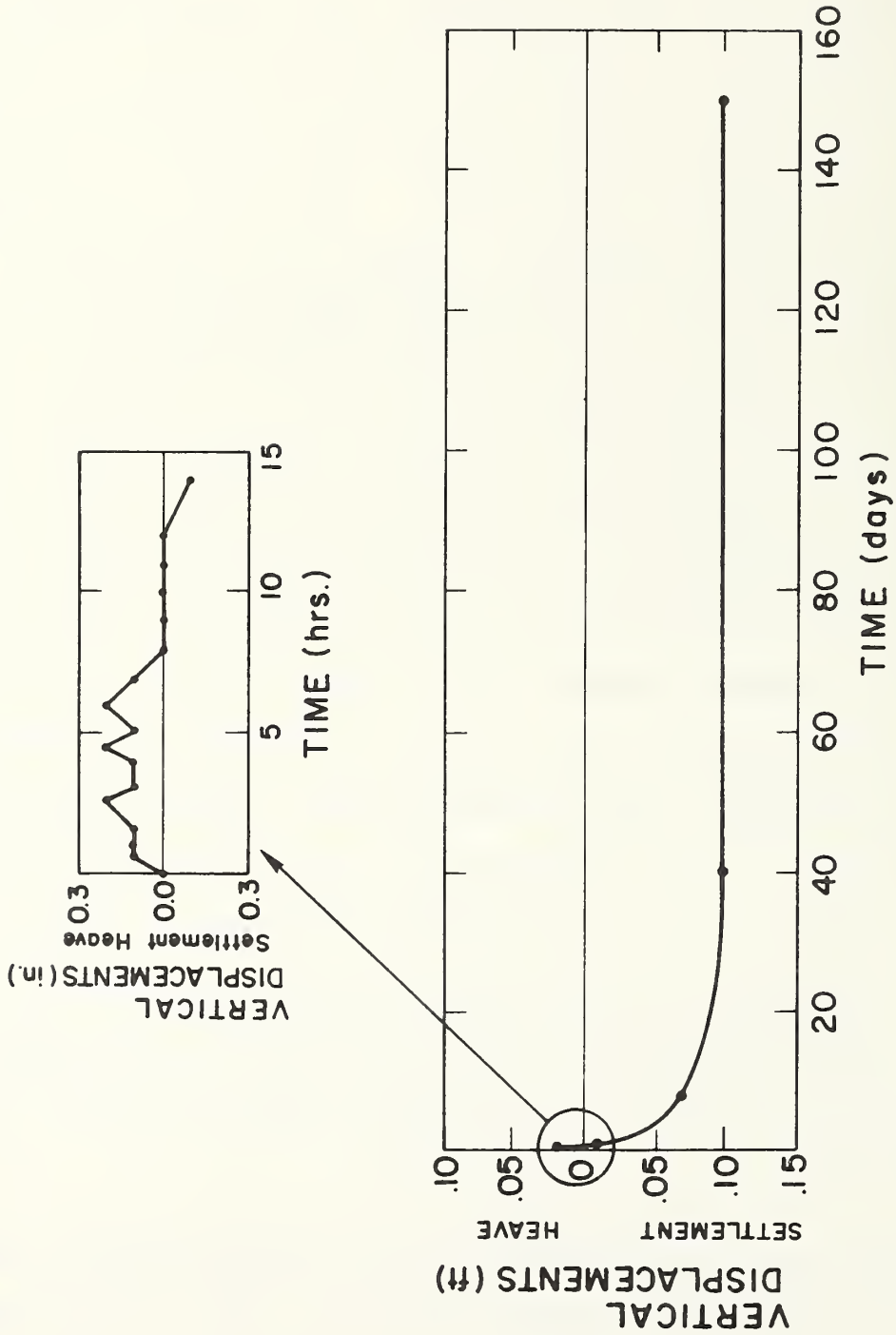

Figure 2.6: Observed Ground Movements, Versus Time For An Earth Balance Shield in San Francisco (After Clough, et al., 1982)

The degree of the time dependent movements also appears to be a function of the degree of disturbance produced by the tunneling techniques. The more the disturbance, the larger the time-dependent movements. All of the information available suggests that the movements are, in large part, due to consolidation phenomena related to the dissipation of excess pore pressures.

2.4.2 Liner Loads and Shapes

The load acting on a liner and the horizontal diameter of the liner have been observed to generally increase with time, Peck (1969). Many field measurements of this type have been reported for tunnels in London clay, and limited results have been reported for other soils.

Figures 2.7 and 2.8 show typical increases in liner loads and horizontal tunnel diameter for two different strength clays. The Chicago data is for a tunnel constructed in 1940 where the soft clay had a shear strength of 700 psf (34 kN/m^2), Terzaghi (1943). The London data is for a tunnel constructed in 1957 where the stiff clay had a shear strength of about 8 Ksf (380 kN/m^2), Ward and Thomas (1965). Although there is much scatter in this type of data, the general trend is usually the same. A steady increase occurs with sudden changes in the observations caused by a change in air pressure or a passing neighbor tunnel.

Of course, the trend of liner loads increasing with time must logically halt at some time if failures are to be prevented. This end point when liner loads become constant is not known for any of the reported data, since the measurements, were not extended over a long

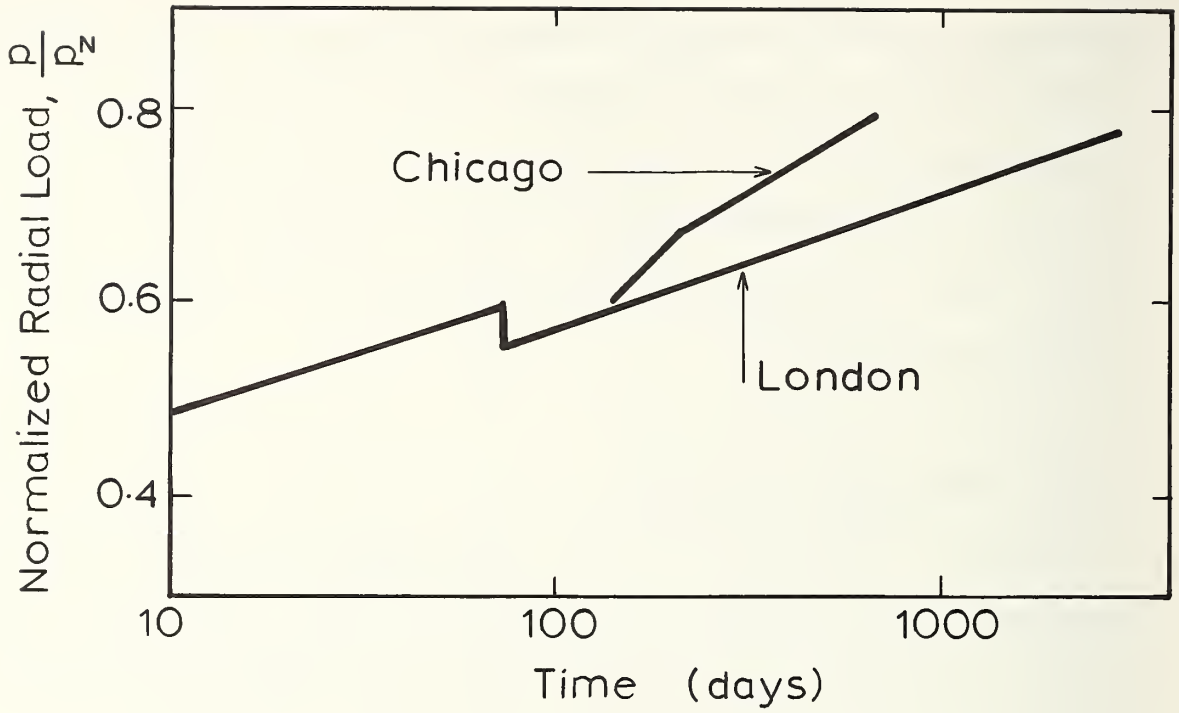

Figure 2.7: Variation of Radial Load on the Liner with Time

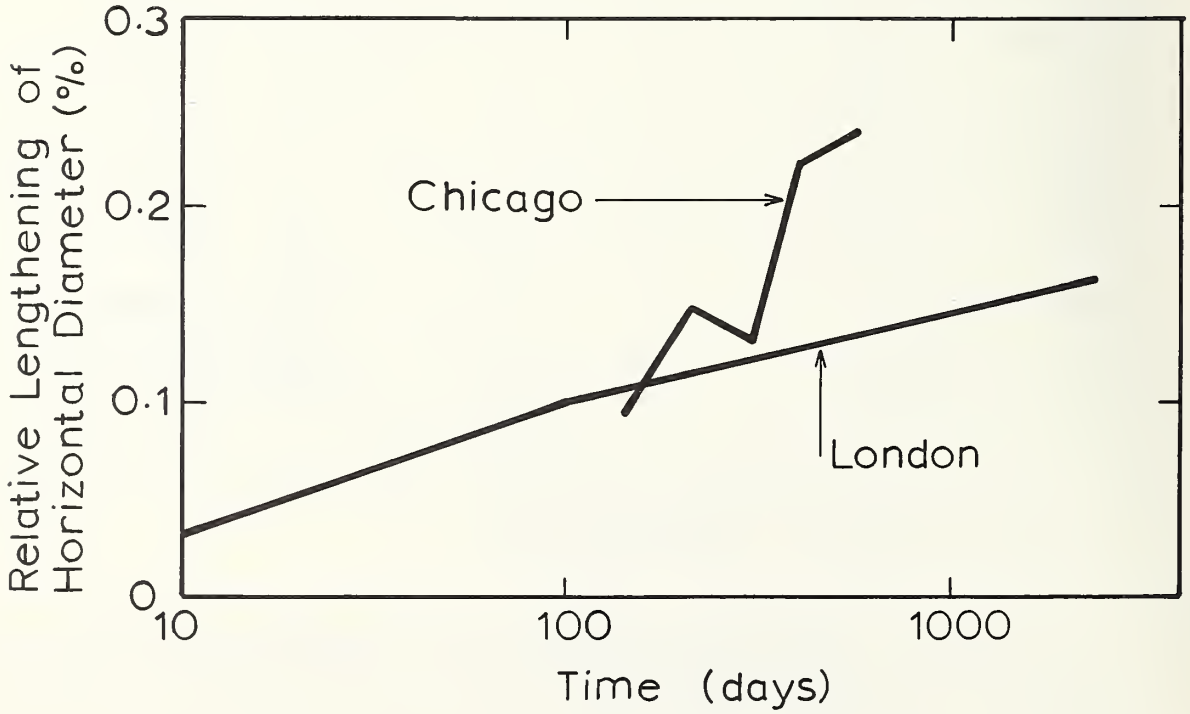

Figure 2.8: Variation of Horizontal Diameter with Time

enough period of time. If this effect were due entirely to consolidation, it should be expected that the load and diameter changes would cease when the consolidation process is completed. However, there are likely several causes, such as creep, leakage into the liner in addition to consolidation and the problem is not clearly understood.

2.4.3 Summary

Field data documenting the effect of pore pressure dissipation on tunnel behavior is scarce. The data available suggests there are significant ground movements and liner load changes caused by consolidation effects. However, at this point the cause of this behavior is only poorly understood. In fact, there are a number of factors that likely contribute to the time-dependent behavior of tunnels in clay. It would appear that these effects may be examined using the finite element method.

2.5 FINITE ELEMENT MODELLING OF THE CONSTRUCTION PROCEDURE

The finite element method is a very useful tool for analyzing stress conditions in a body of soil which may have varying soil properties and be subjected to complex boundary conditions. Elasto-plastic material laws may be used, pore pressures may be calculated along with stresses, strains and displacements. The tunnel excavation and liner installation procedure may be simulated. With calibrations against field behaviors, finite element programs using elasto-plastic parameters can be used for reliable prediction of ground movement problems.

2.5.1 Plane Strain Assumption

A tunnel heading is most accurately modelled using a three-dimensional mesh. However, this becomes extremely costly for an elasto-plastic consolidation analysis. It is possible to reduce the problem to a two-dimensional problem under certain conditions.

First, it is assumed that movements into the face of the tunnel are controlled. This can readily be done using an advanced shield or compressed air. Second, it is assumed that the permeability of the soil is such that the construction procedure takes place in undrained conditions. Thus, the tunnel heading will have advanced a considerable distance before the excess pore pressures begin to dissipate, so that the consolidation process will take place under plane strain conditions. This assumption is quite reasonable since advances of 65 feet (20 m) per day can be achieved and for most clays a negligible amount of consolidation will occur in the first few days.

2.5.2 Tunnel Excavation

First, initial stresses are set up in the finite element mesh, (see Figure 2.9). Then the excavation of the tunnel is simulated by relieving the in-situ stresses around the tunnel opening. Equivalent loads are applied at the nodal points surrounding the opening in order to model this excavation. A detailed account of this procedure is given by Mana (1978).

2.5.3 Liner Installation

The liner is modelled using eight noded isoparametric elements which have been found to give good results when subjected to bending forces. The stiffness of the liner is reduced to account for the flexibility introduced by using bolted liner segments rather than a cast in place concrete liner. The liner elements are in place from the start of the analysis, but are initially inactive. They are activated when the nodal point at the crown of the tunnel has moved sufficiently to simulate a closure of the tail void. Using this procedure the size of the tail void may be altered to simulate shield design and construction performance. The weight of the liner is included in the analysis, since the weight of a concrete liner is equal to a significant proportion of the weight of the excavated soil.

2.5.4 Soil Model

An elasto-plastic soil model is needed to provide a good representation of the stress-strain behavior of clay, since it will undergo yielding as it moves into the tail void. The Cam clay model, which has been chosen for this work, has been developed at Cambridge University over the past 15 years. This model uses a capped yield surface and a hardening rule based on isotropic compression theory. Gunn (1977) has used Cam clay in a finite element code to predict the drained behavior of tunnels in clay. His results were compared with model test results performed by Orr (1976) and Seneviratne (1977). Agreement was observed between the finite element and test results for surface settlements and for contours of volumetric and shear strain. Details of the Cam clay model used are given in Chapter III.

2.5.5 Consolidation

Excess pore pressures are built up during excavation and liner installation. The construction is assumed to take place in undrained conditions. The excess pore pressures are then allowed to dissipate. The surface settlements and liner stresses are altered as a result of this consolidation. A detailed discussion of the consolidation theory used is presented in Chapter IV.

2.5.6 Summary

The construction of a tunnel in clay may be modelled in plane strain. The in-situ stresses are setup first, and this is followed by excavation of the soil. The tunnel liner is then activated when movement of the soil into the tunnel opening has closed the tail void. The finite element program uses an elasto-plastic soil model. Excess pore pressures are calculated by adding pore pressure degrees of freedom to the nodal points. Loads are applied in small increments, and the solution remains accurate when strains become large.

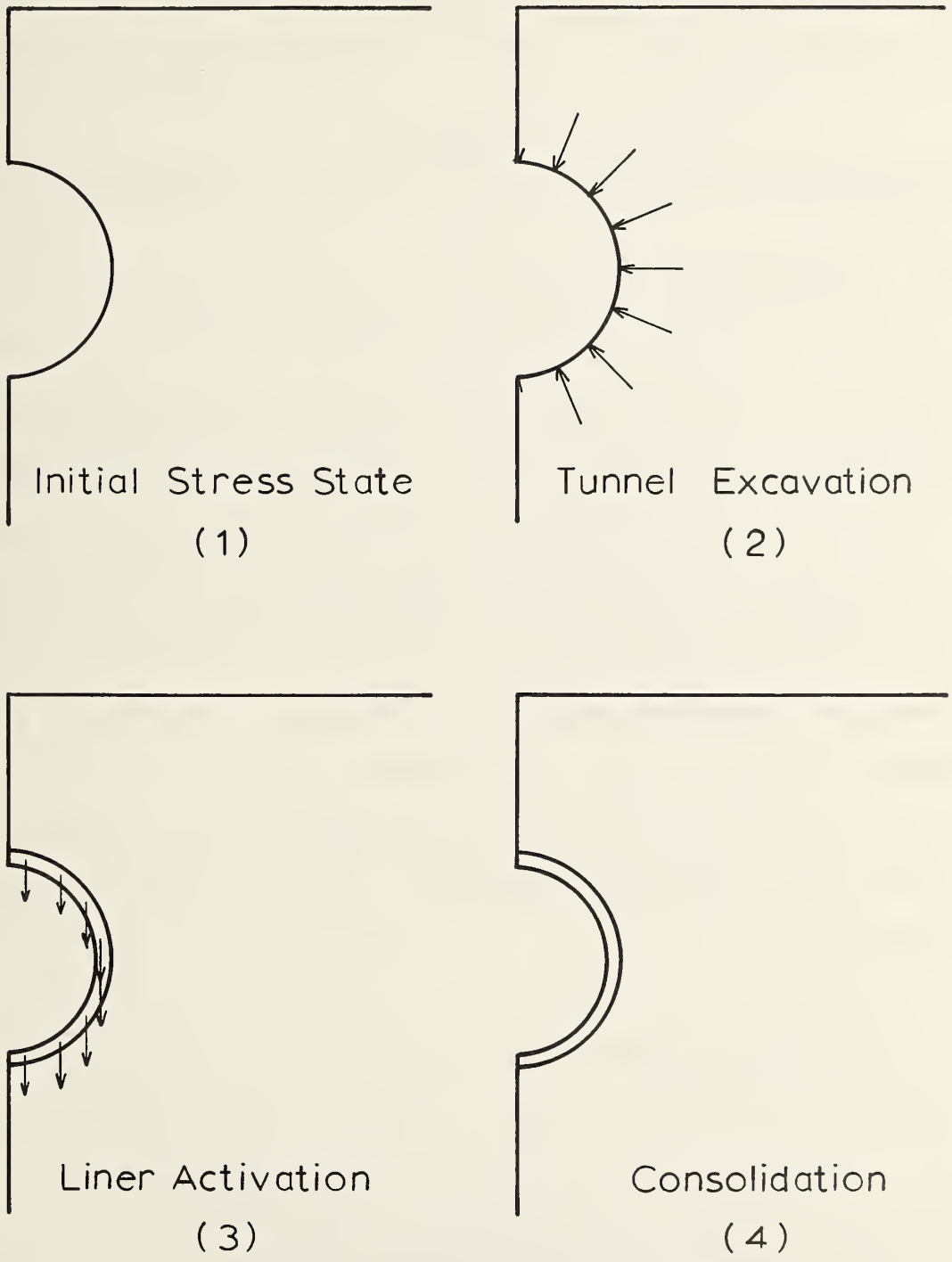

Figure 2.9: Procedure for Simulation of Tunnel Construction

Chapter 3

DEVELOPMENT OF THE CAM CLAY SOIL MODEL FOR USE IN A FINITE ELEMENT CODE

3.1 INTRODUCTION

In this chapter a path will be traced from the equations that define the Cam clay soil model to the development of FORTRAN subroutines that calculate the stress-strain matrix for use in a finite element code.

The finite element code is designed to obtain solutions to problems of combined non-linear material and geometric behavior, in particular, problems related to the construction of tunnels in saturated clays. To solve the non-linear equilibrium equations, incremental element stiffness matrices, [K], are calculated and assembled into a global incremental stiffness matrix. The corresponding equations are solved to determine the incremental dispacements. Element stiffness matrices are calculated from

$$[K] = \int_V [B]^T[D][B]dV \tag{3.1}$$

where [B] is a matrix relating strains to displacements,

[D] is a matrix relating stresses to strains.

Incremental stresses may be calculated from these displacements and added to the stresses that existed at the start of the increment, Marcal (1969), Zienkiewicz (1977).

Thus, to calculate the incremental stiffness matrix, it is necessary to determine the relationship between incremental stresses and incremental strains

$$\{d\sigma'\} = [D]\{d\epsilon\} \tag{3.2}$$

where $\{d\sigma'\}$ is a vector of incremental effective stresses,

$\{d\epsilon\}$ is a vector of incremental strains.

In accordance with the standard sign convention for soil mechanics, compressive stresses are taken as positive and a reduction in volume is taken as a positive volumetric strain.

In a cartesian coordinate system the effective stress vector is given by

$$\{\sigma'\} = (\sigma_x' \ \sigma_y' \ \sigma_z' \ \tau_{yz} \ \tau_{zx} \ \tau_{xy})^T \tag{3.3}$$

The corresponding strain vector is given by

$$\{\epsilon\} = (\epsilon_x \ \epsilon_y \ \epsilon_z \ \gamma_{yz} \ \gamma_{zx} \ \gamma_{xy})^T \tag{3.4}$$

The pore water pressure does not affect the effective stress-strain matrix. The total stress is given in the usual way for direct stresses as

$$\sigma = \sigma' + u \tag{3.5}$$

where u is the pore water pressure.

3.2 THE CAM CLAY MODEL

3.2.1 Introduction

To predict the response of soil it is necessary to use a mathematical model. The earliest researchers chose an elastic model. Soil was first modelled as an elasto-plastic work hardening model by Drucker, Gibson and Henkel (1957). Using this idea in conjunction with critical state theory, the Cam clay model was developed by Roscoe and Schofield (1963), and by Roscoe, Schofield and Thurairajah (1963). The yield surface was later changed from the original bullet shape to an elliptical shape in Modified Cam clay, Roscoe and Burland (1968). This is the version of the Cam clay model that will be used.

The state of a point in a soil continuum is defined by two generalized stress parameters, p' and q, and the voids ratio e, Gunn (1977). The mean effective stress is defined as

$$p' = \frac{\sigma_x' + \sigma_y' + \sigma_z'}{3} \tag{3.6}$$

The octahedral shear stress is defined by

$$q = \frac{1}{\sqrt{2}} \sqrt{(\sigma_y'-\sigma_z')^2+(\sigma_z'-\sigma_x')^2+(\sigma_x'-\sigma_y')^2+6\tau_{yz}^2+6\tau_{zx}^2+6\tau_{xy}^2} \tag{3.7}$$

3.2.2 Yield Surface

If an element of soil is loaded until it reaches the yield surface, any further loading will cause yielding so that the modulus of the soil

will change as the yield surface expands. If this element is then unloaded the soil will behave elastically again. This yielding does not coincide with failure, which occurs when the soil is unable to take any further load.

The elasto-plastic material behaves elastically provided its state in p'-q-e space remains below the yield surface. The projection of this surface on the p'-q plane for a given preconsolidation pressure p'_c is an ellipse. Many other shapes of the yield surface in the p'-q plane have been proposed. The earliest work by Drucker, Gibson and Henkel (1957) used a spherical cap. Early work in Cam clay used a bullet shape, Schofield and Wroth (1968). An exponential cap was used by DiMaggio et al (1971), and a conical cap has been developed more recently by Prevost and Hoeg (1975). Figure 3.1 shows the yield curve whose equation is

$$F = \frac{q^2}{M^2} + p'(p'-p'_c) = 0 \tag{3.8}$$

where M is the slope of the failure line. The significance of this line is explained in the next section.

3.2.3 Failure Envelope

Failure may be said to occur when strains continue to increase without any increase in stresses. This happens when yielding coincides with the critical state so that

$$q = Mp' \tag{3.9}$$

Figure 3.1 also shows the failure line. When $q < Mp'$ stable strain hardening occurs. Thus, if an outward probe is made, the yield surface will expand. When $q > Mp'$ unstable strain softening occurs. In this case, if an outward probe is made, the yield surface collapses.

The finite element code was developed for making predictions in problems for which $q < Mp'$ and thus produces positive definite stiffness matrices. Critical state may also be handled by the program provided that the problem is strain controlled. Thus, stress controlled problems that reach critical state and strain softening problems were not solved in this work.

3.2.4 Flow Rule

The normality principle is used so that the plastic strain increment vector is normal to the yield surface. This is always the case for associative plasticity, Hill (1950). Recently it has been suggested, Banerjee and Stipho (1978), that a non-associative law should be used. This recommendation is based on experimental evidence by Lewin and Burland (1970), who found that the plastic strain increment vector deviates from the outward normal to the yield surface. Nevertheless, for many cases associative plasticity has given good results , and because it leads to a symmetric stiffness matrix, the cost savings are significant.

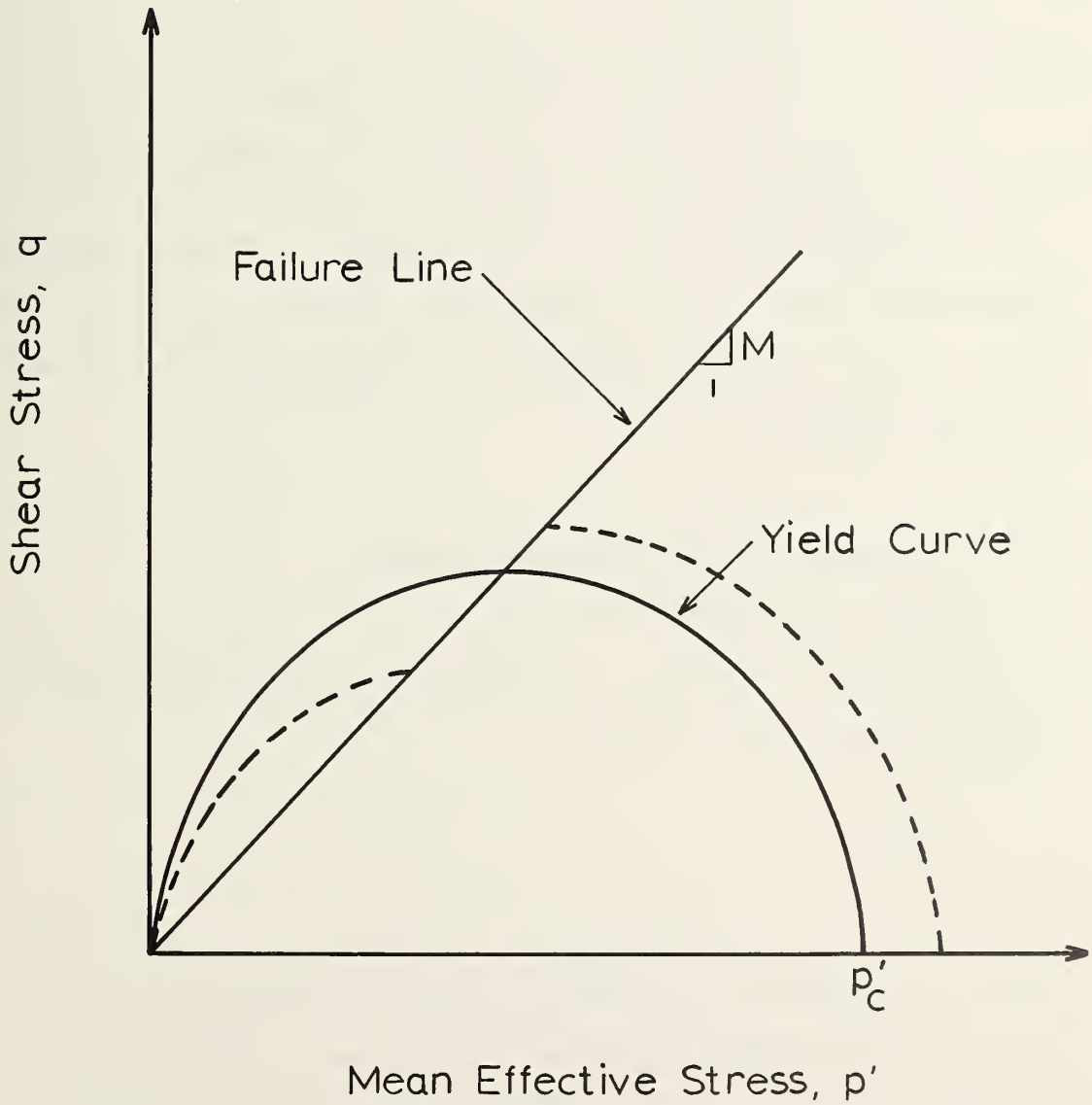

Figure 3.1: Cam clay Yield Model

3.2.5 Hardening Rule

When yielding occurs, the size of the elliptical yield curve is altered since p_c', the hardening parameter, changes. This parameter is governed by the virgin isotropic consolidation curve shown in Figure 3.2 and is given by

$$e = e_1 - \lambda \log_e p_c' \tag{3.10}$$

where e_1 is the value of the voids ratio for unit p_c',

λ is the slope of the virgin isotropic consolidation curve.

In practice this curve may deviate slightly from a straight line when plotted on semi-log graph paper. For this reason, Chang and Duncan (1977) chose to interpolate the line from a set of experimental data fed into their program.

3.3 ELASTIC EFFECTIVE STRESS-STRAIN BEHAVIOR

Below the yield surface, Cam clay is a non-linear elastic material. The bulk modulus, K, may be determined from the elastic rebound line, (see Figure 3.2), and is given by

$$K = \frac{1+e}{\kappa} p' \tag{3.11}$$

where κ is the slope of the rebound isotropic consolidation curve. One further elastic property needs to be specified, since the others are related by

$$E = 3K(1-2\nu) = 2G(1+\nu) \tag{3.12}$$

where E is Young's modulus,

G is the shear modulus,

ν is Poisson's ratio.

For some problems it may be convenient just to specify Poisson's ratio; a value of 0.3 for clays usually gives satisfactory results. However, it is preferred that the shear modulus be specified. This value need not be a constant, but may vary with depth. This method was used for the tunnel analyses in this report.

Thus, the elastic stress-strain matrix may be given by, Timoshenko and Goodier (1970),

$$[D^e] = \frac{1}{3}\begin{bmatrix} 3K+4G & 3K-2G & 3K-2G & 0 & 0 & 0 \\ 3K-2G & 3K+4G & 3K-2G & 0 & 0 & 0 \\ 3K-2G & 3K-2G & 3K+4G & 0 & 0 & 0 \\ 0 & 0 & 0 & 3G & 0 & 0 \\ 0 & 0 & 0 & 0 & 3G & 0 \\ 0 & 0 & 0 & 0 & 0 & 3G \end{bmatrix} \tag{3.13}$$

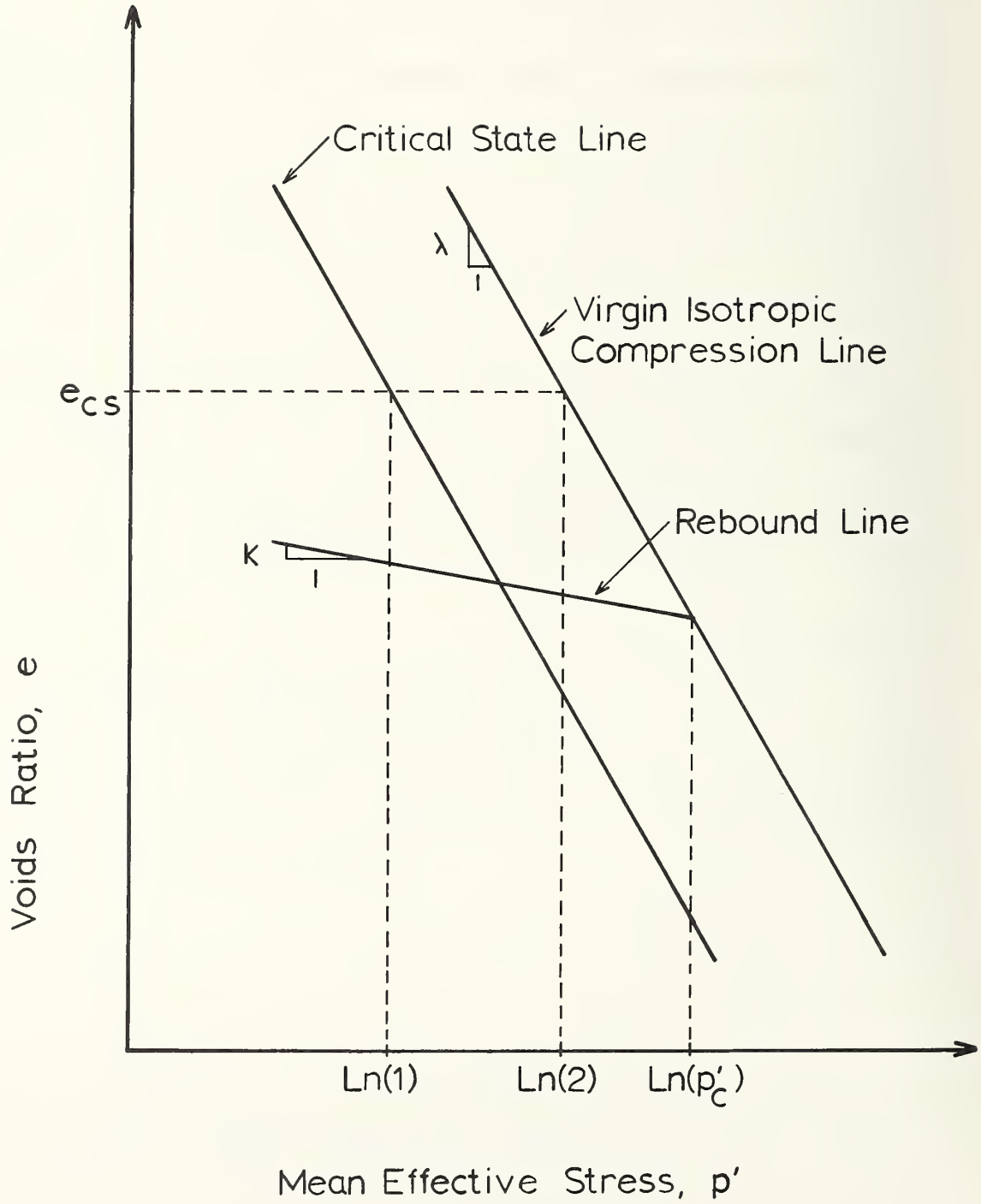

Figure 3.2: Cam clay Hardening Model

3.4 ELASTO-PLASTIC EFFECTIVE STRESS-STRAIN BEHAVIOR

3.4.1 Derivation of the Stress-Strain Matrix

It is now necessary to derive an elasto-plastic stress-strain matrix for a capped yield model. The yield surface given in equation (3.8) may be rewritten as

$$F(\{\sigma'\}T, p_c') = 0 \tag{3.14}$$

Taking the total derivative gives

$$dF = \left\{\frac{\partial F}{\partial \sigma'}\right\}^T \{d\sigma'\} + \frac{\partial F}{\partial p_c'} dp_c' = 0 \tag{3.15}$$

The flow rule is stated as

$$\{d\epsilon^p\} = \phi \left\{\frac{\partial F}{\partial \sigma'}\right\} \tag{3.16}$$

where ϕ is a proportionality constant, and superscripts e and p refer to the elastic and plastic components respectively. Since the volumetric plastic strain increment is given by

$$d\epsilon_v^p = d\epsilon_x^p + d\epsilon_y^p + d\epsilon_z^p \tag{3.17}$$

The flow rule may be rewritten as

$$d\epsilon_v^p = \phi \frac{\partial F}{\partial p'} \tag{3.18}$$

The total strain is the sum of the elastic and plastic components,

$$\{d\epsilon\} = \{d\epsilon^e\} + \{d\epsilon^p\} \tag{3.19}$$

Substituting equations (3.2) and (3.16) into (3.19) gives

$$\{d\epsilon\} = [D^e]^{-1}\{d\sigma'\} + \phi \left\{\frac{\partial F}{\partial \sigma'}\right\} \tag{3.20}$$

From (3.15), (3.18) and (3.20)

$$\left\{\frac{\partial F}{\partial \sigma'}\right\}^T [D^e]\left[\{d\epsilon\} - \phi \left\{\frac{\partial F}{\partial \sigma'}\right\}\right] + \phi \frac{\partial F}{\partial p_c'} \frac{dp_c'}{d\epsilon_v^p} \frac{\partial F}{\partial p'} = 0 \tag{3.21}$$

Solving equation (3.21) for ϕ and substituting into equation (3.20) gives

$$[D] = [D^e] - \frac{[D^e]\left\{\frac{\partial F}{\partial \sigma'}\right\}\left\{\frac{\partial F}{\partial \sigma'}\right\}^T [D^e]}{\left\{\frac{\partial F}{\partial \sigma'}\right\}^T [D^e]\left\{\frac{\partial F}{\partial \sigma'}\right\} - \frac{\partial F}{\partial p_c'} \frac{dp_c'}{d\epsilon_v^p} \frac{\partial F}{\partial p'}} \tag{3.22}$$

This is the final form of the elasto-plastic stress-strain matrix.

3.4.2 Calculation of the Derivatives

Equation (3.22) is a general form of the incremental effective stress-strain matrix for any elasto-plastic material with a capped yield model. To evaluate this matrix for the Cam clay model it is necessary to calculate all of the derivatives in this equation.

To evaluate the vector $\{\partial F/\partial \sigma'\}$, the chain rule for partial differentiation may be used as follows

$$\left\{\frac{\partial F}{\partial \sigma'}\right\} = \frac{\partial F}{\partial p'}\left\{\frac{\partial p'}{\partial \sigma'}\right\} + \frac{\partial F}{\partial q}\left\{\frac{\partial q}{\partial \sigma'}\right\} \tag{3.23}$$

Differentiating equation (3.5) with respect to σ' gives

$$\left\{\frac{\partial p'}{\partial \sigma'}\right\} = \begin{Bmatrix} 1/3 \\ 1/3 \\ 1/3 \\ 0 \\ 0 \\ 0 \end{Bmatrix} \tag{3.24}$$

Differentiating equation (3.7) with respect to σ' gives

$$\left\{\frac{\partial q}{\partial \sigma'}\right\} = \frac{1}{2q}\begin{Bmatrix} 3(\sigma_x'-p') \\ 3(\sigma_y'-p') \\ 3(\sigma_z'-p') \\ 6\tau_{yz} \\ 6\tau_{zx} \\ 6\tau_{xy} \end{Bmatrix} \tag{3.25}$$

Differentiating the yield curve, equation (3.8), with respect to p' gives

$$\frac{\partial F}{\partial p'} = 2p' - p_c' \tag{3.26}$$

Differentiating the yield curve, equation (3.8), with respect to q gives

$$\frac{\partial F}{\partial q} = \frac{2q}{M^2} \tag{3.27}$$

Substituting the terms calculated in (3.24) through (3.27) into equation (3.23) gives

$$\left\{\frac{\partial F}{\partial \sigma'}\right\} = \left\{\begin{array}{c} \dfrac{2p'-p_c'}{3} + \dfrac{3(\sigma_x'-p')}{M^2} \\ \dfrac{2p'-p_c'}{3} + \dfrac{3(\sigma_y'-p')}{M^2} \\ \dfrac{2p'-p_c'}{3} + \dfrac{3(\sigma_z'-p')}{M^2} \\ \dfrac{6\tau_{yz}}{M^2} \\ \dfrac{6\tau_{zx}}{M^2} \\ \dfrac{6\tau_{xy}}{M^2} \end{array}\right\} \tag{3.28}$$

The remaining derivatives to be calculated concern the work hardening parameter. Differentiating the yield curve, equation (3.8), with respect to p_c' gives

$$\frac{\partial F}{\partial p_c'} = -p' \tag{3.29}$$

The final derivative may be calculated as follows

$$\frac{dp_c'}{d\epsilon_v^p} = \frac{dp_c'}{de}\,\frac{de}{d\epsilon_v^p} \tag{3.30}$$

Differentiating equation (3.11) gives

$$\frac{dp_c'}{de} = -\frac{p_c'}{\lambda} \tag{3.31}$$

And the relationship between voids ratio and plastic volumetric strain is

$$\frac{de}{d\epsilon_v^p} = -\frac{\lambda(1+e_0)}{\lambda-\kappa} \tag{3.32}$$

where e_0 is the voids ratio at the start of the increment. Thus, the hardening parameter, A, is given by

$$A = -\frac{\partial F}{\partial p_c'}\frac{dp_c'}{d\epsilon_v^p}\frac{\partial F}{\partial p'} \tag{3.33}$$

or

$$A = \frac{p'p_c'(2p'-p_c')(1+e_0)}{\lambda-\kappa} \tag{3.34}$$

From these equations the stress-strain matrix may be calculated for the Cam clay model when the yield surface has been reached.

3.5 MATERIAL PARAMETERS REQUIRED

For a soil model to be useful, the material parameters that describe the model should be few and easily obtainable from conventional laboratory tests. Cam clay may be described by the following five parameters:

1. λ, the slope of the virgin isotropic consolidation curve

2. κ, the slope of the rebound isotropic consolidation curve

3. e_{cs}, the voids ratio for unit p' on the critical state line

4. M, the slope of the failure line in p'-q space

5. G, the elastic shear modulus

The first three parameters may be readily obtained from an isotropic consolidation test. The slope of the failure line, M, may be calculated from the friction angle ϕ', obtained from a set of drained triaxial tests, since

$$M = \frac{6 \sin \phi'}{3 - \sin \phi'} \tag{3.35}$$

The final elastic constant, G, for a particular confining stress σ_3', can be determined as one third of the initial gradient of the deviatoric stress axial strain curve of an undrained triaxial test, Wroth and Zytynski (1977).

Since the shear modulus usually varies with depth in practice, using a single value for this parameter is a simplification. The shear modulus may be written

$$G = mc_u \tag{3.36}$$

where c_u is the shear strength,

m is a multiplier.

The multiplier may be assumed to be a constant. The shear strength may be assumed to vary linearly with depth; for example, it is equal to approximately 0.3 times the effective vertical stress for many normally consolidated clays. A further sophistication may be added by assuming that a desiccated layer exists above any normally consolidated zone, thus prohibiting the value of G from becoming zero at the surface. This is the type of approach used in the tunnel analyses.

There are other material parameters which are needed in order to set up the initial stresses in a problem. The following parameters are required for this purpose:

1. γ, the density of the soil

2. k_0, the coefficient of earth pressure at rest

3. OCR, the overconsolidation ratio

Details as to how the initial stresses are set up in the program will be given in the chapter VI.

3.6 REDUCTION TO ONE- AND TWO-DIMENSIONAL PROBLEMS

The effective stress-strain matrix has been derived to this point in the chapter in its most general form for use in three-dimensional problems. However, for many applications the problem reduces to two dimensions; for example, a long embankment may be analyzed as a plane strain problem, or a triaxial test may be treated as an axisymmetric problem. Some problems even reduce to a single dimension; for example,

consolidation of a thin clay layer under a large area of uniform load. Other problems approximate to these conditions, such as consolidation around a tunnel. Thus, for the sake of simplicity and considerably reduced computer costs, it is often desirable to solve problems of fewer than three dimensions.

3.6.1 Axisymmetric

Consider a problem which has the y axis as the axis of symmetry. Then τ_{yz}, and τ_{zx} may be set to zero. For this reason the original 6x6 stress-strain matrix reduces to a 4x4.

3.6.2 Plane Strain

For a problem with the longitudinal axis aligned along the z axis, τ_{yz} and τ_{zx} may be set to zero. And although ϵ_z is zero, the value of σ_z is not necessarily zero. Also the relationship

$$\sigma_z = \nu(\sigma_x+\sigma_y) \tag{3.37}$$

does not hold for an elasto-plastic material such as Cam clay. Thus, this problem also reduces to a 4x4.

The importance of σ_z for analysis of deep circular tunnels was shown by Pender (1980). He found that pore pressure changes during the construction of a lined tunnel depended on σ_z, and differred drastically from those predicted using the Stress Path Method, (Lambe and Marr 1979), where σ_z is neglected. Early versions of the Cam clay model which were used in finite element programs also neglected the effect of σ_z (Simpson and Wroth 1972). The effect of σ_z is included in the tunnel analyses in this report.

3.6.3 One Dimension

All the shear stresses are zero in a problem that reduces to one dimension. Thus, the stress-strain matrix reduces to a 3x3. Further simplifications could be made when initial stress conditions allow two of the direct stresses to be identical.

3.7 FULLY DRAINED AND UNDRAINED BEHAVIOR

In chapter IV the soil model is expanded to include a consolidation capability by adding a pore pressure degree of freedom to the nodal points. However, fully drained and undrained problems may be solved in a more simple way. The equations presented in this chapter apply for a drained analysis. For an undrained analysis, when calculating the stress-strain matrix, the bulk modulus of water is added to the bulk modulus of the soil. This bulk modulus is a very large number when compared with the shear modulus of the soil. Thus, the effect is to produce no volume change (for numerical reasons a very small amount of volume change is necessary), but to allow shearing to take place. This method is preferable to the usual method of setting Poisson's ratio close to 0.5.

During the stress recovery cycle, the stress-strain matrix should be computed without adding the bulk modulus of water. The effective stress increment is then obtained. The pore pressure may be obtained by multiplying the small volume change by the bulk modulus of water.

3.8 FINITE ELEMENT ALGORITHMS

3.8.1 Introduction

FORTRAN subroutines for calculating the stress-strain matrix for Cam clay and for calculating the updated stresses in the stress recovery cycle are given in Appendix B.

It is useful to understand this part of the program design. During the assembly of the global stiffness matrix, stiffness matrices are calculated for each element using the numerical technique of gaussian integration. The stress-strain matrix, [D], is calculated at each integration point. Since this matrix depends on the stress state and history of that integration point, these stresses must be stored from one increment to the next.

3.8.2 Stress-Strain Matrix

The stress-strain matrix subroutine is called for each integration point and computed according to equation (3.22). First the elastic component , $[D^e]$, is computed. The stress state is examined, and if it is below the yield surface, the behavior is elastic and thus no further calculations are required. If the stress state lies on the yield surface, the remainder of the formula in equation (3.22) must be calculated.

For cyclic problems, the stress state may lie on the yield surface even though the soil is unloading. To accommodate this possibility, it is necessary to be allow the program to repeat or iterate an increment

until the guess (unloading or loading) made in the assembly cylcle is matched by the correct response in the recovery cycle. Since the problems analyzed in this work are generally not cyclic, this capability has been omitted. The problem may be overcome, where necessary, by taking very small load increments.

3.8.3 Stress Updating

The stress-strain matrix and the strain-displacement matrix are recovered from temporary storage, where they are preserved from the assembly cycle. The incremental stresses are then calculated from

$$\{d\sigma'\} = [D][B]\{dx\} \tag{3.38}$$

where $\{dx\}$ is a vector of the incremental displacements. These incremental stresses are added to the total stresses which existed at the start of the increment. The yield surface is updated if it has expanded during the increment. The updated voids ratio is calculated from

$$e = e_{cs} - \kappa \log_e p' - (\lambda-\kappa) \log_e \left(\frac{p_c'}{2}\right) \tag{3.39}$$

The updated quantities p', q, e and p_c' are saved for each integration point along with the stresses and strains.

3.9 COMPARISON OF THE FINITE ELEMENT RESULTS WITH TEST DATA

At this stage it is desirable to test the response of the finite element code using the Cam clay model. This is done by analyzing the

problem of drained triaxial tests on normally consolidated Weald clay. The experimental tests were performed by Bishop and Henkel (1971). The material properties used are shown in Table 3.1.

TABLE 3.1

Weald Clay Material Parameters

κ	0.031
λ	0.088
e_{cs}	1.0575
M	0.882
G	434.8 psi

The finite element mesh used is shown in Figure 3.3. The test was simulated using one four noded axisymmetric isoparametric element. The initial stresses were set equal to the value of σ_3', which was 30 psi, and then the test was run by applying displacement increments in the negative y direction to nodes 1 and 2. Thus, a strain controlled test was simulated, and hence problems of instabilty at failure were avoided. Results are shown in Figure 3.4 and excellent agreement was obtained between experimental and finite element results.

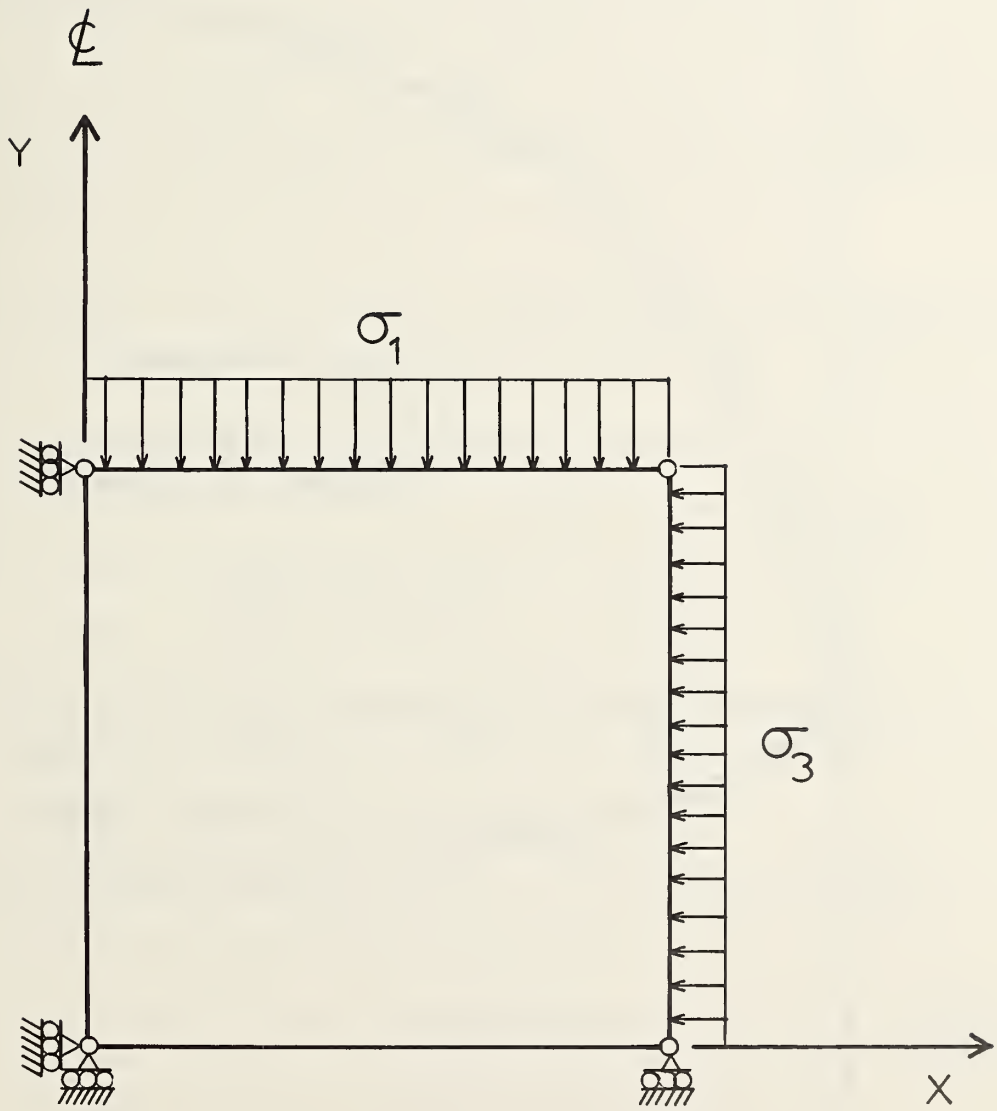

Figure 3.3: Finite Element Mesh for Triaxial Tests

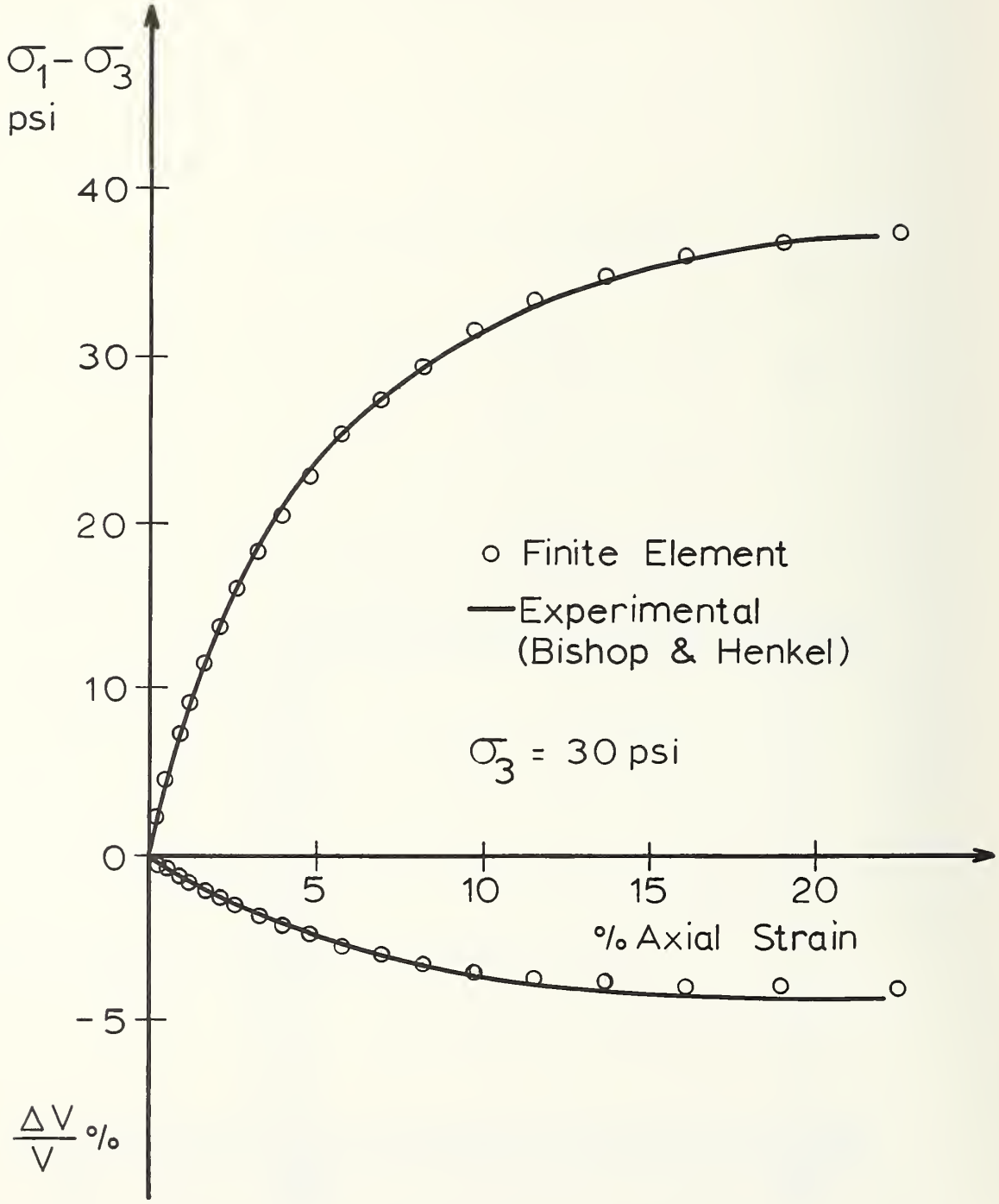

Figure 3.4: Drained Triaxial Compression Tests on Weald Clay

Chapter 4

EXTENDING THE MODEL TO INCLUDE CONSOLIDATION

4.1 INTRODUCTION

The settlement of soils under load due to the squeezing out of the pore water is a process called consolidation. This phenomenon was first explained by Terzaghi (1925) for the case of one-dimensional consolidation. The theory was later generalized to three dimensions by Biot (1941).

A solution to the problem of consolidation involves coupling the equations of elasticity with those of fluid flow. To solve these equations using a finite element scheme, the problem must be discretized in both the space and time domains. Sandhu and Wilson (1969) proposed a finite element procedure for the case of seepage in an elastic medium. Small, Booker and Davis (1976) used a different technique to find a solution to the problem of elasto-plastic consolidation of soil. It is this method that is used here, since Cam clay is a work hardening elasto-plastic material. Only the essential parts of the theory will be outlined; readers interested in the complete mathematical solution are referred to appropriate papers in the text.

4.2 GOVERNING EQUATIONS

In this section the partial differential equations governing the elasto-plastic consolidation of soil will be presented. Appropriate boundary conditions will also be given. Double suffix notation is used, and a superior dot denotes material differentiation with respect to time.

The governing equations are

1. Equilibrium between the incremental stresses and the incremental body forces:

$$\frac{\partial \dot{\sigma}_{ij}}{\partial x_j} - \dot{F}_i = 0 \tag{4.1}$$

where σ_{ij} are the components of the total stress tensor,

x_j are the coordinates in a cartesian reference frame,

F_i are the components of body force.

2. Stress-strain relation between the incremental effective stresses and the incremental strains:

$$\dot{\sigma}_{ij}' = \dot{\sigma}_{ij} - \dot{p}\delta_{ij} = D_{ijkl}\dot{\epsilon}_{kl} \tag{4.2}$$

where σ_{ij}' are the components of the effective stress tensor,

p is the pore water pressure,

δ_{ij} is the Kronecker delta,

D_{ijkl} are the coefficients of the stress-strain law,

ϵ_{kl} are the components of the strain tensor.

3. Darcy's law for the rate of flow of water through soil:

$$\dot{v}_i = -\frac{k_{ij}}{\gamma_w}\frac{\partial \dot{p}}{\partial x_j} \tag{4.3}$$

where v_i are the components of the superficial velocity vector,

k_{ij} are the coefficients of the permeability matrix,

γ_w is the unit weight of water.

4. And finally, relationship between the rate of volume decrease of the element and the rate at which water is expelled, assuming the pore water is incompressible relative to the soil skeleton:

$$\frac{\partial \dot{v}_i}{\partial x_i} = \frac{\partial \dot{\epsilon}_v}{\partial t} \tag{4.4}$$

where ϵ_v is the volumetric strain,

t is the time.

To model problems accurately, many different types of boundary conditions must be applied. The following four are common in practice, and may be used in the finite element program:

1. To simulate a constrained boundary, the displacement increment is set to zero:

$$\dot{u}_i = 0 \tag{4.5}$$

where u_i are the displacements.

2. To allow free displacements, the applied tractions must be in equilibrium with the stresses:

$$\dot{\sigma}_{ij}n_j = -\dot{T}_i \tag{4.6}$$

where n_j is the outward normal to the surface,

T_i are the applied tractions.

3. To simulate a pervious boundary, the pore pressure must be allowed to remain constant:

$$\dot{p} = 0 \tag{4.7}$$

4. To simulate an impervious boundary, water must not be allowed to cross the boundary:

$$n_i\dot{v}_i = 0 \tag{4.8}$$

A solution to these equations was found by Booker (1973).

4.3 FINITE ELEMENT FORMULATION

The consolidation problem may be discretized using finite elements. A pore pressure degree of freedom is added to the usual displacement degrees of freedom at the nodal points. The spatial integrations may then be performed using gaussian quadrature, and a marching process is used to perform the time integration.

Shape functions are used to relate the continuous value of the displacements, u, to the nodal values, $\{\delta\}$.

$$\{u\} = \{N_u\}^T\{\delta\} \tag{4.9}$$

where $\{N_u\}$ are the shape functions.

Shape functions may also be used to relate the continuous values of the pore pressure, p, to the nodal values, $\{q\}$.

$$p = \{N_p\}^T\{q\} \tag{4.10}$$

where $\{N_p\}$ are the shape functions.

Both sets of shape functions depend on the particular type of finite element used. The shape functions may use the same or different orders of interpolation, and thus a pore pressure degree of freedom need not necessarily exist at each nodal point. This will be discussed further in Section 4.10.

The coupled equations for an element may be written in matrix form, Carter, Booker and Small (1979):

$$\begin{bmatrix} K & -L^T \\ -L & -\beta dt\Phi \end{bmatrix} \begin{bmatrix} d\delta \\ dq \end{bmatrix} = \begin{bmatrix} f \\ ndt + \Phi q_0 dt \end{bmatrix} \tag{4.11}$$

where the element stiffness matrix, [K], is given in the usual way by

$$[K] = \int_V [B]^T[D][B]dV \tag{4.12}$$

The matrix [L] couples the stiffness equations with those of fluid flow, and is given by

$$[L]^T = \int_V \{B_v\}^T \{N_p\}^T dV \tag{4.13}$$

where the volumetric strain-displacement vector, $\{B_v\}$, is given by

$$\epsilon_v = \{B_v\}\{\delta\} \tag{4.14}$$

This vector is easily calculated from the strain-displacement matrix, since

$$\{B_v\} = (\ 1 \quad 1 \quad 1 \quad 0 \quad 0 \quad 0\ )\ [B] \tag{4.15}$$

The fluid flow matrix is given by

$$[\Phi] = \frac{1}{\gamma_w} \int_V [E]^T [k]^T [E] dV \tag{4.16}$$

where [k] is the permeability matrix, and where

$$[E]^T = \left[\left\{\frac{\partial N_p}{\partial x}\right\} \quad \left\{\frac{\partial N_p}{\partial y}\right\} \quad \left\{\frac{\partial N_p}{\partial z}\right\} \right] \tag{4.17}$$

Also, {f} is the incremental load vector,

$\{q_0\}$ are the pore pressures at the beginning of the increment,

β is an integration parameter, which is discussed in more detail in Section 4.11.

Finally, the existence of a hydrostatic pore pressure distribution is taken care of by adding the following term to the load vector:

$$\{n\} = \int_V [E]^T[k]^T\{i_g\}dV \tag{4.18}$$

where $\{i_g\}$ is a vector containing the direction of the gravitational field.

4.4 MATERIAL PARAMETERS REQUIRED

In order to extend the Cam clay model to include the effect of consolidation, only two further material properties need to be specified. These are as follows:

1. γ_w, the density of water or other pore fluid.
2. [k], the components of the permeability matrix.

Since the density of water is known, it just remains to find the components of the permeability matrix. These may be obtained from laboratory or field tests. Different values of horizontal and vertical permeabilities may be used.

4.5 REDUCTION TO ONE- AND TWO-DIMENSIONAL PROBLEMS

In Section 3.6 it was shown that for problems with fewer than three dimensions, the computation of the stress-strain matrix is simplified, as is the computation of the fluid flow matrix, [Φ]. Computation of the coupling matrix, [L], however, remains unchanged.

For problems that reduce to two dimensions, i.e., plane strain or axisymmetric, the order of [E] is reduced, since

$$\left\{\frac{\partial N_p}{\partial z}\right\} = 0 \tag{4.19}$$

The permeability matrix is also reduced, so that for horizontal or vertical bedding,

$$[k] = \begin{bmatrix} k_x & 0 \\ 0 & k_y \end{bmatrix} \tag{4.20}$$

For problems that reduce to one dimension, further simplification is permitted:

$$[E]T = \left\{\frac{\partial N_p}{\partial x}\right\} \tag{4.21}$$

and

$$[k] = [k_x] \tag{4.22}$$

4.6 FINITE ELEMENT ALGORITHMS

A marching process is used to perform the integration through time. This involves calculating the stress state at some future time, $t+\Delta t$, from the current stress state at time, t, due to the excess pore pressures existing at time t. The process can then be marched forward by taking successive time increments, Δt. These time increments are read in with the load increment data for each increment.

At each increment the coupled set of equations needs to be recalculated. This is done using gaussian integration over each element. The element matrices are then assembled into a global stiffness matrix. A schematic diagram of the element matrices that need to be calculated is shown in Figure 4.1. It should be noted that the element stiffness matrix is symmetric. The parts A1, A2 and A3 are calculated regardless of whether the consolidation option is being used. The element stiffness matrix is stored in the computer program in a vector. This vector stores the elements of the stiffness matrix column by column, but only down to and including the diagonal. This procedure has two advantages: first no storage is wasted; and second, when consolidation is included, it is no trouble to add the additional columns. The parts B1, B2 and B3 correspond to the fluid flow equations, while C1 is the coupling matrix. FORTRAN subroutines for the calculation of parts B1, C1 and B3 are given in Appendix B.

As an example, the matrices needed for the addition of pore pressures will be shown for a simple element. The element chosen is an isoparametric one-dimensional element with three nodes. The element is named L3P2 since it is a link element with displacement degrees of freedom at three nodes, and pore pressure degrees of freedom at two nodes. The element is shown in Figure 4.2.

The shape functions that describe the displacement field are

$$\{N_u\} = \begin{Bmatrix} -\xi(1-\xi)/2 \\ \xi(1+\xi)/2 \\ 1-\xi^2 \end{Bmatrix} \tag{4.23}$$

The shape functions that describe the pore pressure field are

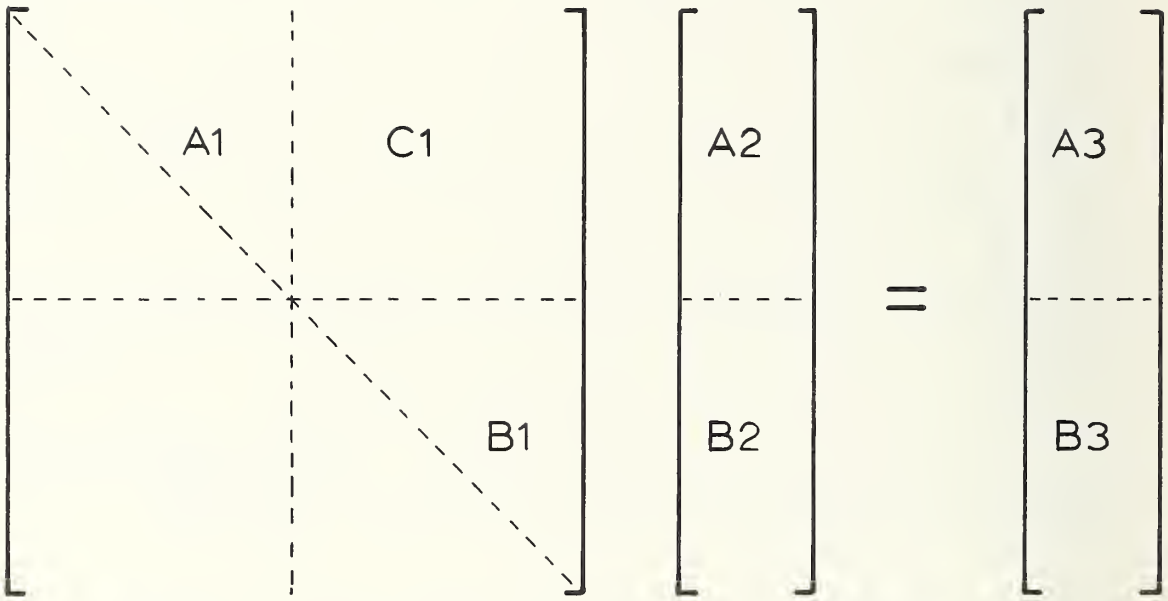

Figure 4.1: Schematic of the Element Equations

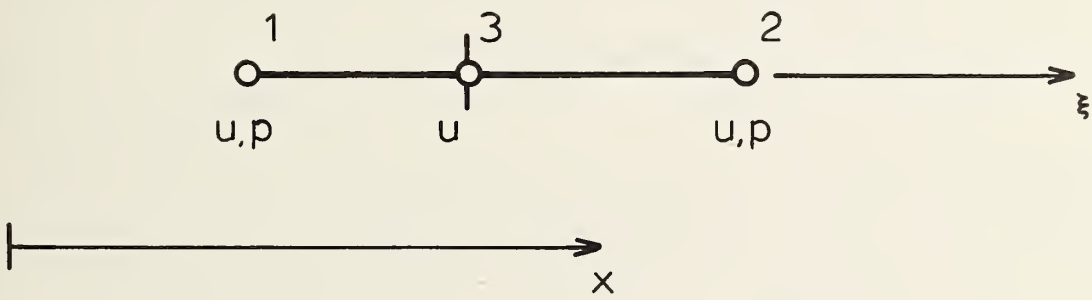

Figure 4.2: Element L3P2

$$\{N_p\} = \begin{Bmatrix} (1-\xi)/2 \\ (1+\xi)/2 \end{Bmatrix} \tag{4.24}$$

The permeability matrix reduces to a 1x1 with this component being k_x. If there is no acting gravitational field, $\{i_g\}$ is zero. The flow matrix becomes

$$[\Phi] = \frac{k_x}{\gamma_w} \int_{-1}^{+1} [E]^T[E] \, |J_p| \, d\xi \tag{4.25}$$

where $|J_p|$ is the determinant of the Jacobian for the pore pressure shape functions, and is given by

$$|J_p| = \left(-\frac{1}{2}x_1 + \frac{1}{2}x_2 \right) \tag{4.26}$$

Also,

$$[E]^T = \begin{Bmatrix} -1/2 \\ 1/2 \end{Bmatrix} \tag{4.27}$$

The coupling matrix becomes

$$[L]^T = \int_{-1}^{+1} [B_v]^T[N_p]^T \, |J_u| \, d\xi \tag{4.28}$$

where $|J_u|$ is the determinant of the Jacobian for the displacement shape functions, and is given by

$$|J_u| = \left(\xi - \frac{1}{2}\right)x_1 + \left(\xi + \frac{1}{2}\right)x_2 - 2\xi x_3 \tag{4.29}$$

Since there are two Jacobians for this one element, some confusion may arise over which one to use. When node 3 is placed midway between nodes 1 and 2, the values of both Jacobians become identical.

4.7 VERIFICATION OF ONE-DIMENSIONAL SEEPAGE

In this section the seepage capability of the program is tested. The porous medium is assumed rigid so that only the flow characteristics are tested. Thus, consolidation does not take place, and the coupling matrix, [L], is not tested. Two problems are analyzed; the first is one-dimensional seepage and the second is radial seepage.

4.7.1 Vertical Drainage

A one-dimensional flow problem was analyzed. The pore pressure at depth x=10ft is given as p=1000psf, and at depth x=100ft it is given as zero. The governing differential equation is

$$\frac{d}{dx}\left(k_x \frac{dp}{dx}\right) = 0 \tag{4.30}$$

Assuming a constant value for the permeability, k_x, the equation may be integrated twice and the boundary conditions applied. The expected linear distribution of pore pressure is found to be

$$p = \frac{100}{9}(100 - x) \tag{4.31}$$

The finite element mesh consisted of ten L3P2 elements. Fourteen time increments were used to allow the solution to stabilize. The size of the time increment increases in a logarithmic fashion, and is dependent on the value of k_x chosen. The results are shown in Figure 4.3. No difference is visible between the theoretical results and those from the finite element analysis.

4.7.2 Radial Drainage

An axisymmetric flow problem was analyzed. The pore pressure on the inside of a thick porous pipe with inside radius, r=10in, is p=1000psi, and the pressure on the outside, r=100in, is zero. The problem is axisymmetric and also plane strain. The governing differential equation, written in polar coordinates, is

$$\frac{d}{dr}\left(k_r\, r\, \frac{dp}{dr}\right) = 0 \tag{4.32}$$

After integrating this equation twice and applying the boundary conditions, the pore pressure distribution is given by

$$p = 1000\left(2 - \frac{\log_e r}{\log_e 10}\right) \tag{4.33}$$

The finite element mesh used was similar to that used in the previous problem, The same time increments were also utilized. The results are shown in Figure 4.4, and the results of the finite element analysis appear to agree exactly with the theory.

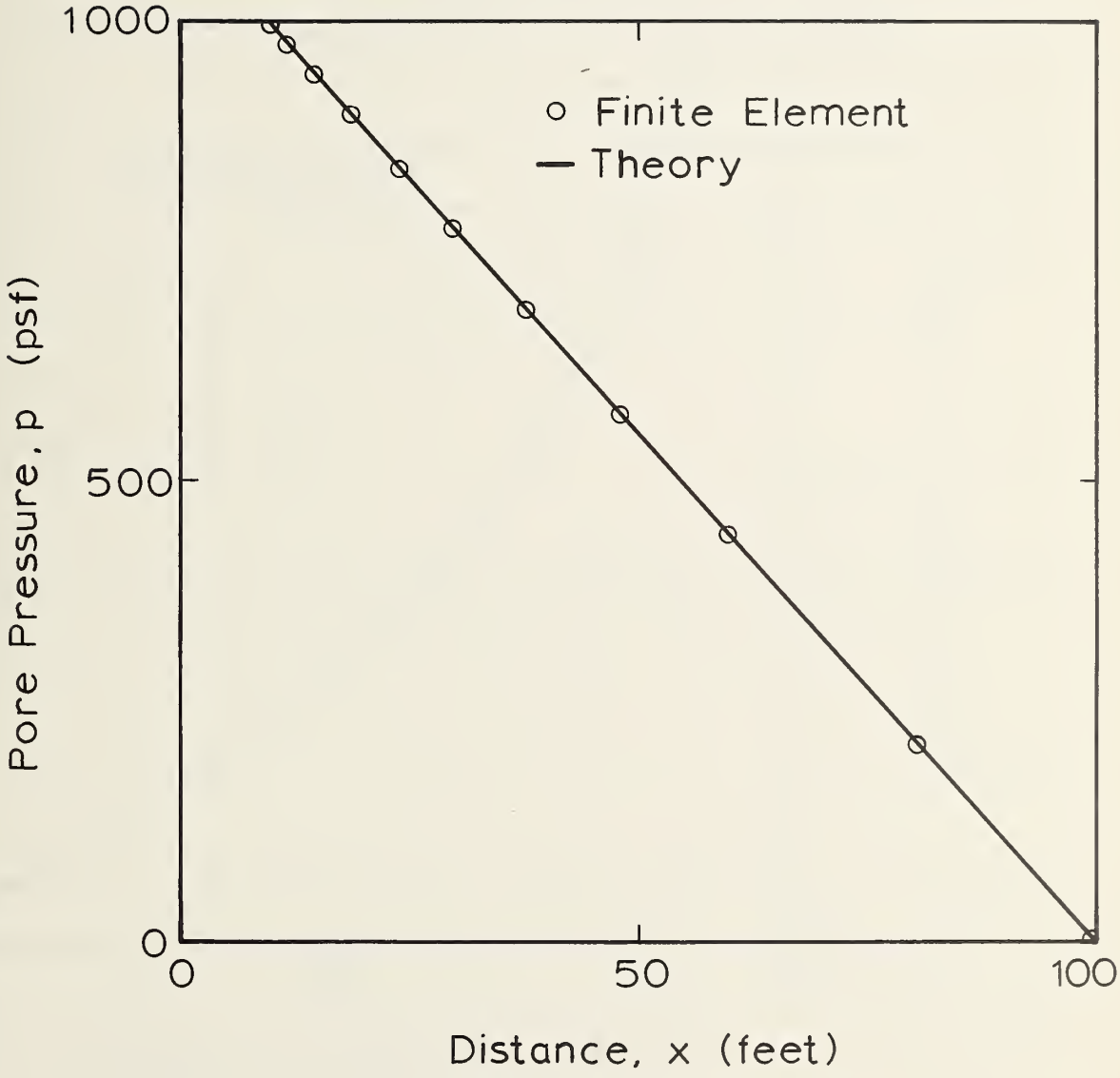

Figure 4.3: Pore Pressure Distribution for Vertical Drainage

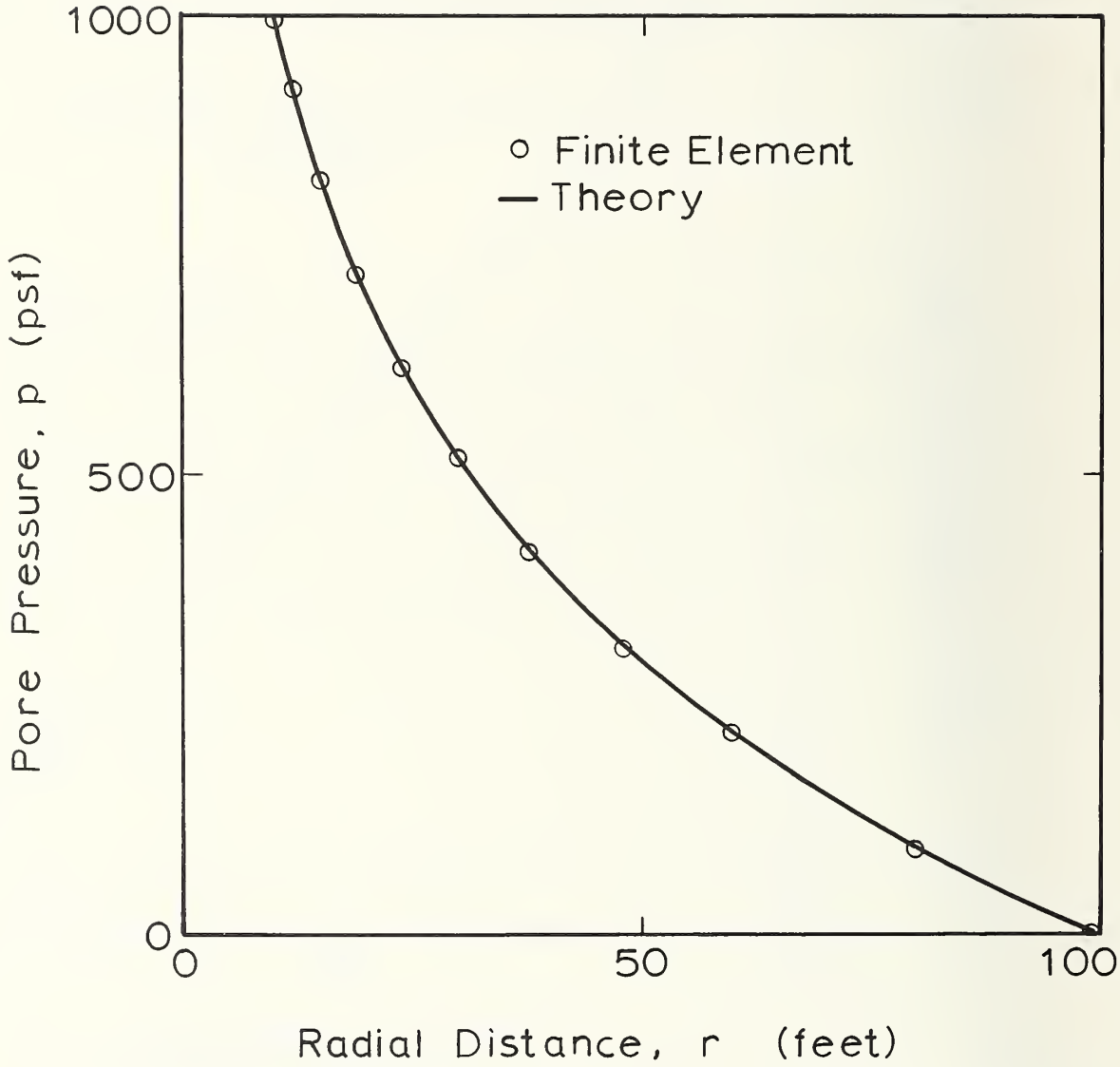

Figure 4.4: Pore Pressure Distribution for Radial Drainage

4.8 VERIFICATION OF ONE-DIMENSIONAL CONSOLIDATION

One-dimensional consolidation occurs when a uniform load is applied to a clay layer and drainage is allowed to occur in the vertical direction only. Thus, settlement occurs with time as the excess pore pressure is allowed to dissipate. If the soil skeleton is assumed to behave elastically, the consolidation process obeys Terzaghi's consolidation equation, as defined by Lambe and Whitman (1969):

$$c_v \frac{\partial^2 u_e}{\partial z^2} = \frac{\partial u_e}{\partial t} - \frac{\partial \sigma_z}{\partial t} \tag{4.34}$$

Thus, the excess pore pressure, u_e, is dependent on the time, t, and the depth, z. The applied vertical stress is σ_z, and c_v is given by

$$c_v = \frac{k_z}{\gamma_w} E_c \tag{4.35}$$

where E_c is the constrained Young's modulus, equal to E when Poisson's ratio is zero. The solution may be written in non-dimensional form, Taylor (1948), so that the excess pore pressure is related to the initial pore pressure, u_0, by

$$u_e = \sum_{m=0}^{\infty} \frac{2u_0}{M} \sin(MZ)\, e^{-M^2 T} \tag{4.36}$$

where

$$M = \frac{\pi}{2}(2m+1) \tag{4.37}$$

The non-dimensional height is $Z = z/H$, where H is the drainage distance. The non-dimensional time is given by

$$T = \frac{c_v t}{H^2} \tag{4.38}$$

The percentage of consolidation for the clay layer is given by

$$U = 1 - \sum_{m=0}^{\infty} \frac{2}{M^2} e^{-M^2 T} \tag{4.39}$$

The finite element mesh used to verify the consolidation capability of the program consisted of five L3P2 elements, and is shown in Figure 4.5. The boundary conditions chosen correspond to single drainage, since the bottom node was made impervious and the top node pervious. The bottom node is fixed and a uniform load was applied to the top node. Fourteen time increments were chosen; each five increments represent a tenfold increase in time.

The finite element results obtained are shown in Figures 4.6 and 4.7, plotted along with the theoretical values calculated from the above formulae. The results are in good agreement. More accurate results can be obtained by refining the part of the mesh near the load, since the excess pore pressure gradient is large in this area. This is especially true shortly after the application of load. Better results also may be obtained by taking more small time increments at the start of the analysis. Thus, the results improve at greater times.

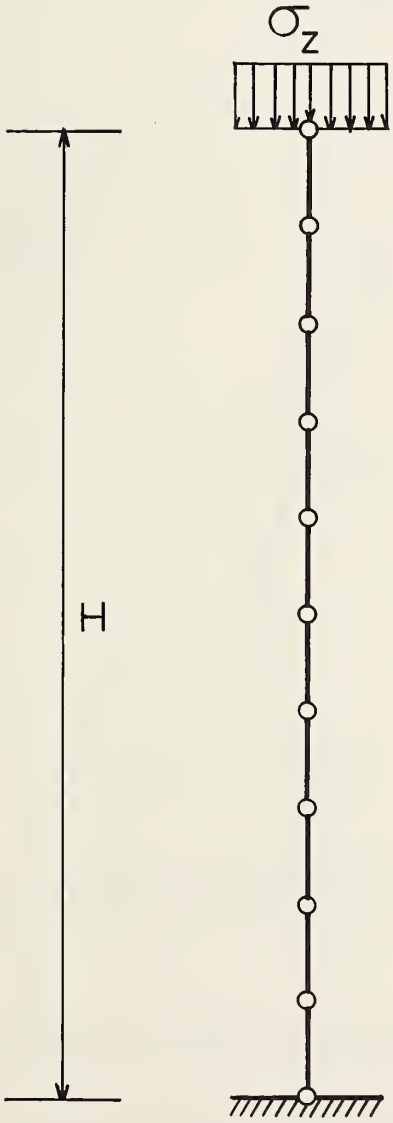

Figure 4.5: Finite Element Mesh for One-Dimensional Consolidation

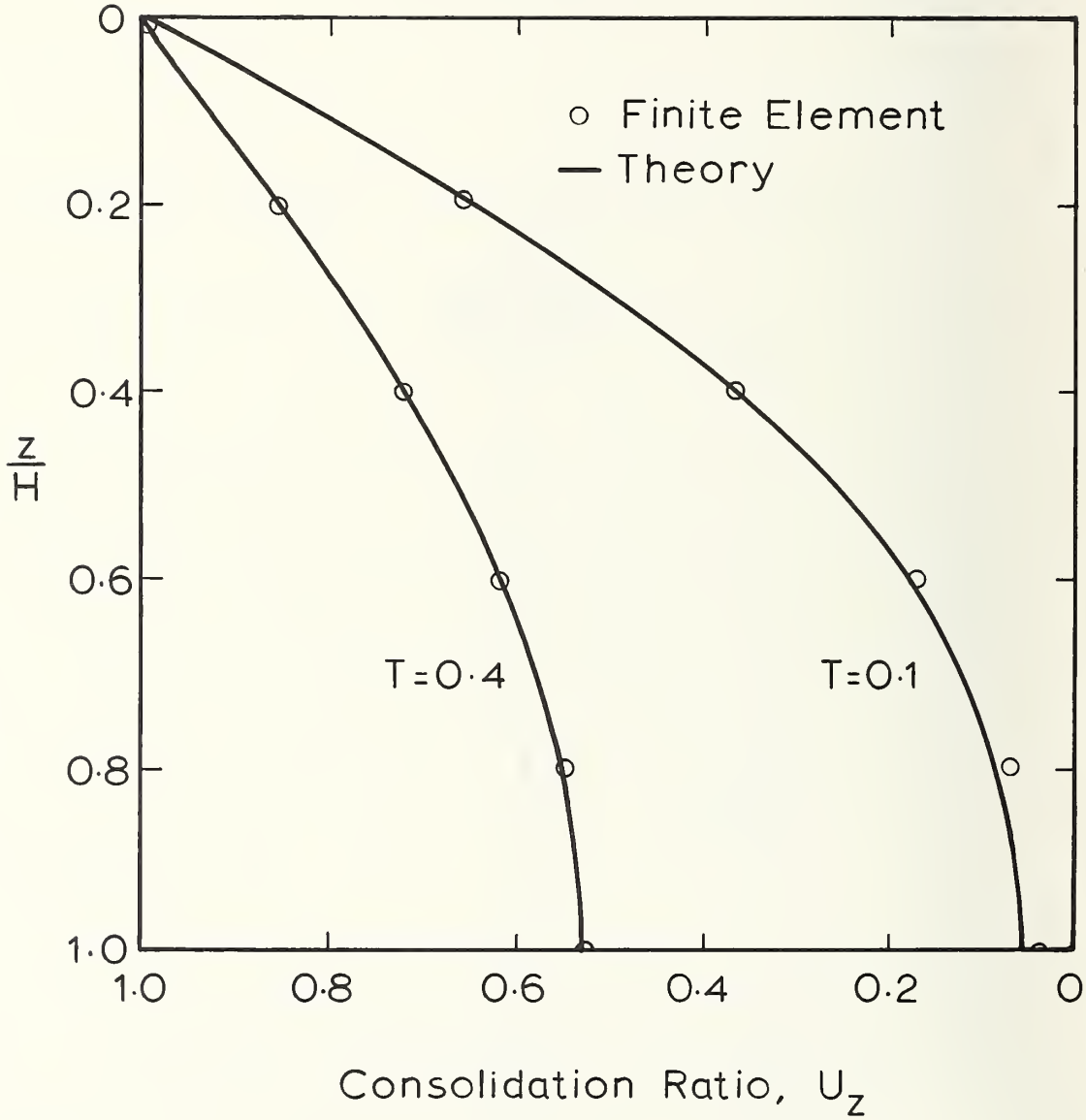

Figure 4.6: Excess Pore Pressures for One-Dimensional Consolidation

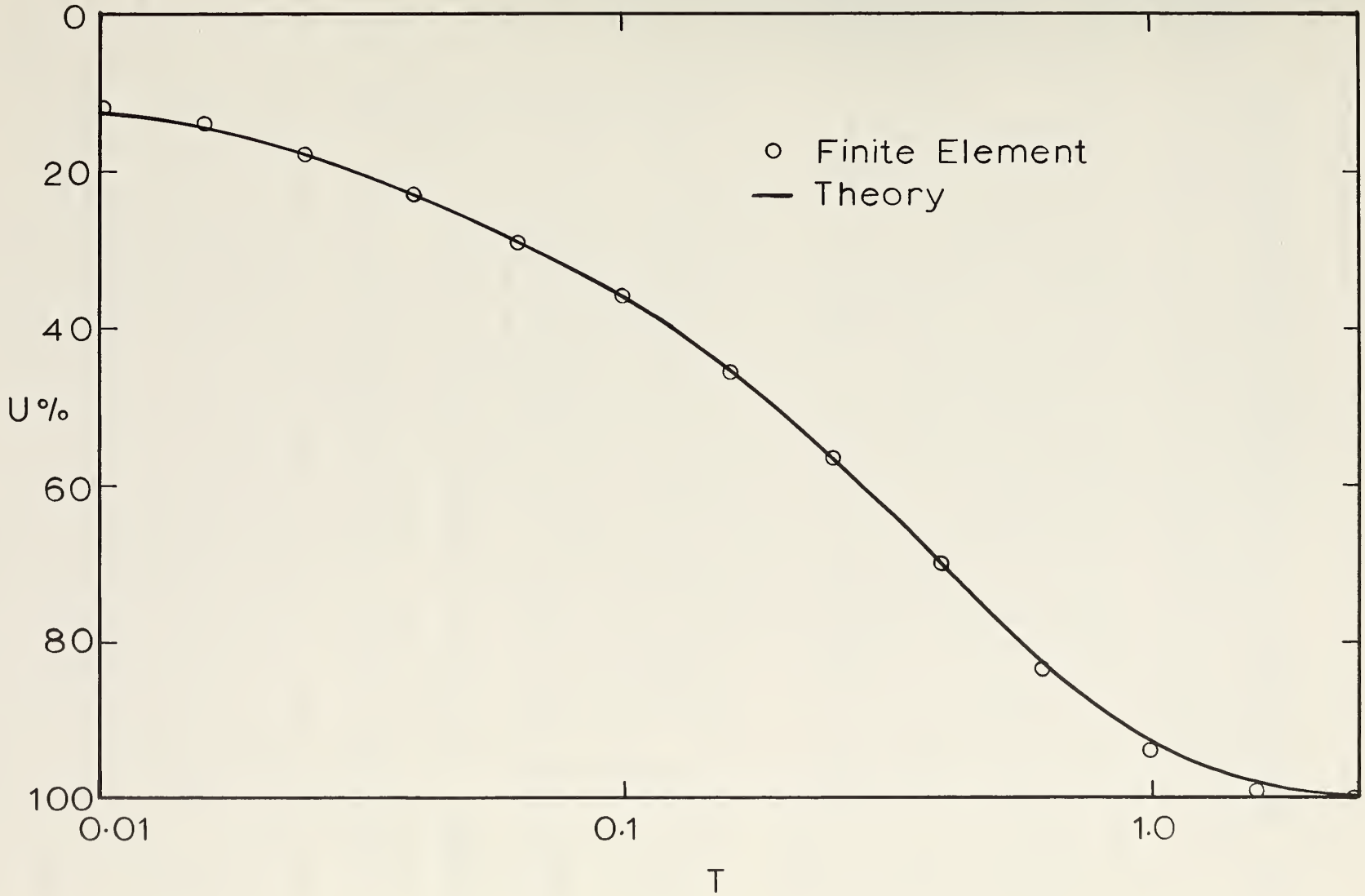

Figure 4.7: Settlement Versus Time for One-Dimensional Consolidation

4.9 CONSOLIDATION OF A CLAY LAYER UNDER A UNIFORM STRIP LOAD

The coupled set of equations which governs the consolidation process is such that closed form solutions have only been obtained for problems with very simple boundary conditions. The case of a strip load on an elastic half space was solved by Schiffmann, Chen and Jordan (1969). A closed form solution has also been obtained for the problem of a strip load on an elastic layer with a smooth base, Gibson, Schiffmann and Pu (1970). However, problems in the field do not often approximate the above boundary conditions, and thus, these solutions can rarely be applied.

A more useful problem is that of consolidation of an elastic clay layer under a uniform strip load with a rough rigid impervious base. While no closed form solutions for this problem exist, a finite element approach presented by Christian, Boehmer and Martin (1972) provides results which can be used to check those obtained by the present program. The finite element mesh used is shown in Figure 4.8, and consists of seventy Q8P4 elements in plane strain. The Q8P4 element is an isoparametric eight noded quadrilateral element with pore pressure degrees of feedom at the corner nodes. Water is allowed to drain at the surface, while the base is impervious. The boundary conditions on the edge furthest from the load have little effect on the solution. As a matter of preference these nodes are fixed in order to reduce the number of degrees of freedom in the problem. Fourteen time increments were chosen in the same manner as those used for the problem of one-dimensional consolidation.

The settlement results are plotted against non-dimensional time for the load center and the load edge in Figure 4.9. These are compared to one-dimensional consolidation settlement results. The results agree with those reported by Christian, Boehmer and Martin (1972).

4.10 EFFECT OF ELEMENT CHOICE ON SOLUTION ACCURACY

During the course of this work a number of different finite elements was used, depending upon the application. Hence, some effort was expended to determine the most superior element. All elements have an isoparametric formulation. This enabled geometries with curved surfaces, such as tunnels, to be easily modelled by higher order elements. The following elements were programmed:

1. Q4P4, a four-noded quadrilateral element with a pore pressure degree of freedom at each node.
2. Q8P4, an eight-noded quadrilateral element with a pore pressure degree of freedom at the corner nodes.
3. Q8P8, an eight-noded quadrilateral element with a pore pressure degree of freedom at each node.
4. L2P2, a two-noded link element with a pore pressure degree of freedom at each node.
5. L3P2, a three-noded link element with a pore pressure degree of freedom at the end nodes.

It should be noted that the L2P2 element is obtained by the degeneration of the Q4P4 element into one dimension. Similarly, if the Q8P4 element is degenerated into one dimension, the L3P2 element is obtained. This study focused upon the quadrilateral elements since the same considerations of choice may then be applied to the linear elements.

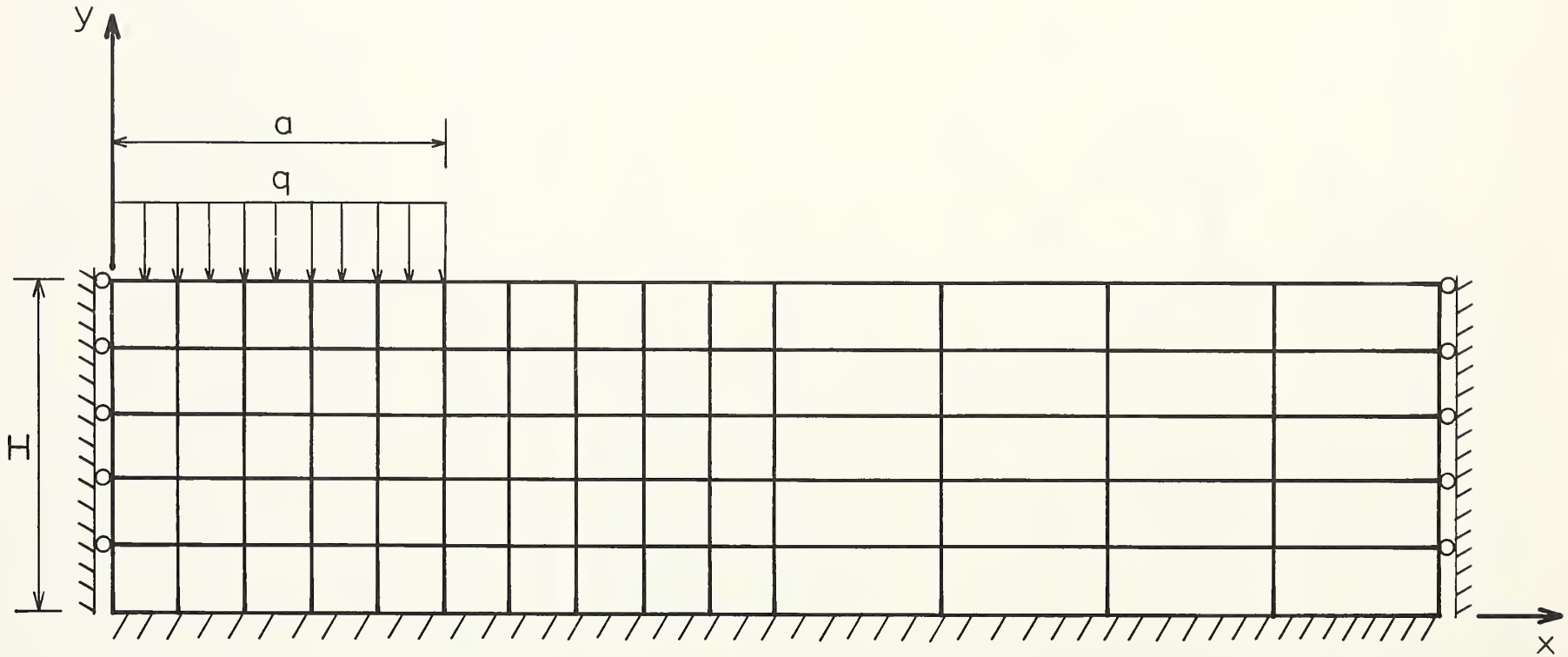

Figure 4.8: Finite Element Mesh for Strip Load on a Clay Layer

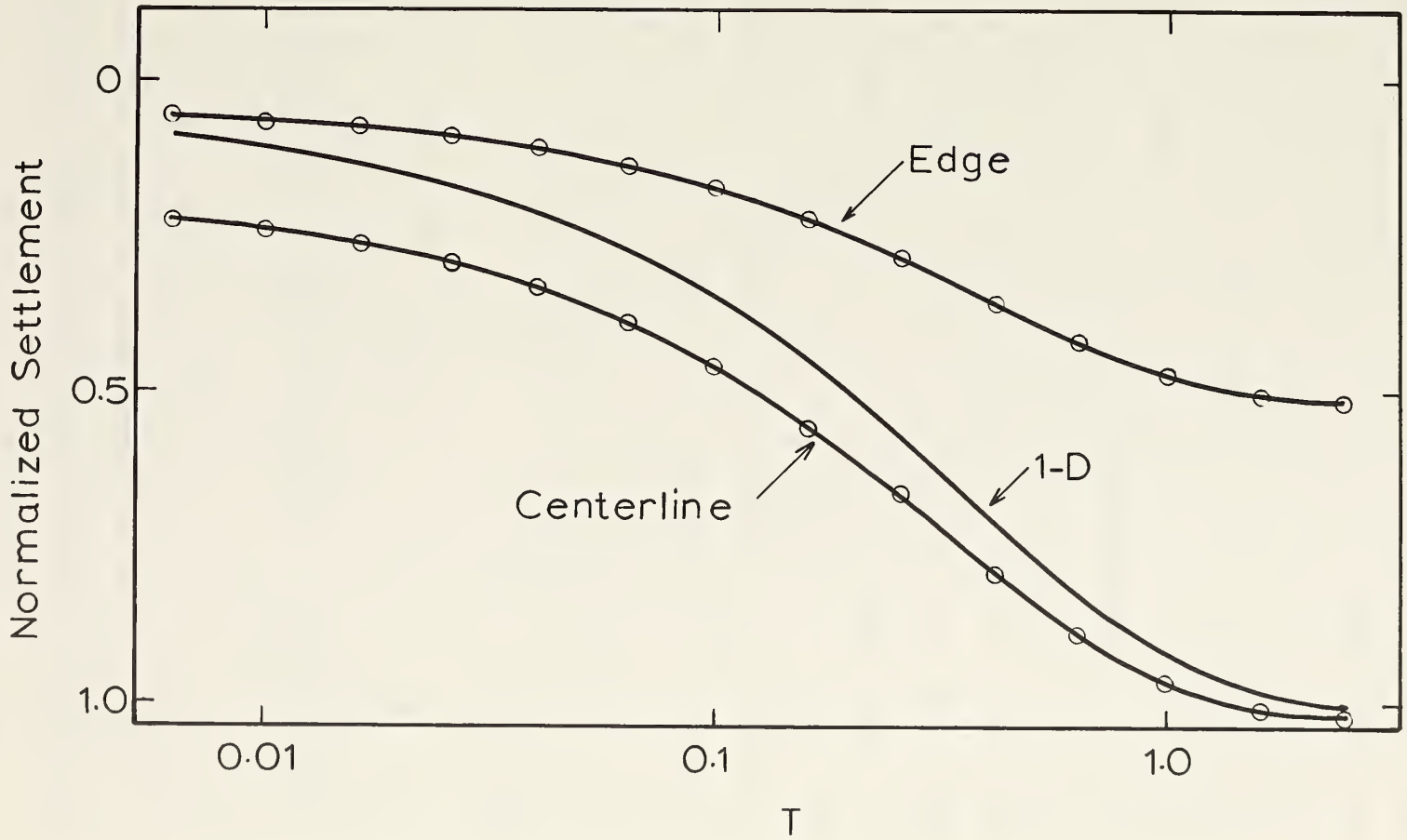

Figure 4.9: Settlement versus Time for Strip Load on a Clay Layer

The problem of one-dimensional consolidation was approached using both the Q8P8 and Q8P4 elements. The same numbers of elements and time steps were used. It is found that small oscillations of excess pore water pressure exist through space for the Q8P8 element at any given time, but not for the Q8P4 element, (see Figure 4.10.) At first, this might seem surprising since there are more pore pressure degrees of freedom for the case using the Q8P8 element. The reason for this appears to be the matching of the stress and pore pressure distributions across the elements. Considering the Q8P8 element, it is seen that the displacement shape functions are quadratic. Thus, the stress variation across the element is linear, while the pore pressure variation across the element is quadratic. This mismatch between the orders of interpolation for stress and pore pressure is probably the reason for the apparently poor showing of the Q8P8 element. The Q8P4 element has equal orders of interpolation for stresses and pore pressures. For this reason, hybrid elements have become popular for coupled problems, for example Osaimi (1976).

A comparison between the Q8P4 and Q4P4 elements was made using the strip loading problem described in Section 4.9. The same numbers of elements and time increments were used. The prediction of settlement for the two elements was very close even though for the Q4P4 element there were many fewer displacement degrees of freedom. However, the prediction of pore pressures using the Q4P4 element produced large oscillations in time for a given point in space, (see Figure 4.11.)

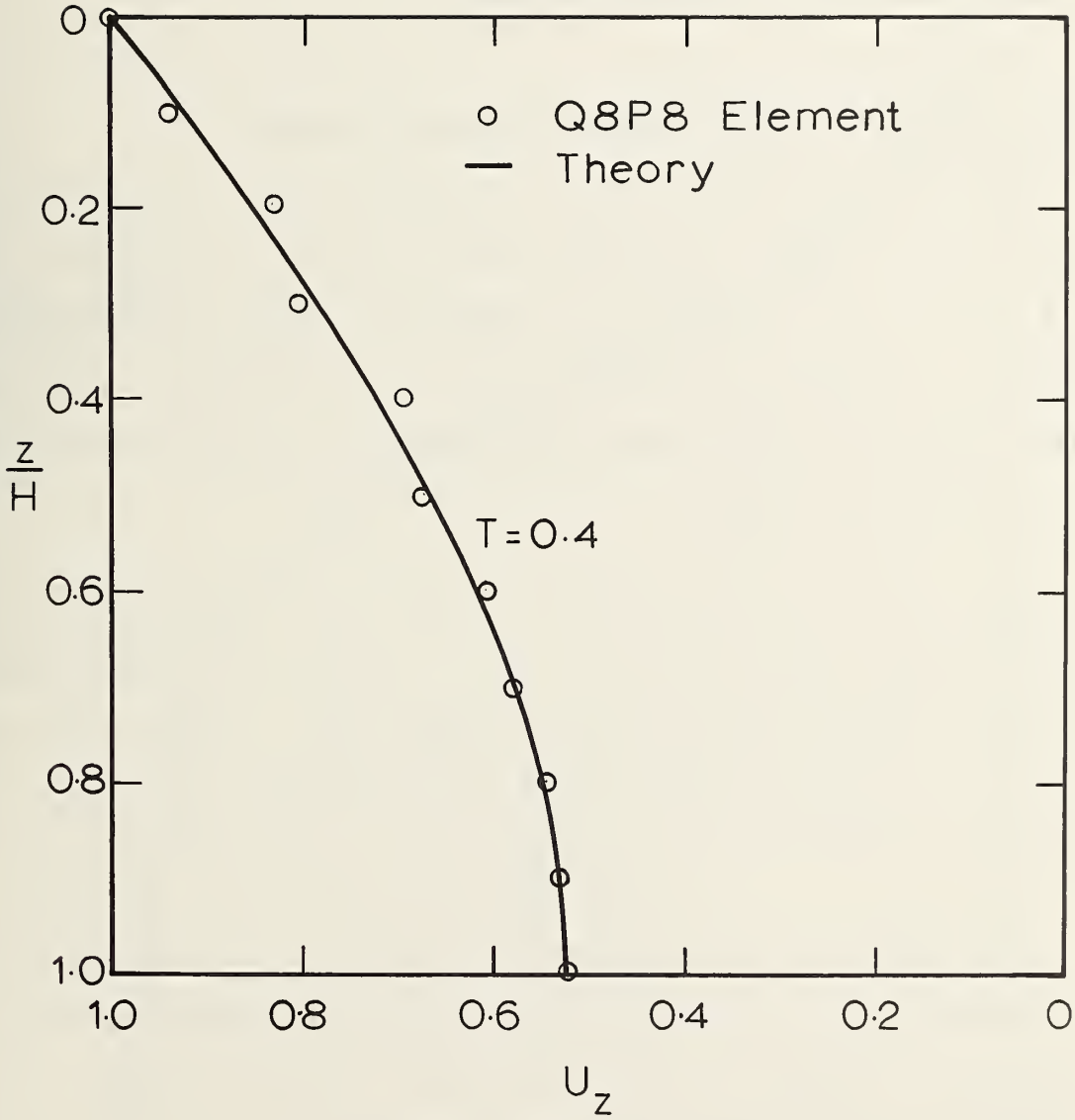

Figure 4.10: Oscillations in Space for the Q8P8 Element

Sandhu, Liu and Singh (1977) studied various elements for one-dimensional problems. They found serious deficiences for elements such as the Q8P8. This is supported by the one- and two-dimensional studies presented here, and thus, the Q8P4 element was chosen as being the most suited for the tunnel analyses.

4.11 EFFECT OF INTEGRATION RULE ON SOLUTION ACCURACY

During the marching process an integration rule, defined by the value of β, was used. Values of β from zero to one may be chosen. When $\beta = 0.5$ the rule corresponds to a trapezoidal rule, and when $\beta = 0.67$ the rule corresponds to a parabolic rule. It can be shown, Booker and Small (1975), that for β greater than or equal to one half, the solution is unconditionally stable.

The effect of β on the solution for the excess pore pressure during one-dimensional consolidation was tested. A mesh of five Q8P8 elements was used and the results are shown in Figure 4.12. It can be seen that for values of β greater than 0.5 the solution becomes damped, while for values of β less than 0.5, oscillations in the solution become large.

As a result of this study, $\beta = 0.5$ was used for the tunnel analyses. It was also found that accurate solutions could be obtained while using five time increments to cover a tenfold increase in time. This procedure was also used in the tunnel analyses.

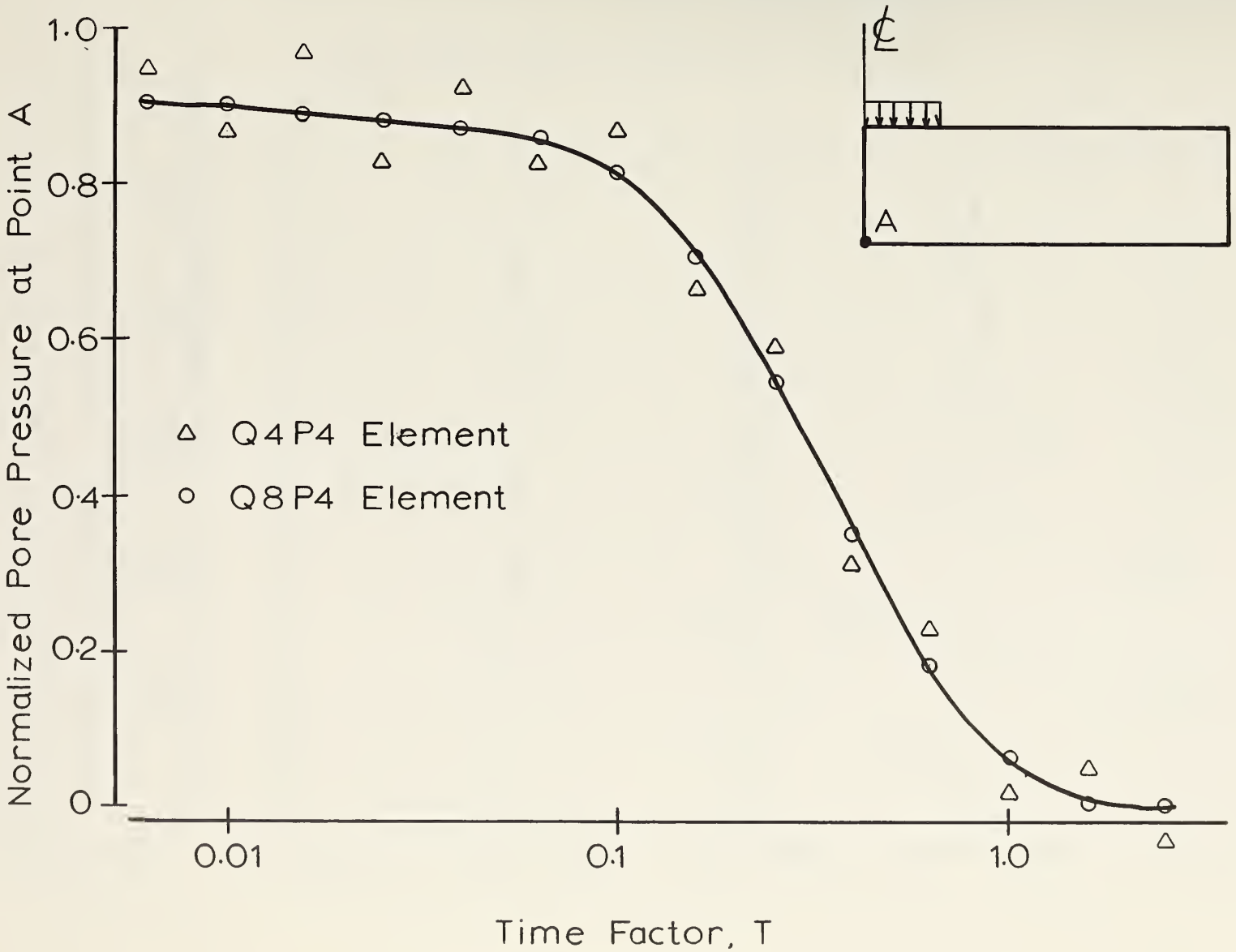

Figure 4.11: Oscillations in Time for the Q4P4 Element

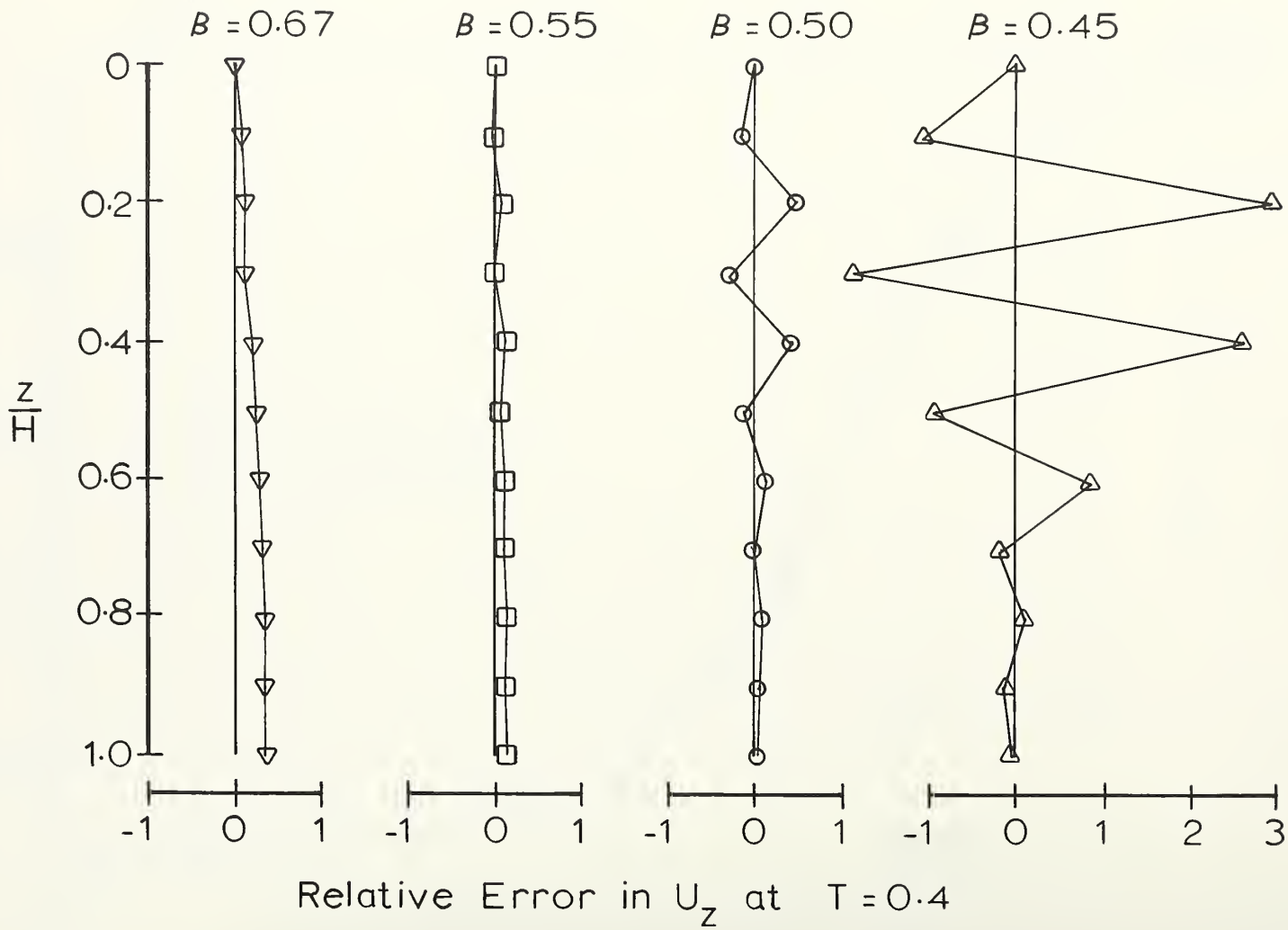

Figure 4.12: Effect of Integration Rule on Solution Accuracy

Chapter 5

FINITE ELEMENT FORMULATION FOR LARGE DEFORMATIONS

5.1 INTRODUCTION

For structures built with materials such as steel and concrete, it is unusual for displacements or strains to become large. However, in geotechnical engineering the modulus values for soil may be small, thereby producing large deformations. For example, large settlements are often observed when embankments are constructed on soft clay or peat. In this report, the primary application is to that of shield tunneling; in this case, the strains may range from small to large depending upon the soil conditions and construction technique. The most likely location for large strains is in the area of the tail void which is created as the shield advances. Here, the soil is temporarily unsupported and can collapse against the liner, leading to large strain effects. Obviously, this is most likely to occur where the soil is a soft clay or a non-selfsupporting medium like sand. Grouting behind the liner segments is designed to prevent this collapse, but if the soil is weak enough, the grouting will come too late.

5.2 CHOOSING A REFERENCE FRAME

To include the effect of finite deformations, additional terms need to be added to the stiffness matrix. In order to compute these terms, it is necessary to distinguish between two possible reference frames.

In a Lagrangian analysis, the coordinate system remains fixed in space. This method leads to an unsymmetric stiffness matrix, Hibbitt, Marcal and Rice (1970). This is an undesirable result, since the solution of the resulting equations requires approximately twice as many operations on a digital computer. However, if the stress-strain law is already unsymmetric, as is the case for non-associative plasticity, then this method may be desirable, Carter, Booker and Davis (1977).

In a Eulerian analysis the coordinate system is fixed in the material. This method is approximated by taking small load increments and updating the nodal coordinates after each increment. This method should more precisely be called an 'updated Lagrangian' analysis. McMeeking and Rice (1975) used this approach to obtain a symmetric stiffness matrix, and this is the method used here.

5.3 CHOOSING APPROPRIATE MEASURES OF STRESS AND STRAIN

When the finite element equations are derived from the virtual work equations, care must be taken in the definition of stress. The relationship between different measures of stress is given by Yamada and Wifi (1977). The equilibrium equations are most conveniently written in terms of nominal or Lagrange stress. However, a symmetric stress measure such as Cauchy stress, σ, or Kirkoff stress, τ, is more desirable. Furthermore, the stress-strain law must be written using a stress measure that is frame indifferent. The Jaumann rate of Kirkoff stress fulfills this requirement, Malvern (1969). It should be pointed out that other rates of stress also exist. The Jaumann rate is denoted by a superior star.

The stress-strain law may then be written as

$$\overset{*}{\tau}_{ij} = D_{ijkl}\, e_{kl} \tag{5.1}$$

where the deformation rate tensor is given by

$$e_{ij} = \frac{1}{2}\left(\frac{\partial v_i}{\partial x_j} + \frac{\partial v_j}{\partial x_i} \right) \tag{5.2}$$

The Cauchy true stress increment is

$$d\sigma_{ij} = \overset{*}{\tau}_{ij} - \sigma_{ij}\, e_{ii} + \sigma_{ik}\, \omega_{ki} + \sigma_{jk}\, \omega_{kj} \tag{5.3}$$

where the skew symmetric spin tensor is given by

$$\omega_{ij} = \frac{1}{2}\left(\frac{\partial v_i}{\partial x_j} - \frac{\partial v_j}{\partial x_i} \right) \tag{5.4}$$

The decision to use the Jaumann rate of Kirkoff stress in the stress-strain law is arbitary. Thus, the Jaumann rate of Cauchy stress could have been used where

$$\overset{*}{\tau}_{ij} = \overset{*}{\sigma}_{ij} + \sigma_{ij}\, e_{ii} \tag{5.5}$$

5.4 INITIAL STRESS STIFFNESS MATRIX

The initial stress stiffness matrix, $[K_s]$, must be added to the conventional stiffness matrix to give the total structure stiffness matrix.

$$[K] = \int_V [B]^T[D][B]\, dV + [K_s] \tag{5.6}$$

The initial stress stiffness matrix was derived by McMeeking and Rice (1975), and is given by

$$[K_s] = \int_V \left\{ [N_k]^T{}_{,i}\, \sigma_{ij}\, [N_k]_{,j} - 2\, [B_{ki}]^T\, \sigma_{ij}\, [B_{kj}] \right\} dV \tag{5.7}$$

where $[B_{ij}]$ is expressed, in terms of the shape functions, as

$$[B_{ij}] = \frac{1}{2} \left\{ [N_i]_{,j} + [N_j]_{,i} \right\} \tag{5.8}$$

This matrix arises from two sources. The variation of the strain-displacement matrix gives one term, since for small strains this variation is zero. This is often referred to as the 'initial stability matrix', Zienkiewicz (1977). The other term comes from the more precise definition of stress. The initial stability contribution is dependent on the stress level, and thus an eigenvalue problem may be solved, Cook (1974).

$$|K_0 + \lambda K_s| = 0 \tag{5.9}$$

where K_0 is the stiffness matrix, excluding the initial stability terms, and λ is the eigenvalue dependent on the stress level. Thus, this eigenvalue problem is similar to a buckling load problem.

A FORTRAN subroutine which calculates this initial stress stiffness matrix for the case of plane strain is given in Appendix B. The subroutine computes the matrix for an element using an algorithm derived by Derbalian (1978). The element matrix may be written in partitioned form as

$$[k_s] = \int_{-1}^{1}\int_{-1}^{1} \begin{bmatrix} [k_{11}] & [k_{12}] \\ [k_{21}] & [k_{22}] \end{bmatrix} |J| \, d\mu d\nu \tag{5.10}$$

where the submatrices are given by

$$[k_{11}] = \frac{1}{2}(\sigma_{22} - \sigma_{11})[S_{\nu\nu}] - \sigma_{11}[S_{\mu\mu}] \tag{5.11}$$

$$[k_{12}] = -\frac{1}{2}(\sigma_{11} + \sigma_{22})[S_{\mu\nu}] - \sigma_{12}([S_{\mu\mu}] + [S_{\nu\nu}]) \tag{5.12}$$

$$[k_{21}] = [k_{12}]^T \tag{5.13}$$

$$[k_{22}] = \frac{1}{2}(\sigma_{11} - \sigma_{22})[S_{\mu\mu}] - \sigma_{22}[S_{\nu\nu}] \tag{5.14}$$

and where, for example

$$[S_{\mu\nu}] = \left\{\frac{\partial N}{\partial \mu}\right\}\left\{\frac{\partial N}{\partial \nu}\right\}^T \tag{5.15}$$

The computation of this matrix was found to add significantly to the cost of calculating the stiffness matrix. Hence, the program option to use the initial stress stiffness matrix should be used with caution.

5.5 UPDATING STRESSES AND DISPLACEMENTS

After the displacement increment has been calculated, the total stresses must be updated by adding the incremental stresses. In a large strain analysis this stress increment must first be modified to allow for rotations. This is achieved using the following equations for the plane strain case, Derbalian (1978):

$$d\sigma_{11} = \overset{*}{\tau}_{11} - \sigma_{11}e - 2R\sigma_{12} \tag{5.16}$$

$$d\sigma_{22} = \overset{*}{\tau}_{22} - \sigma_{22}e + 2R\sigma_{12} \tag{5.17}$$

$$d\sigma_{12} = \overset{*}{\tau}_{12} - \sigma_{12}e + R(\sigma_{11} - \sigma_{22}) \tag{5.18}$$

$$d\sigma_{33} = \overset{*}{\tau}_{33} - \sigma_{33}e \tag{5.19}$$

where the rate of dilation is given as

$$e = e_{11} + e_{22} \tag{5.20}$$

and the spin is given by

$$R = \frac{1}{2}\left(\frac{\partial v_2}{\partial x_1} - \frac{\partial v_1}{\partial x_2}\right) \tag{5.21}$$

A FORTRAN subroutine which calculates this true stress increment for the case of plane strain is given in Appendix B.

At the end of each increment the coordinates of the nodal points are updated by adding the corresponding displacement increments. This process allows the reference frame to move with the material.

It has been pointed out, Gibson, England and Hussey (1967), that for large deformation problems the velocity of the pore fluid in Darcy's law needs to be the relative velocity of the fluid to the solid. By updating the coordinate system this objective is achieved.

5.6 RESIDUAL LOAD CORRECTION

The modulus values for a Cam clay material that is yielding will not remain constant throughout the load increment. Hence, equilibrium will not exist exactly at the end of the increment. Stress corrections due to the rotation of elements, which were discussed in the previous section, may lead to further deviations from the equilibrium state.

To correct for this situation, the out-of-balance forces are calculated at the end of each increment, and then applied as nodal loads during the next increment. These forces may be obtained from

$$\{\Psi\} = \int_V [B]^T\{\sigma\}\, dV - \{f\} \tag{5.22}$$

where $\{f\}$ is a vector containing the total nodal loads.

These forces should be small compared to the applied loads or support reactions. If they become large, the solution is becoming unstable and smaller load increments should be used.

5.7 VERIFICATION OF STRESS CORRECTION DUE TO ROTATIONS

To verify the stress correction due to finite rotations, one element was rotated through 45^0 in the x-y plane. The element was prestressed in the x direction. The solution was compared to the exact solution obtained using the Mohr's circle transformation. Two separate computer runs were performed, one using 25 increments of rotation and the other using 50 increments. The results, shown in Table 5.1, indicate that the program yields correct results which come closer to the exact solution as more increments are used.

TABLE 5.1

Rotation of Stresses

	σ_{xx}	σ_{yy}	σ_{xy}
Before rotation	1.000	0.000	0.000
Mohr circle	0.500	0.500	0.500
50 increments	0.506	0.494	0.512
25 increments	0.513	0.487	0.525

5.8 LARGE DEFORMATION ONE-DIMENSIONAL CONSOLIDATION

Finite element solutions are found for the case of one-dimensional elastic consolidation with large deformations. In this case rotations do not occur and the initial stress stiffness matrix was not computed. Hence, the only correction used from that of small strain theory was to update the reference frame after each increment.

The mesh used consisted of five L3P2 elements. Nineteen time increments were used with the full load applied on the first increment. The final theoretical settlement may be obtained by integrating the strain

$$d\epsilon = \frac{d\sigma}{E} \tag{5.23}$$

Let the final stress be q, and the initial and final depths of the clay layer be H_0 and H respectively. Thus,

$$\int_{H_0}^{H} - \frac{dh}{h} = \int_{0}^{q} \frac{d\sigma}{E} \tag{5.24}$$

Thus, the ratio of the final depth to the initial is given by

$$\frac{H}{H_0} = e^{-q/E} \tag{5.25}$$

Four finite element runs were made with different values of the ratio q/E. The results are given in Table 5.2.

The percent consolidation is plotted against the time factor in Figure 5.1. As expected, the clay layer consolidates more quickly at higher strains. This can be attributed to the progressively shorter drainage paths that are obtained during the consolidation process when the final settlements are large. These results are in agreement with the finite difference results of Olson and Ladd (1979), and the finite element results of Carter, Small and Booker (1977).

TABLE 5.2

Final Settlements Computed by Different Methods

q / E	% final settlement small strain theory	% final settlement large strain theory	% final settlement finite element	% error between FE and LST
0.00001	0.001	0.001	0.001	0.1
0.1	10.0	9.5	9.6	1.1
0.5	50.0	39.3	40.9	4.1
1.0	100.0	63.2	68.4	8.2

Mesri and Rokhsar (1974) found that small strain theory gave reasonable consolidation results up to strains of 32 percent. Because much smaller strains are expected in the tunnel analyses, and in view of the good results obtained using just the updated reference frame, the computation of the initial stress stiffness matrix will be omitted for subsequent work in this report.

5.9 SUMMARY

An updated Lagrangian formulation has been outlined which enables problems involving large strains to be solved accurately with a symmetric stiffness matrix. For problems with intermediate strains, a less expensive option is available in which only the nodal coordinates are updated between increments.

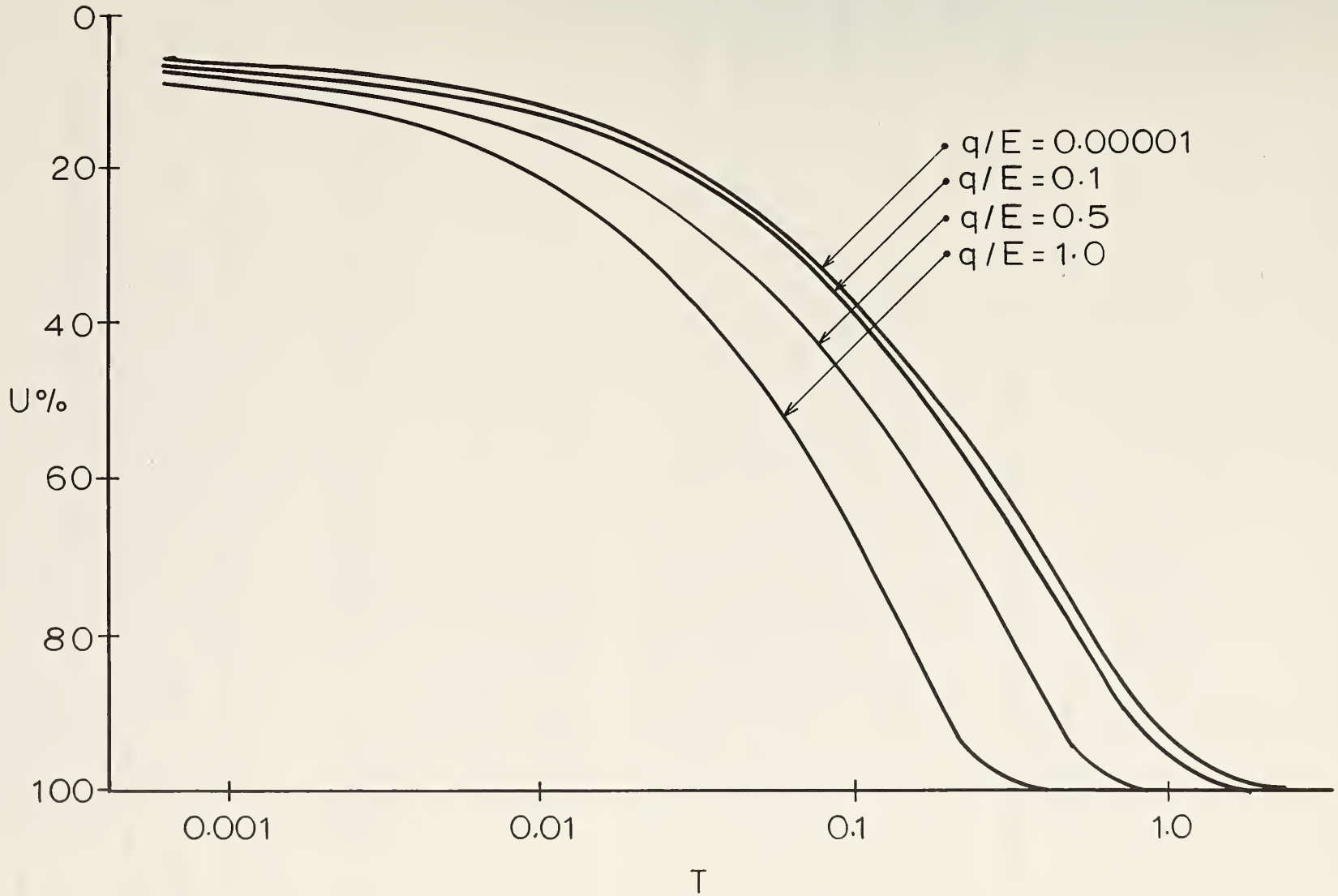

Figure 5.1: Effect of Large Strains on One-Dimensional Consolidation

Chapter 6

CONSOLIDATION ANALYSES OF TUNNELS

6.1 INTRODUCTION

Tunnels are constructed in many different shapes and sizes, and they may pass through an even greater variety of soil profiles. When analysing a proposed tunnel, these site characteristics would be used in defining the finite element mesh and soil properties. For the purpose of gaining an understanding of the behavior of tunnels due to consolidation, a typical large diameter tunnel in a homogeneous clay layer was analysed. Parametric studies were then performed to determine the effects on the behavior due to:

1. Stiffness of the liner
2. Size of the tail void
3. Soil strength
4. Permeability of the soil
5. Initial pore pressures set up by outward shoving at the tunnel face.

This is by no means a complete list of the factors influencing the behavior of a tunnel, but it does serve to cover some of the more important ones. The last item is directed at the question of effects of the initial pore pressures created by a pressurized face shield, as noted in Chapter II.

6.2 PROBLEM DEFINITION

6.2.1 Geometry

The finite element mesh used is shown in Figure 6.1. The soil is modelled using 66 eight-noded isoparametric quadrilateral elements with pore pressure degrees of freedom at the corner nodal points (Q8P4). The tunnel liner is modelled using 8 eight-noded isoparametric quadrilateral elements (Q8).

The tunnel is located at a depth of 44 feet (13.5 m) to the springline. A rigid base is assumed at a depth of 88 feet (27 m) below the surface. The outside diameter of the tunnel is 26 feet (8 m). The finite element mesh extends horizontally to a distance equal to 11 radii from the center of the tunnel. This will ensure that the boundary has an insignificant effect on the results.

The concrete liner is assumed to be 20 inches (0.5 m) in thickness, a value typical of that used in practice for this size tunnel.

6.2.2 Soil Conditions

The soil is assumed to be a homogeneous clay layer with shear strength increasing with depth as shown in Figure 6.2. A desiccated layer with a uniform shear strength is assumed near the surface. The parameters used are typical of Boston Blue Clay. This soil was simulated since it is typical of soft clays in urban areas and since there is an abundance of data on it.

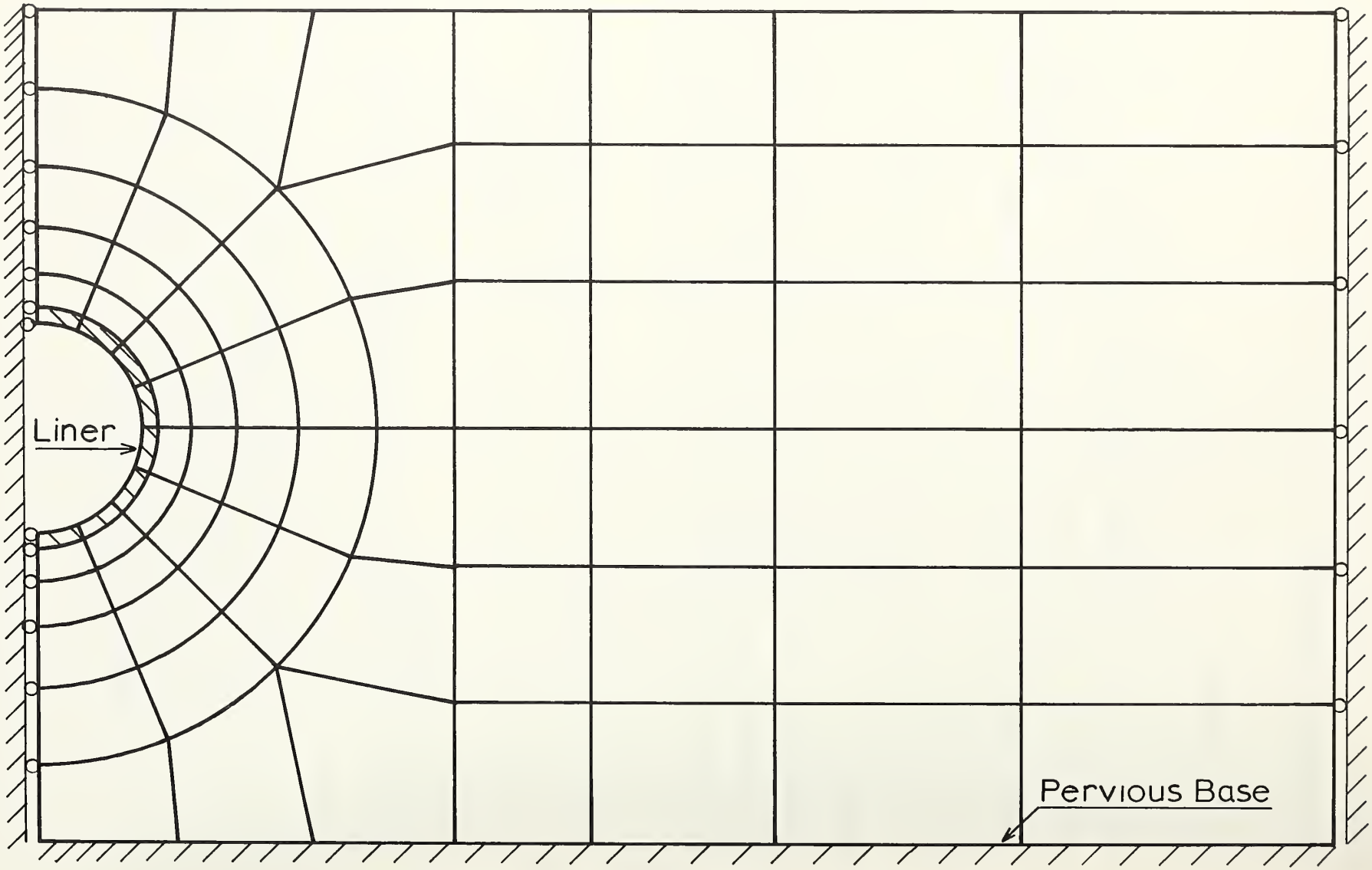

Figure 6.1: Finite Element Mesh for Tunnel Analyses

Two shear strength profiles below the desiccated crust were used; the first corresponds to an overconsolidation ratio, OCR, of one and the second to an OCR of two. The coefficient of lateral earth pressure at rest, k_0, and the ratio of the shear strength to the effective vertical stress are dependent on the OCR and are given in Table 6.1, based upon results reported by Ladd et al. (1977).

Parameters for the Cam Clay model were obtained from the reference by Carter, Randolph and Wroth (1979), who had analysed Boston Blue Clay for an embankment problem using the Cambridge model. These parameters are given in Table 6.2. The soil is assigned a density of 115 pcf (18 kN/m^3).

When air pressure is not used, the overstress factor, OFS, may be defined as

$$OFS = \frac{p_z}{c_u} \tag{6.1}$$

where p_z is the total vertical insitu pressure at a depth equal to the depth of the springline.

The OFS has been used in practice as a parameter for predicting the performance of a tunnel, Broms and Bennermark (1967). When OCR=1, the value of OFS is 7.3, and some difficulty may be expected during construction. This could include, for example, a tendency of the shield to tilt. When OCR=2, the value of OFS is 4.9, in which case the tunnel should be constructed without unusual difficulties.

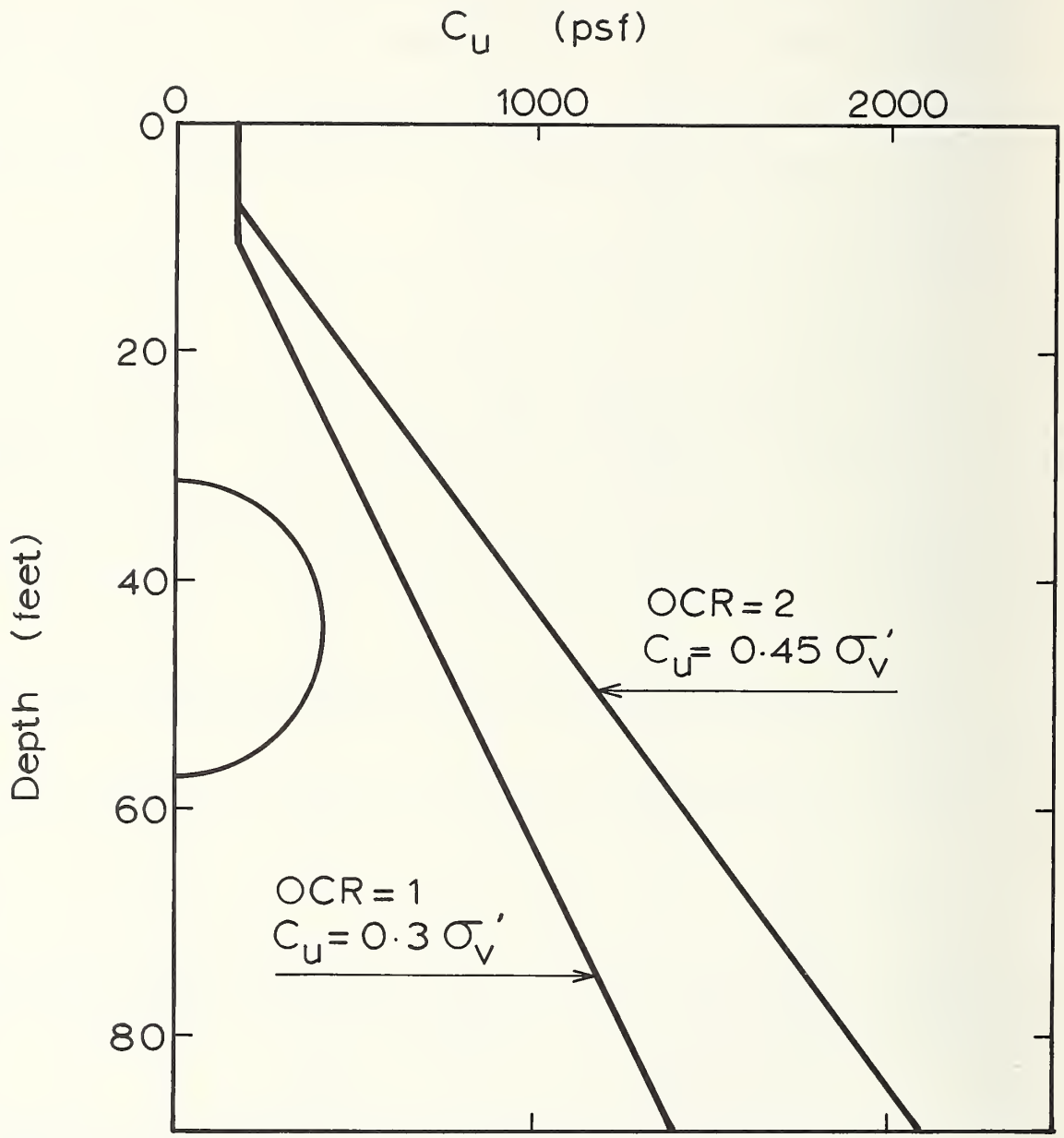

Figure 6.2: Shear Strength Versus Depth

TABLE 6.1

OCR Dependent Parameters

	OCR = 1	OCR = 2
k_0	0.55	0.8
c_u/σ_v'	0.3	0.45

TABLE 6.2

Boston Blue Clay Parameters for Cam Clay Model

κ	0.03
λ	0.15
e_{cs}	1.74
M	1.20
G/c_u	74

The soil was assigned an isotropic permeabilty of 5 x 10^{-7} ft/sec (1.5 x 10^{-5} cm/sec). The actual value chosen is unimportant since it has an effect of just scaling the time dependent results. Results involving actual times, rather than non-dimensional times, will be given in Section 6.7.

6.2.3 Boundary and Initial Conditions

The water table is assumed to be at the surface. Drainage is allowed to occur at the surface and at the base. Thus, the base represents a dense sand layer or permeable bedrock. The tunnel liner is

assumed to be impervious. This may be considered true provided the permeability of the liner is two orders of magnitude lower than the surrounding soil, Fitzpatrick (1980). It is difficult to achieve this degree of waterproofing in a liner, but it is possible with the aid of careful grouting techniques.

Initially there is a hydrostatic pore pressure distribution. The at-rest stresses in the soil are calculated by a simulated gravity turn-on with the appropriate value of k_0.

6.2.4 Liner properties

A concrete tunnel liner is used with a density of 125 pcf (20 kN/m^3). The weight of a concrete liner is a significant percentage of the weight of soil removed from a tunnel during excavation, and hence it must be included in the analysis. The stiffness is calculated using a value of 3000 ksi (20700 kPa) for the Young's modulus of concrete. The liner is assumed to consist of continuous elements; use of the 3000 ksi modulus in this model simulates the effect of a cast-in-place liner. If precast segments were used, their ring stiffness would be less than that of a continuous liner even if they were the same thickness because of the effects of the numerous bolted connections. In order to approximate the reduction in stiffness due to the bolting of the segments, the modulus is reduced by dividing by a 'liner stiffness reduction factor'. In Section 6.4 four different liner stiffness reduction factors were investigated. A reduction factor of 40 was chosen as best representing a typical segmented liner. The shortening of the vertical diameter of the tunnel liner was used as a parameter in making the choice. Values

of this parameter from the finite element analyses were compared with those reported by Deere et al (1969).

The permeability of a segmented liner is typically greater than that of a cast-in-place liner. However, a successful grouting program should be capable of making up the difference.

6.2.5 Construction Performance

The construction performance for the cases with no initial excess pore pressures is modelled by varying the tail void gap. Thus, a small gap represents good control of the shield. Two different values of this tail void gap were used: 2.0 and 3.6 inches (50 and 90 mm). These tail void values represent the distance from the soil as it leaves the tail of the shield to the outside of the liner at the crown. This gap is not uniform. For example, when the crown gap is 3.6 inches, the springline gap is 2.0 inches (50 mm) and the invert gap is 0.8 inches (20 mm). The soil closes in at different rates around the liner. Contact with the liner is assumed to take place at the same time for each point around the liner. In practice this may be the time when the grouting is injected.

In the case analyzed to determine the effects of initial excess pore pressures, it is assumed that a pressurized face shield is used which has caused an initial outward expansion of the soil away from the shield face. This outward expansion actually occurs out of the plane of the tunnel cross-section being analyzed and thus cannot be exactly simulated with the present plane strain approach. In lieu of an exact model, the

initial pore pressures for this analysis are created by an expansion of the tunnel opening in the plane of the finite element mesh, as described subsequently in this chapter.

6.2.6 Summary

Three different parameters were varied in the finite element analyses. Table 6.3 shows the parameters used for the six analyses.

TABLE 6.3

Parameters Used in Finite Element Tunnel Analyses

Run Number	Liner Stiffness Reduction Factor	Crown Tail Void Gap (inches)	OCR	Initial Excess P.P.
1	40	3.6	1	No
2	100	2.0	1	No
3	40	2.0	1	No
4	20	2.0	1	No
5	10	2.0	1	No
6	40	2.0	2	No
7	40	3.2	1	Yes

6.3 BEHAVIOR OF A TYPICAL TUNNEL

The results shown in this section were obtained using an OCR of one for the soil and a tail void gap of 3.6 inches (90 mm) from the liner to the crown of the tunnel. A liner stiffness reduction factor of 40 was used.

The analysis was performed using 63 time increments in the finite element program. Loads may be applied as required during any time increment, however, the incremental time must not be zero in any increment.

Increment 0 corresponds to the initial conditions with at-rest stresses in the soil. The equivalent nodal loads necessary to simulate the excavation of the tunnel are applied during increments 1 through 40. The incremental time for these 40 increments is kept very small to ensure undrained behavior. After increment 15 the soil has closed the tail void and the liner is activated. The weight of the liner was included during increments 16 through 40. The construction of the tunnel is complete after increment 40. The large number of increments used are required because of the non-linear nature of the Cam clay model.

Consolidation was allowed to occur during increments 41 through 63. No loads were applied during this part of the analysis. The time increments are increased on a logarithmic scale, so that each time increment is approximately 1.6 times larger than the previous. Hence, the time increment increases by an order of magnitude every five increments. After increment 63 the excess pore pressures had dissipated.

In discussing the results, four particular stages of construction will be referred to:

1. Initial conditions prior to any construction.

2. When the tail void has closed, just before the liner is activated.

3. After all excavation forces have been applied, but before consolidation. This represents the end of construction.

4. Final conditions, after consolidation is completed.

6.3.1 Settlements

Surface settlement profiles before and after consolidation are shown in Figure 6.3. The maximum surface settlement occured above the tunnel crown as expected. This settlement was 2.08 inches (53 mm) before consolidation. This increased by 32 percent to 2.74 inches (70 mm) after consolidation.

Surface settlement profiles have been found in practice to approximate the error function, Schmidt (1969). For field data the surface settlement, s, at a horizontal distance, x, from the centerline of the tunnel is typically approximated by

$$s = s_{max} \exp\left(- \frac{x^2}{2i^2} \right) \tag{6.2}$$

where i is the horizontal distance from the centerline of the tunnel to the point of inflection of this bell-shaped curve. Plotting the logarithm of settlement against the square of the distance from the centerline of the tunnel the data should fit a straight line, and i may be obtained from the slope of the best-fit line. The width of the

settlement trough may be expressed in non-dimensional form as i/a, where a is the tunnel radius.

The error function is plotted in Figure 6.4 for the surface profiles both before and after consolidation. The data may be seen to fit a straight line very well for both cases. The width of the settlement trough increases from 2.2 before consolidation to 3.1 after consolidation. This confirms that settlements are more widespread as a result of consolidation, Peck (1969).

The volume of the settlement trough, V_s, may be conveniently obtained from

$$V_s = 2.5\ i\ s_{max} \tag{6.3}$$

This is usually expressed as a percentage of the tunnel opening

$$v_s = \frac{V_s}{\pi a^2} \times 100\% \tag{6.4}$$

The volume of the settlement trough was found to be 2.3 percent prior to consolidation. This increased to 4.3 percent after consolidation, showing the effect of consolidation to be significant. Results of the error function analysis will be compared with values obtained with a different soil strength and field data in Section 6.5.

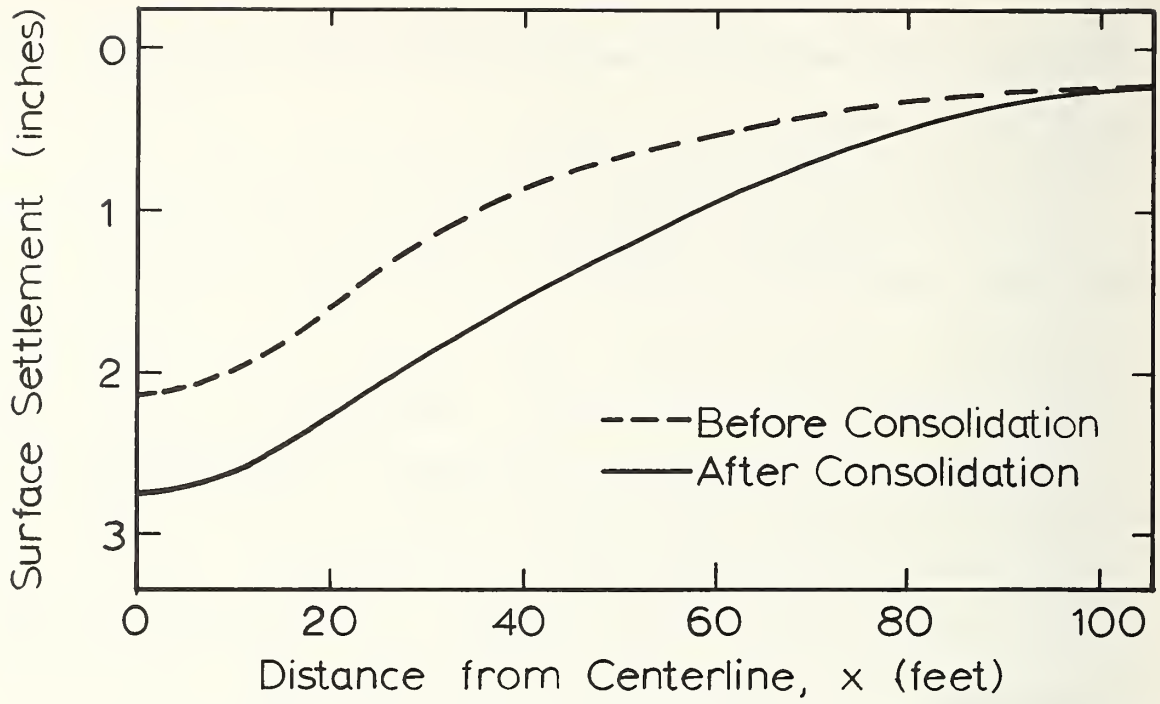

Figure 6.3: Typical Surface Settlement Profiles

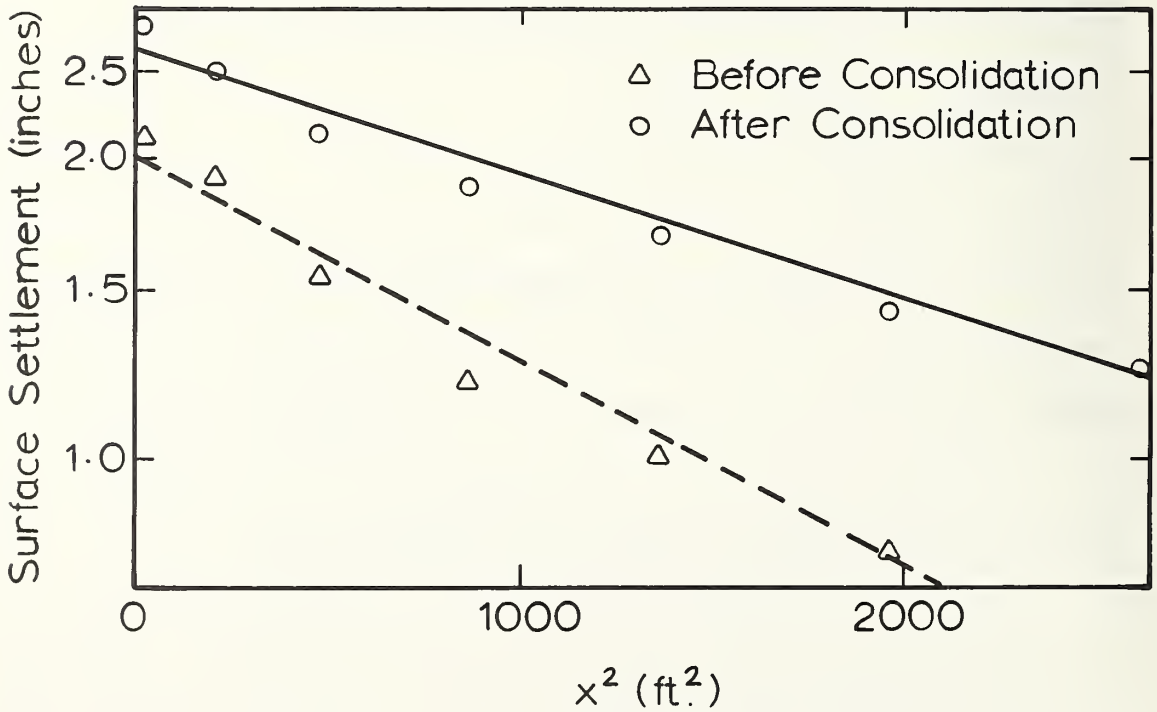

Figure 6.4: Surface Settlements Plotted as an Error Function

Displaced mesh plots before and after consolidation are shown in Figure 6.5. The displacements are scaled by a factor of 30. Before consolidation there is a general movement of the soil towards the tunnel opening, and the springline of the tunnel settles. As consolidation takes place, there is a continued movement of soil above and below the tunnel towards the opening. However, the tunnel undergoes continued ovalization which pushes the soil outward at the springline. The springline also rises to its original level due to the dissipation of negative excess pore pressures below the invert.

For one-dimensional consolidation the degree of consolidation may be simply given as the compression at time T divided by the final compression. However, this definition is not satisfactory when both positive and negative excess pore pressures are dissipating simultaneously because they have a cancelling effect on each other. The excess pore pressure dissipation constant, U_e, is introduced where

$$U_e = \int_A |u_e| \, dA \tag{6.5}$$

Thus, the degree of consolidation may be defined as

$$U = 1 - \frac{U_e}{(U_e)_{max}} \tag{6.6}$$

A non-dimensional time parameter, T, is also introduced

$$T = \frac{kGt}{H^2 \gamma_w} \tag{6.7}$$

where k is the permeability of the soil,

G is the shear modulus at the depth of the springline,

t is the time used in the finite element program,

H is a measure of the drainage distance.

In this case the drainage distance is equal to the depth to the springline.

A plot of U versus T is shown in Figure 6.6. The shape of this curve is similar to curves for other consolidation problems. Most of the consolidation takes place between T=0.005 and T=0.1.

The maximum surface settlement is plotted against T in Figure 6.7. The surface settlement appears delayed when compared to the U versus T curve. This is due to the rapid dissipation of negative excess pore pressures which exist below the invert and have a short drainage path to the permeable base. These negative excess pore pressures do not contribute to the settlement, but do contribute to the degree of consolidation, U. On the other hand, the positive excess pore pressures near the springline have a long drainage path, so that the resulting settlement is delayed.

6.3.2 Excess Pore Pressures

The predicted distribution of excess pore pressures is shown in Figure 6.8 for two stages of construction. The first stage is just prior to tail void closure and the second stage is at the end of construction, before consolidation. The maximum absolute values of these excess pore pressures near three locations are shown in Table 6.4.

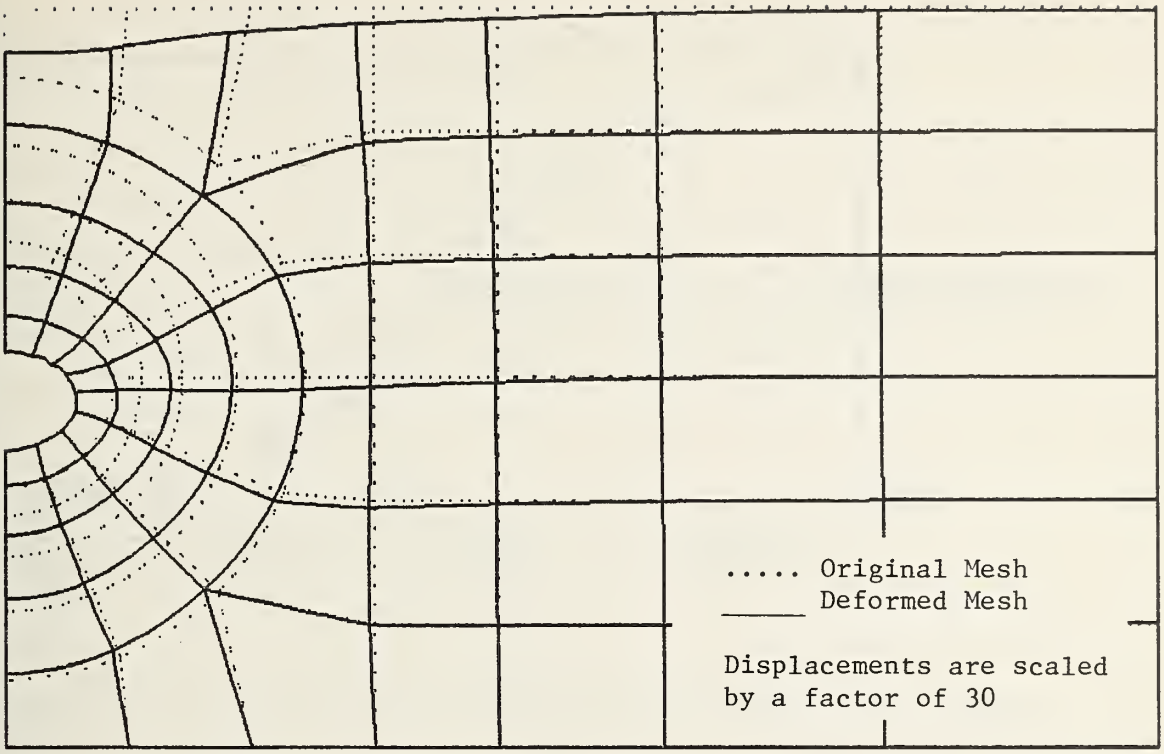

(a) Before Consolidation

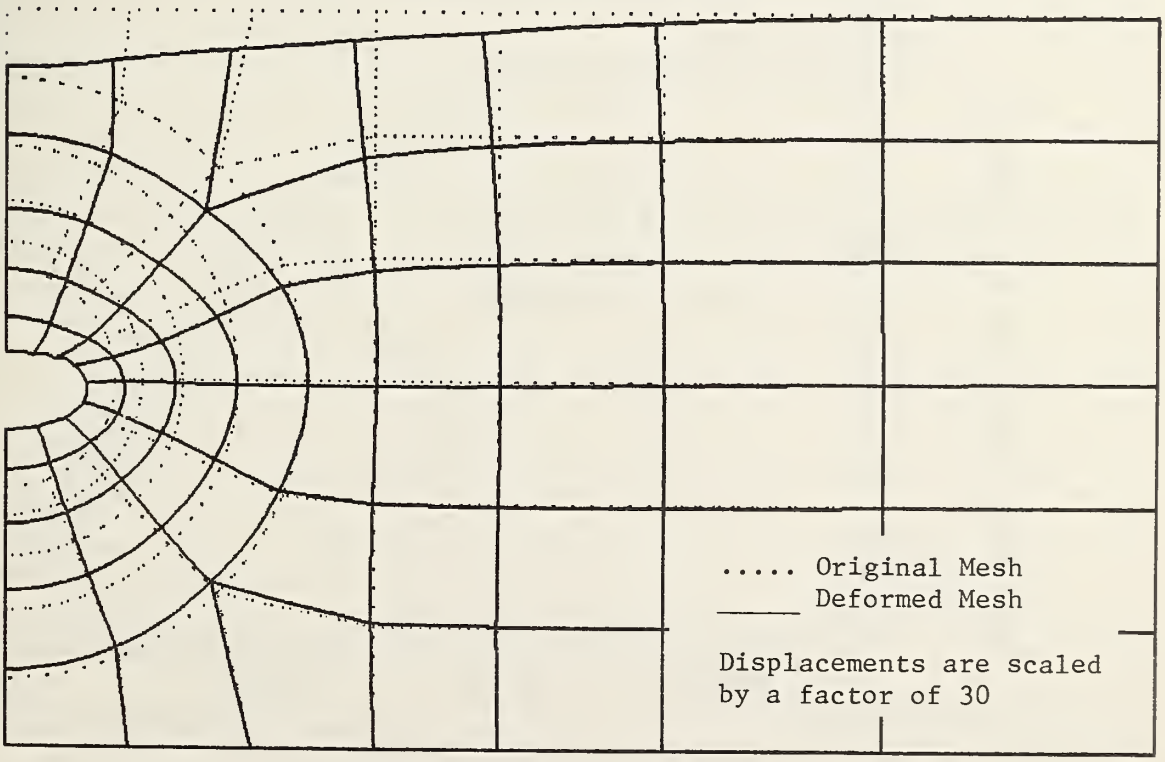

(b) After Consolidation

Figure 6.5: Displaced Mesh Plots for a Typical Tunnel

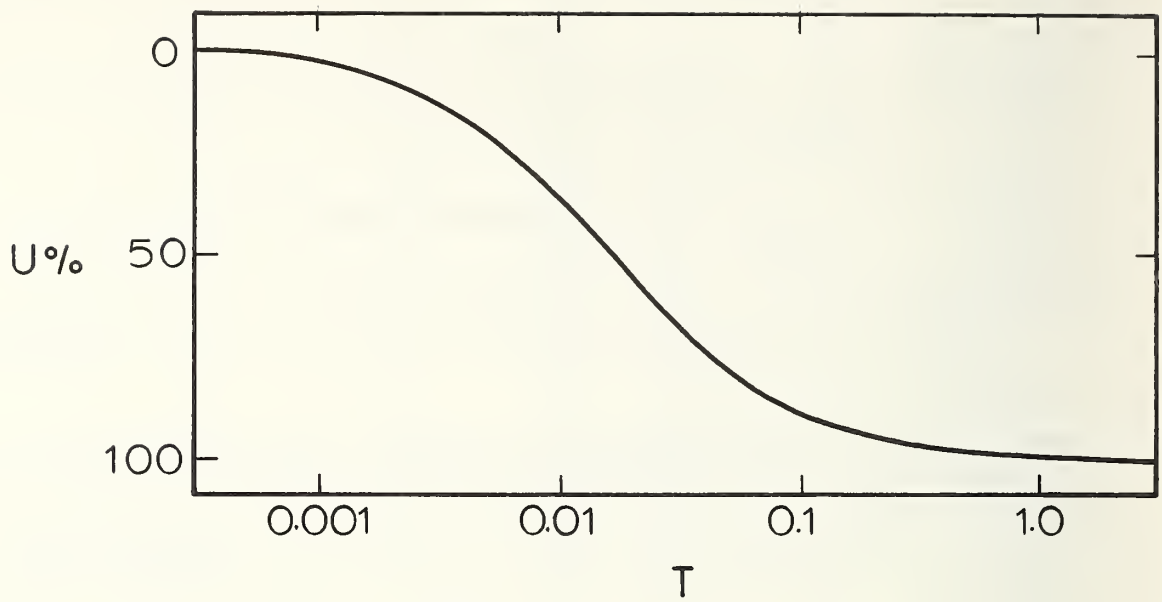

Figure 6.6: Degree of Consolidation Versus Time for a Typical Tunnel

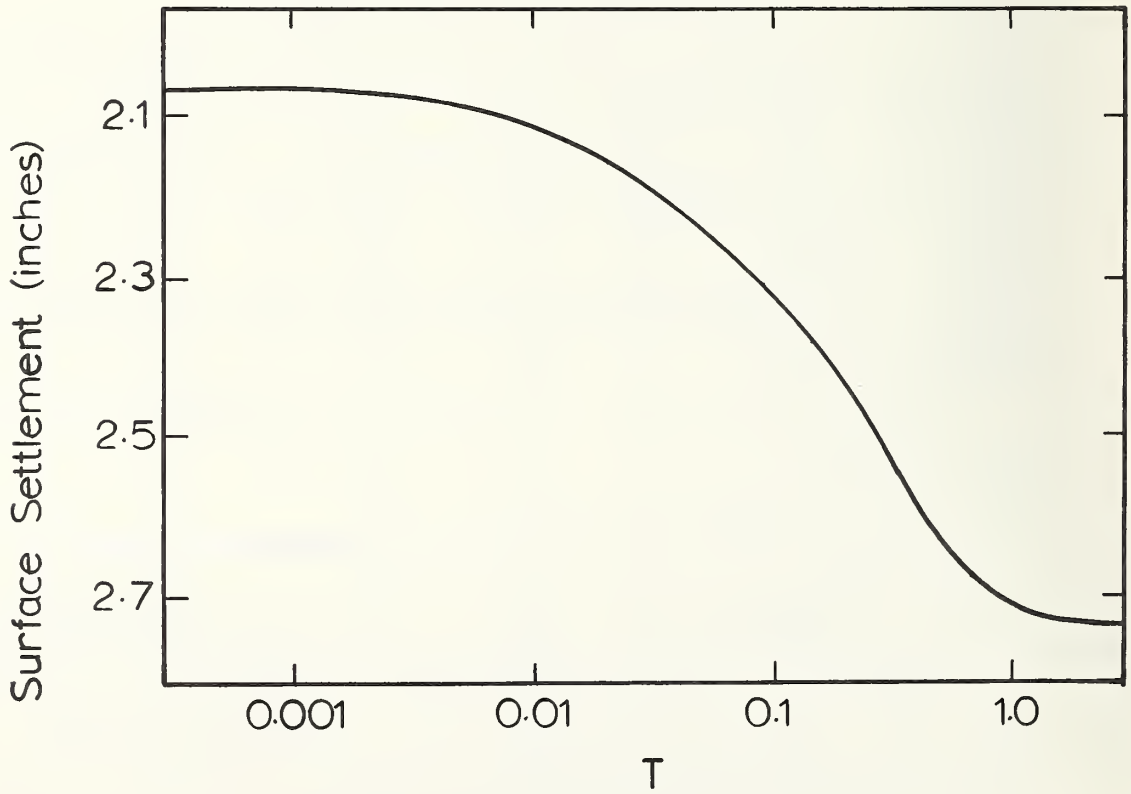

Figure 6.7: Maximum Surface Settlement Versus Time

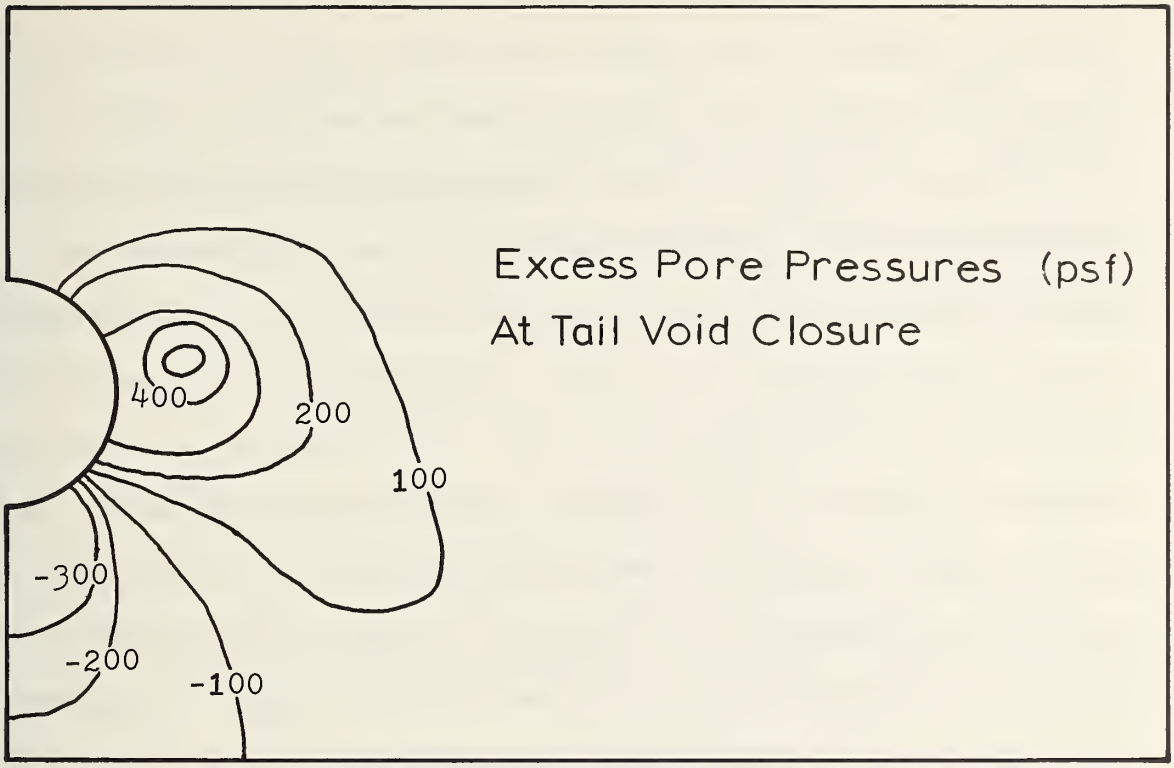

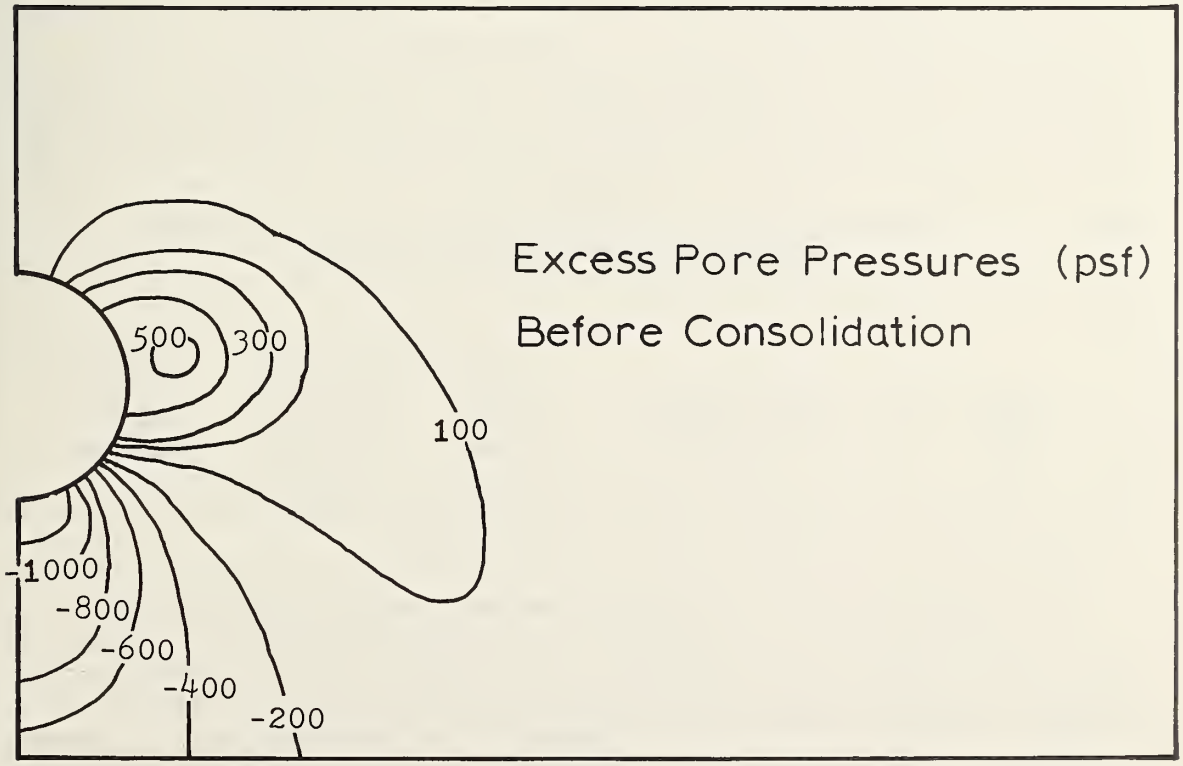

Figure 6.8: Excess Pore Pressure Contours for a Typical Tunnel

The pore pressure contours show two distinct areas. The first is a large area of positive excess pore pressures extending outward from the springline. This bulb of positive excess pore pressures grows slightly from the first stage of construction to the end of construction. The second area lies beneath the invert and consists of very high negative excess pore pressures. Although the extent of this area remains constant as construction takes place, the magnitude of these pore pressures increases significantly. The pore pressures at the crown remain almost constant. The maximum excess pore pressure at the springline corresponds to a 20 percent rise in the hydrostatic pore pressure, while the excess pore pressure at the invert corresponds to a 39 percent drop in the hydrostatic pore pressure.

TABLE 6.4

Excess Pore Pressures Near Tunnel

	Crown	Springline	Invert
Before Liner Installation	10 psf	509 psf	-397 psf
After Liner Installation	-10 psf	549 psf	-1398 psf

The prediction of the negative excess pore pressures in the crown and invert is due to the expansion of the soil into the tunnel opening. Clough and Schmidt (1977) have predicted such behavior based on general principles. The very high values of negative pore pressure predicted in the soil below the invert are in part due to the presence of the

underlying rigid base. This boundary condition creates a situation where the soil is restrained on the lower side while it tries to move into the opening on the upper side, resulting in a stretching effect. The positive pore pressures predicted at the springline are generated because this area is subject to an increase in both shear and normal stress as the tunnel is opened.

6.3.3 Soil Pressures Acting on the Liner

The in-situ stress distribution at the location of a lining prior to the excavation of a tunnel is elliptical. The pressure at the imaginary crown is γz, while at the springline it is $k_0 \gamma z$. If the tunnel is excavated and a perfectly flexible liner installed, the liner will deform until equilibrium is reached. The soil pressure distribution acting on a circular liner will become circular. Direct compressive stresses will exist in the liner and there will be no bending stresses. On the other hand, if a rigid liner were to be installed, the soil pressures acting on the liner would remain unchanged from the in-situ state.

The soil pressures acting on the liner before and after consolidation are shown in Figure 6.9. The in-situ stress state is also shown for comparison. All pressures have been normalized by dividing by the vertical in-situ stress at the springline. It can be seen that the elliptical in-situ distribution becomes more circular after the liner is installed. This behavior is in agreement with Peck's (1969) philosophy, outlined above. The distribution does not become completely circular because the tunnel liner is not perfectly flexible. Thus, equilibrium is maintained by the bending stresses in the liner.

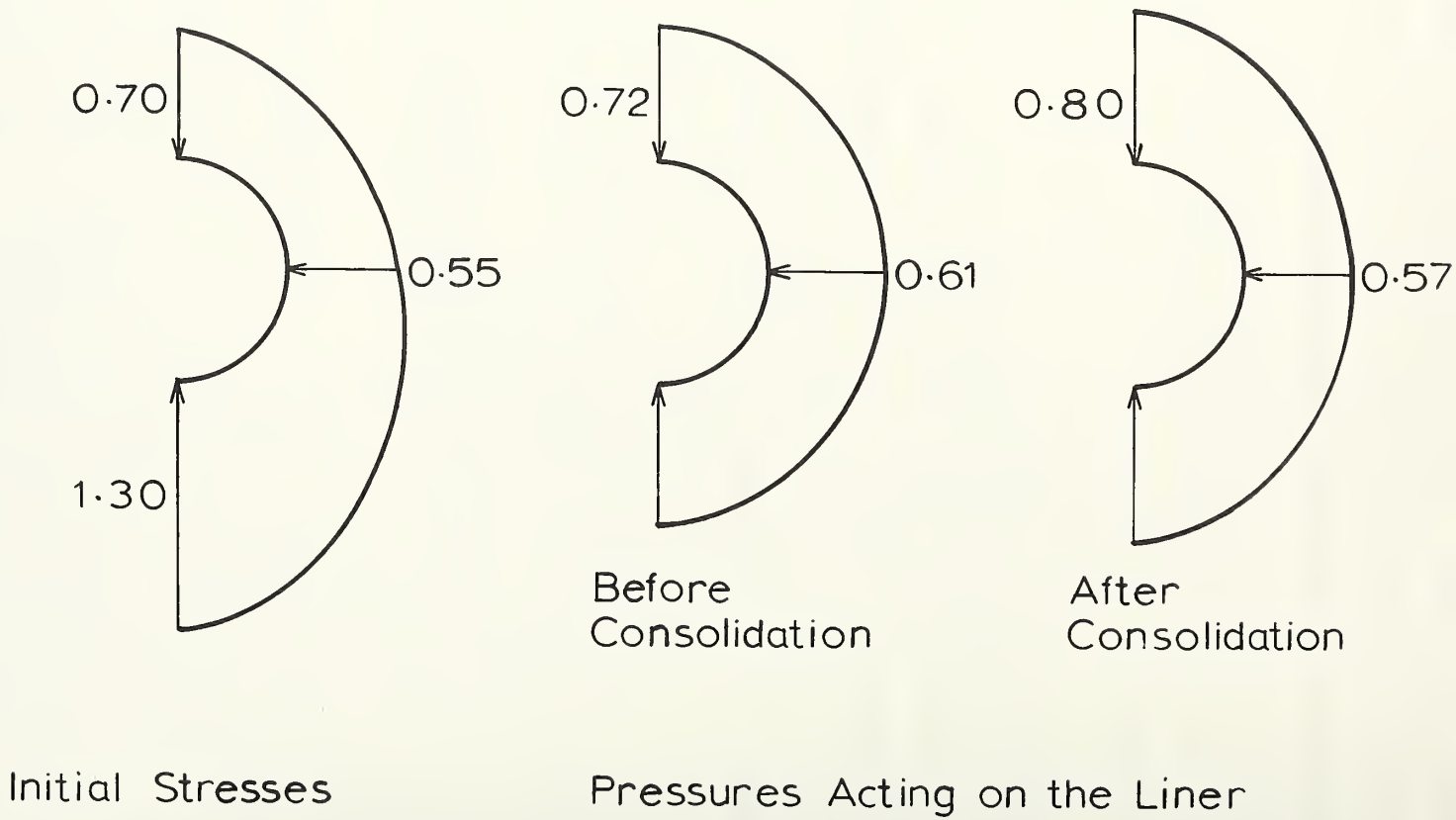

Figure 6.9: Soil Stresses Acting on a Typical Liner

During consolidation, the excess pore pressures near the springline decay, reducing the horizontal pressure acting on the liner. The decay of negative excess pore pressures near the invert causes an increase in vertical pressure on the liner. Thus, the distribution of soil pressure acting on the liner becomes more elliptical as consolidation proceeds.

The average soil pressure acting on the liner is found to increase by 3.1 percent during the consolidation period. Much larger increases with time have been recorded in the field, Peck (1969). There, the soil pressure acting on the liner is often calculated from strain gauges which are attached to the liner. These gauges record the increase in the bending stress as well as the direct stress. It is possible that the average stress may remain constant while the bending stress increases.

The elliptical distribution of soil pressure on the liner may be approximated by two terms from a Fourier series:

$$p = p_0 + p_2 \cos 2\theta \tag{6.8}$$

Generally the average pressure, p_0, is much larger than the other term, p_2. If we assume that the liner behaves as a thin shell with the radius, r, much greater than the thickness, t, then the p_0 term produces a direct compressive stress, given by

$$\sigma_d = \frac{p_0 r}{t} \tag{6.9}$$

No bending stress is produced by this term. The maximum bending stress produced by the p_z term may be obtained from the Novozhilov shell equations, and is given by

$$\sigma_b = \frac{2p_z r^2}{t^2} \tag{6.10}$$

The direct stress for the p_z term is small compared to the bending stress.

The bending component, p_z, was found to more than double during consolidation, as shown in Figure 6.10. This phenomenum is one explanation for the field observations.

The horizontal diameters of tunnel liners have been found to increase with time as consolidation takes place, Peck (1969). This effect may be predicted on the basis of the excess pore pressure distribution before consolidation, and is plotted as a percentage of the initial diameter versus the non-dimensional time parameter, T, in Figure 6.11. The increase falls within the range of those recorded in the field.

Increases in both liner pressures and liner spreading recorded in the field tend to be indefinite. If existing tunnels are to remain safe, however, these increases must eventually stop. The consolidation results shown in Figures 6.10 and 6.11 indicate that these increases do indeed die out. The fact that this has not been recorded in the field may be because tunnels are not monitored long enough after construction.

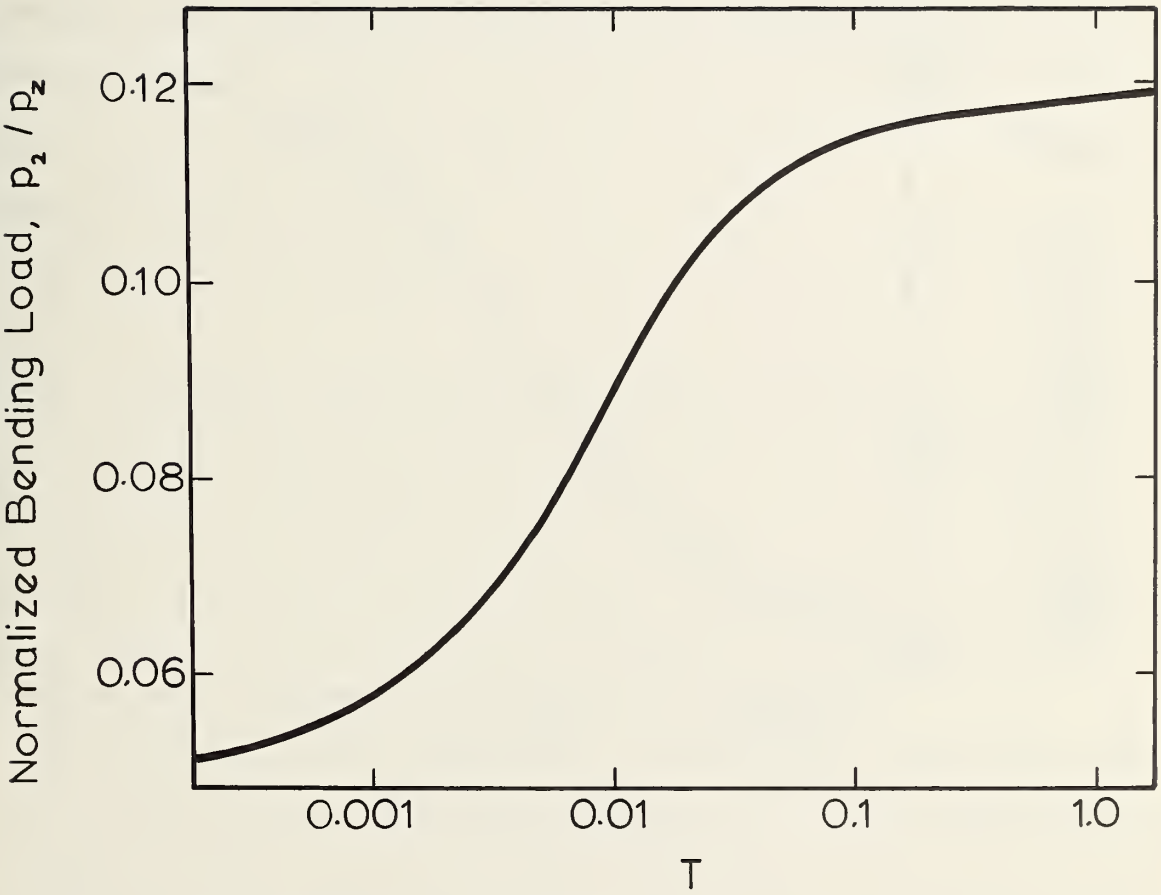

Figure 6.10: Bending Component of Pressure on a Liner Versus Time

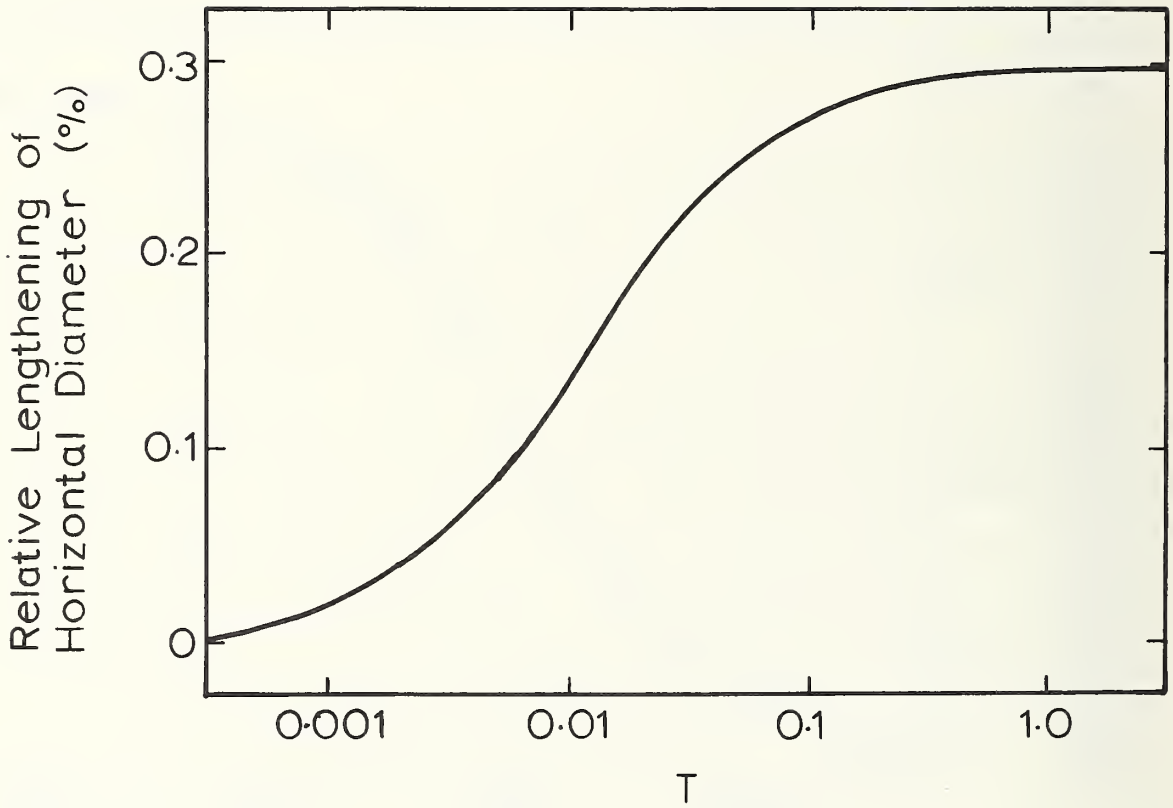

Figure 6.11: Typical Liner Spreading as a Function of Time

6.3.4 Soil Stresses

The stress paths undergone by soil elements close to the tunnel crown, springline and invert are shown in Figure 6.12. The effective stress paths are plotted using the mean effective stress, p', and the octahedral shear stress, q. The p' and q axes were chosen since the Cam clay model was used and since the effect of σ_2 is important. A basic reference line shown on this diagram is the critical state or failure envelope, defined as

$$q = Mp \tag{6.11}$$

Figure 6.12 shows that the soil near the springline moves towards failure during excavation and away from failure during consolidation. The soil near the invert behaves in an opposite manner, that is, it moves away from failure during excavation and towards failure during consolidation. The soil near the crown remains almost on the k_0 line.

Contour plots of the percentage of critical state reveal the areas moving towards failure. The situations before and after consolidation are shown in Figure 6.13. In the at-rest state prior to any soil removal, the percentage of critical state is 53. During consolidation the location in the soil that is nearest to failure moves from near the springline to near the invert.

Relative magnitudes of the principal stresses and their directions are shown before and after consolidation in Figure 6.14. For an unlined tunnel the major principal stresses would be aligned tangent to the tunnel for a soil element next to the tunnel wall.

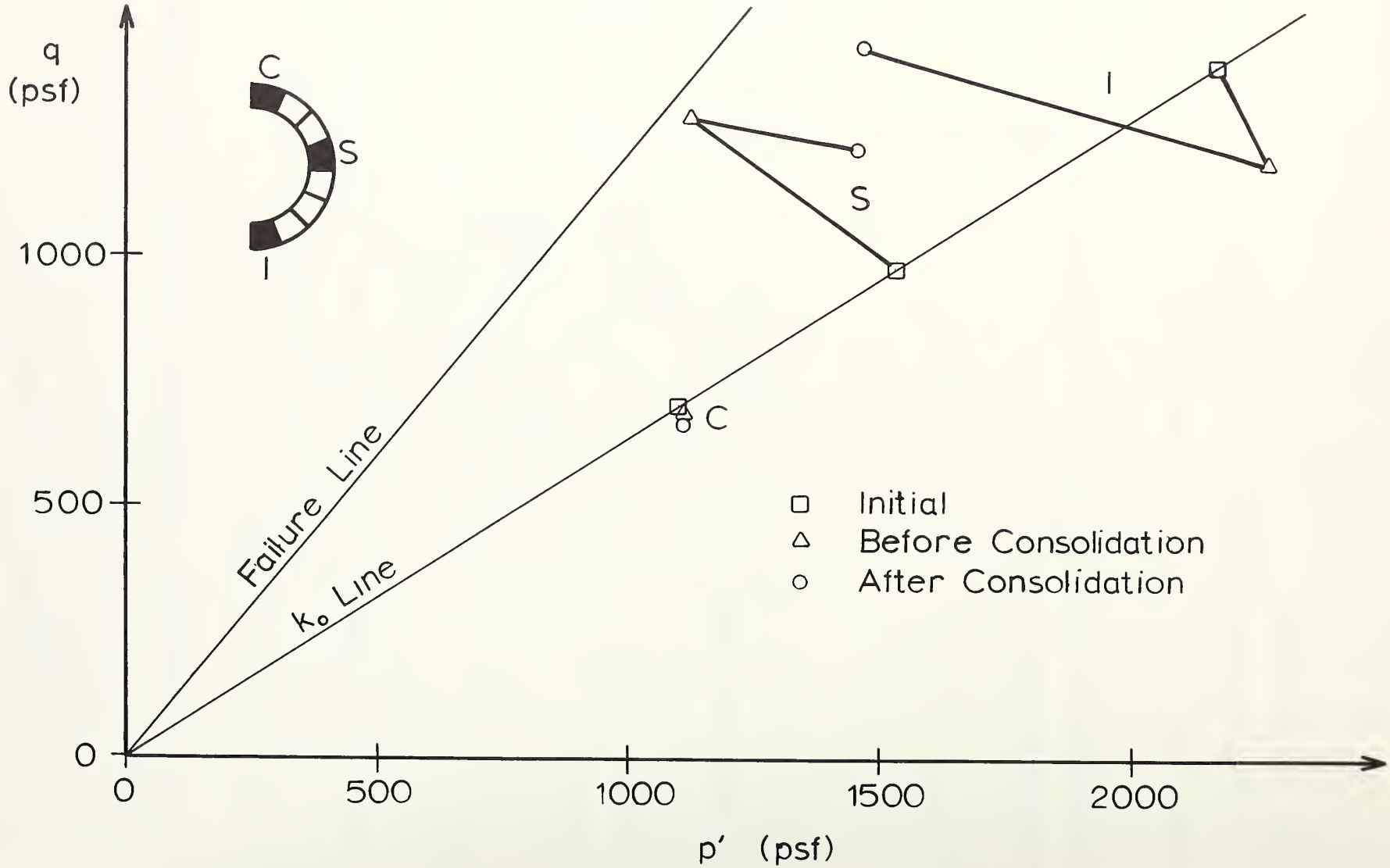

Figure 6.12: Typical Effective Stress Paths for Soil Close to the Liner

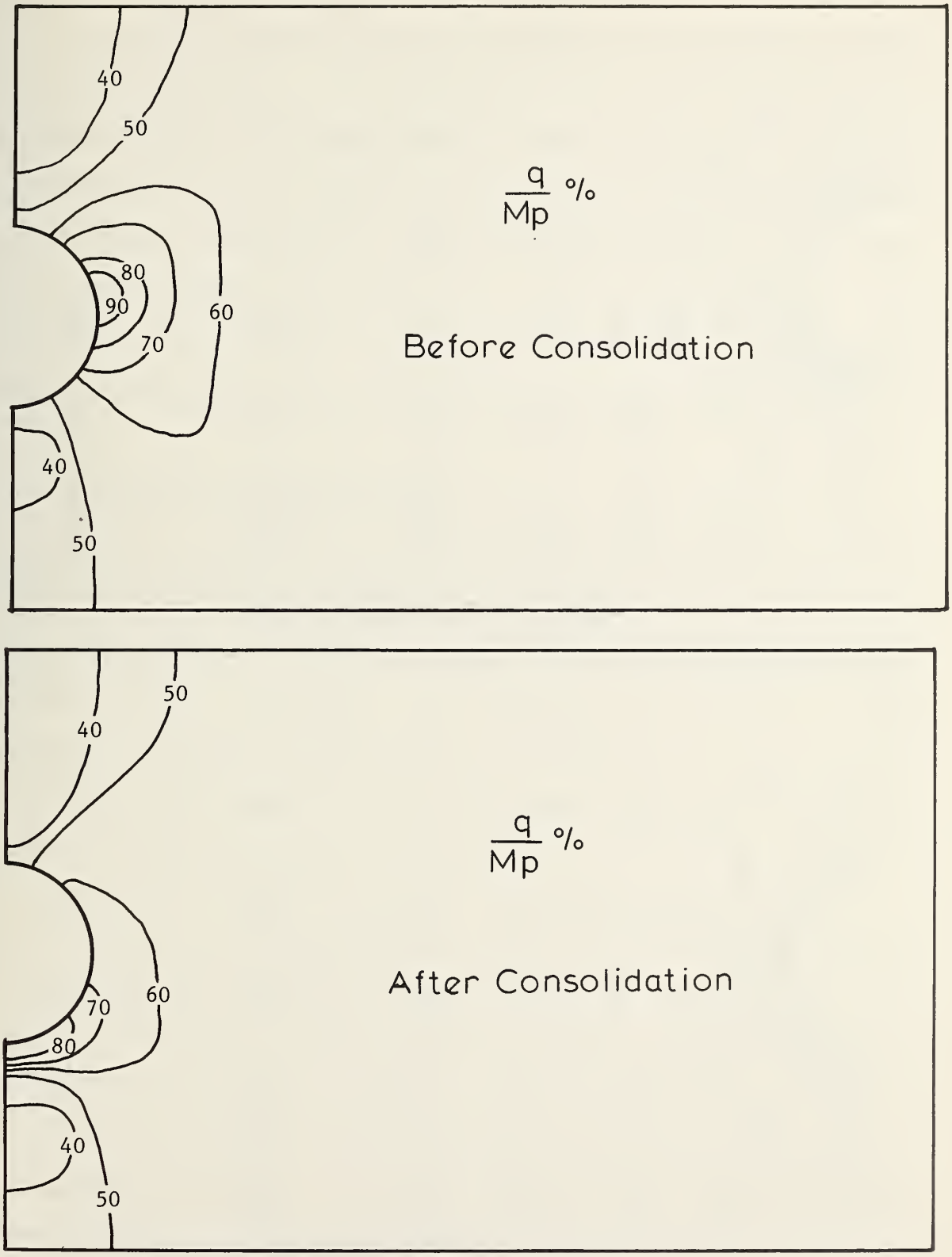

Figure 6.13: Percentage of Critical State Contours for a Typical Tunnel

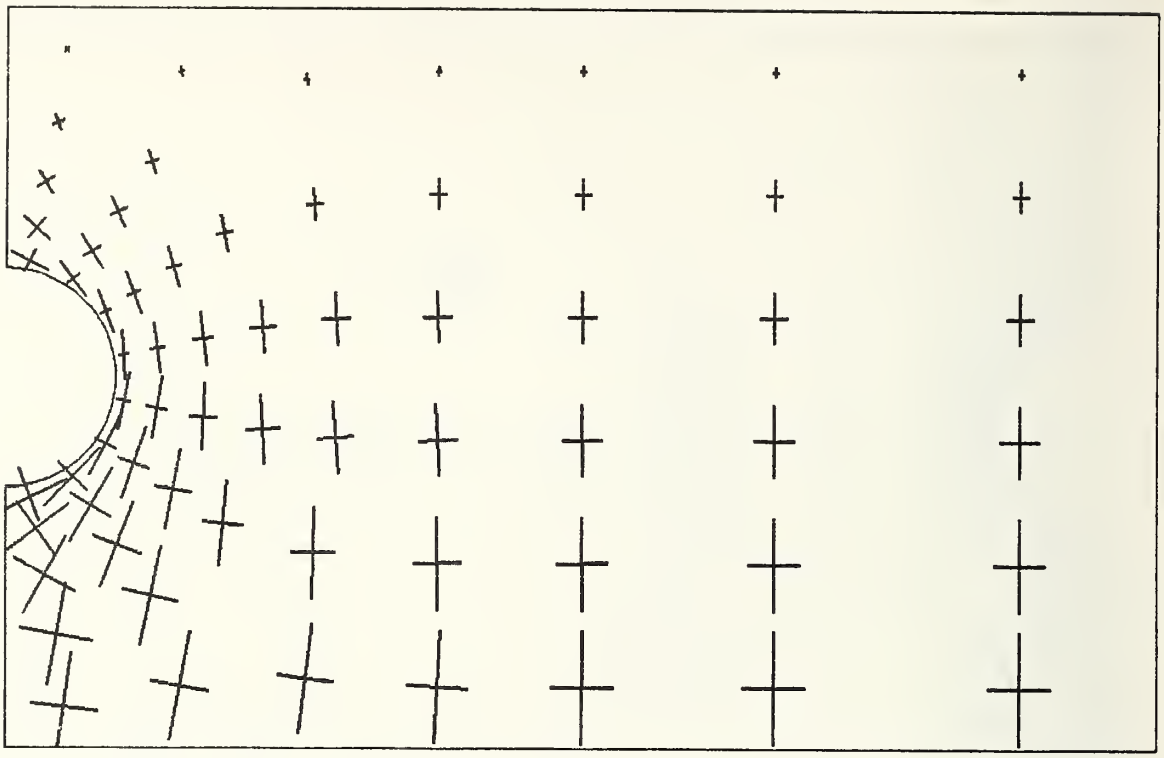

Before Consolidation

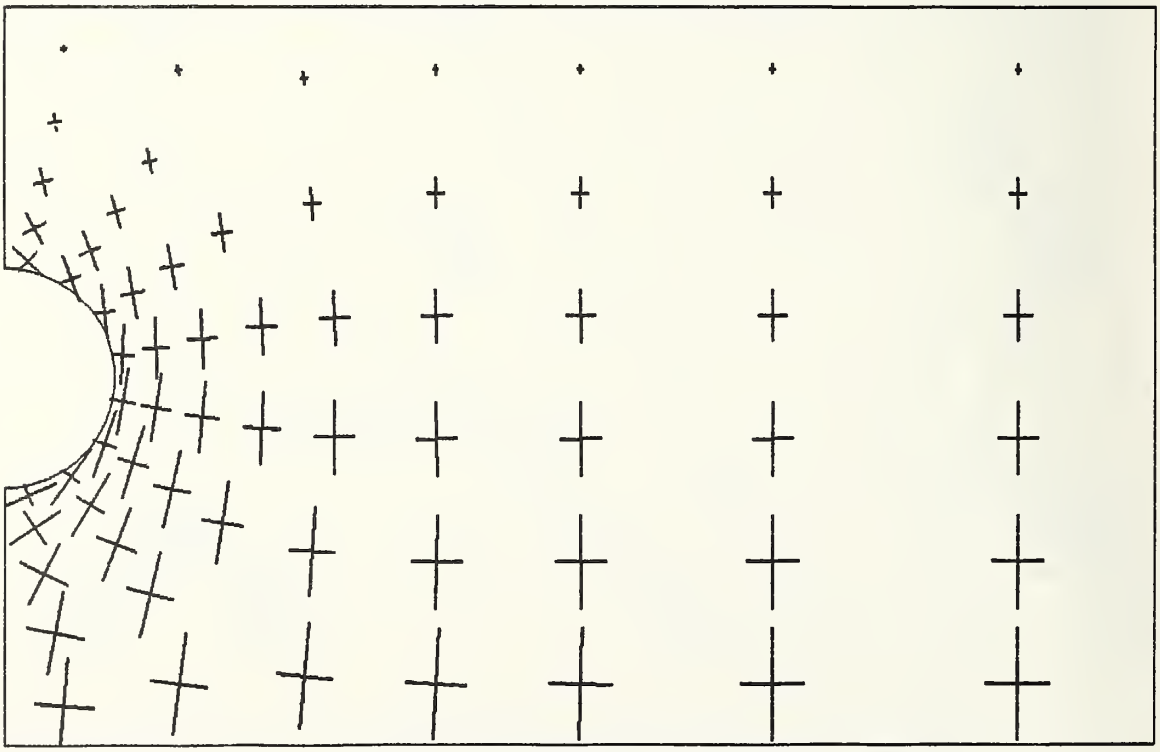

After Consolidation

Figure 6.14; Principal Stresses for a Typical Tunnel

In this case the stress component perpendicular to the tunnel wall is carried by the liner. It should be noted that the direct stress in a direction parallel to the axis of the tunnel, σ_z, is not always the intermediate principal stress, σ_2. For example, after the installation of the liner the stresses at a point near the crown were: σ_x=1336psf, σ_y=1261psf, σ_z=880psf and τ_{xy}=214psf. Thus, σ_z is actually σ_3. This emphasizes the importance of including σ_z in the finite element calculations, even during a plane strain analysis.

6.4 EFFECT OF THE LINER STIFFNESS

The liner used in the finite element program is continuous, while that used in the field is segmented. The bolted joints between segments act as hinges allowing greater movement. In order to simulate this more flexible liner, a reduction factor may be used to reduce the liner stiffness calculated for one which is continuous. A suitable liner stiffness may be chosen as the one which allows liner deformation similar to that observed in the field.

The effect of liner stiffness on tunnel behavior is investigated by varying the elastic modulus for the concrete liner. Four cases were studied with modulus reduction factors of 10, 20, 40 and 100. The liner became more flexible as the reduction factor was increased. Other basic parameters for the finite element computer runs were kept constant. The tail void gap was 2.0 inches (50 mm) and the soil was normally consolidated.

6.4.1 Settlements

Maximum surface settlements are shown for three stages of construction in Table 6.5. The maximum surface settlements before and after consolidation are plotted in Figure 6.15.

TABLE 6.5

Variation of Settlements with Liner Stiffness

Reduction Factor	Maximum Surface Settlement (inches)		
	At Tail Void Closure	Before Consolidation	After Consolidation
10	0.90	0.67	0.38
20	0.90	0.83	0.73
40	0.90	1.05	1.23
100	0.90	1.58	2.24

A flexible liner allows more movement near the tunnel. As a result, a larger zone of soil undergoes a change of stress. When this soil yields it is remolded. The larger the remolded zone, the greater is the extent of excess pore pressure buildup. Greater surface settlements are observed after consolidation for this case.

For very stiff liners the settlement actually gets reduced from the time the tail void is closed until the liner is installed. This result may be explained by examining the excavation procedure, equivalent nodal loads are applied to the nodes on the tunnel wall to simulate the excavation. These loads act in an inward direction. After the crown

displacement is equal to the tail void gap, in this case 2.0 inches, the liner is installed. The remaining portion of the equivalent nodal loads is then applied to the outside of the liner. The downward load at the crown, however, is less than the upward load at the invert. Thus, there is a net upward force applied to the liner. When the liner is very stiff it acts as a rigid body, and so the upward force is translated into an upward movement at the surface. During the consolidation period the settlement is further reduced because of the dissipation of large areas of negative excess pore pressures.

In order to identify a reasonable reduction factor for modelling a typical tunnel, the shortening of the vertical diameter was compared to those reported by Deere et al. (1969). The percentage change in this diameter is given in Table 6.6, and on this basis a reduction factor of 40 was chosen as being the most representative.

TABLE 6.6

Effect of Liner Stiffness on Vertical Diameter Shortening

Reduction Factor	Vertical Diameter Shortening (%)
10	0.4
20	0.6
40	0.9
100	1.4

6.4.2 Liner Stresses

The p_0 and p_2 components of pressure before and after consolidation are shown in Table 6.7. The corresponding stresses are plotted in Figure 6.16. The direct stress increases very slightly with consolidation, while the bending stress approximately doubles.

Further, while the direct stress is only very slightly reduced by using a more flexible liner, the bending stress experiences a large reduction.

TABLE 6.7

Effect of Liner Stiffness on Liner Pressures

Reduction Factor	Pressures as a Percentage of the Vertical Insitu Stress at the Springline			
	Before Consolidation		After Consolidation	
	p_0	p_2	p_0	p_2
10	71.7	9.4	71.9	18.2
20	71.1	7.0	71.6	14.6
40	70.0	5.5	71.0	11.5
100	67.3	4.3	69.3	8.8

6.4.3 Excess Pore Pressures and Soil Stresses

The maximum excess pore pressure near the springline increases with an increase in the flexibility of the liner. These pore pressures are shown in Table 6.8. Their increase is due to the greater movement allowed by a flexible liner.

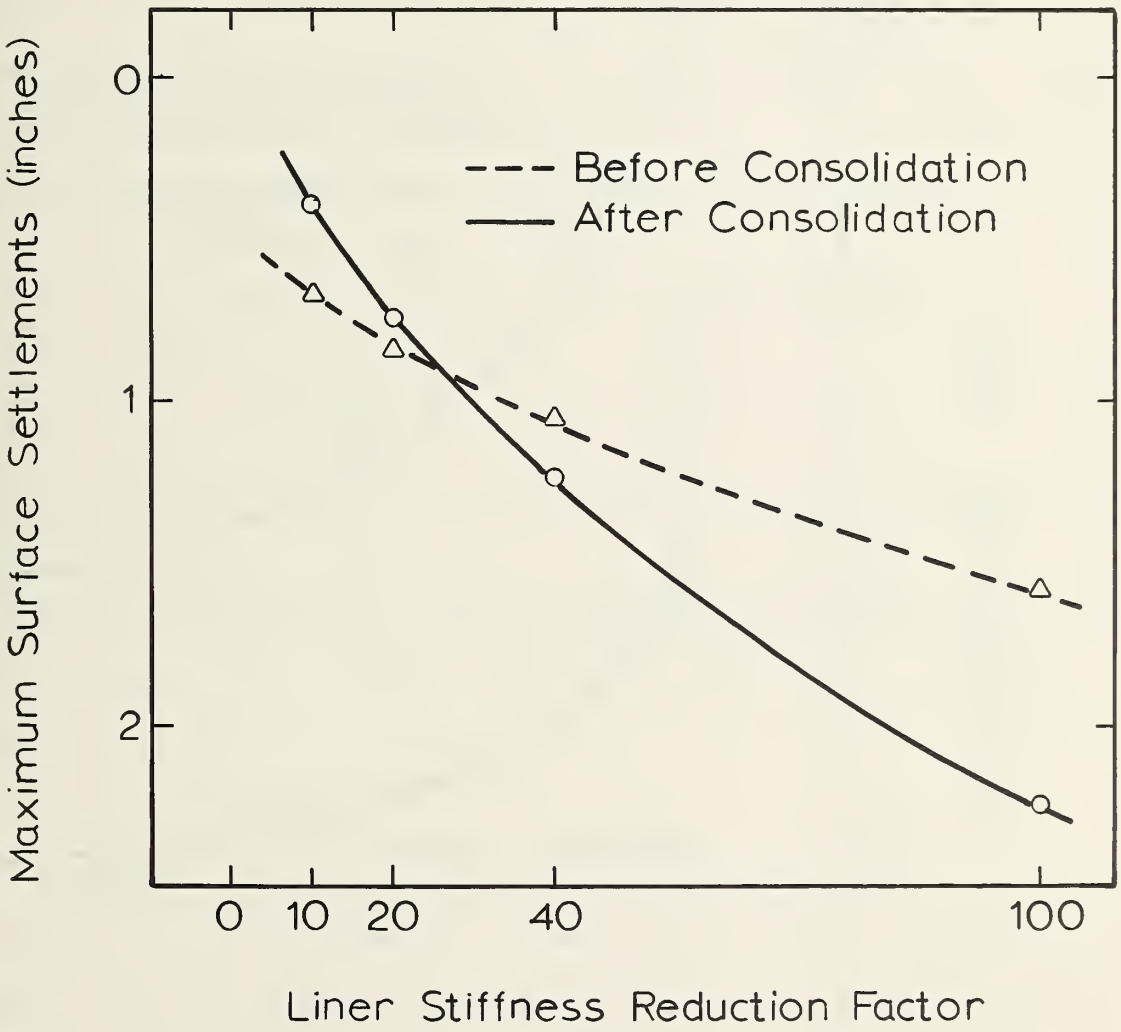

Figure 6.15: Effect of Liner Stiffness on Surface Settlement

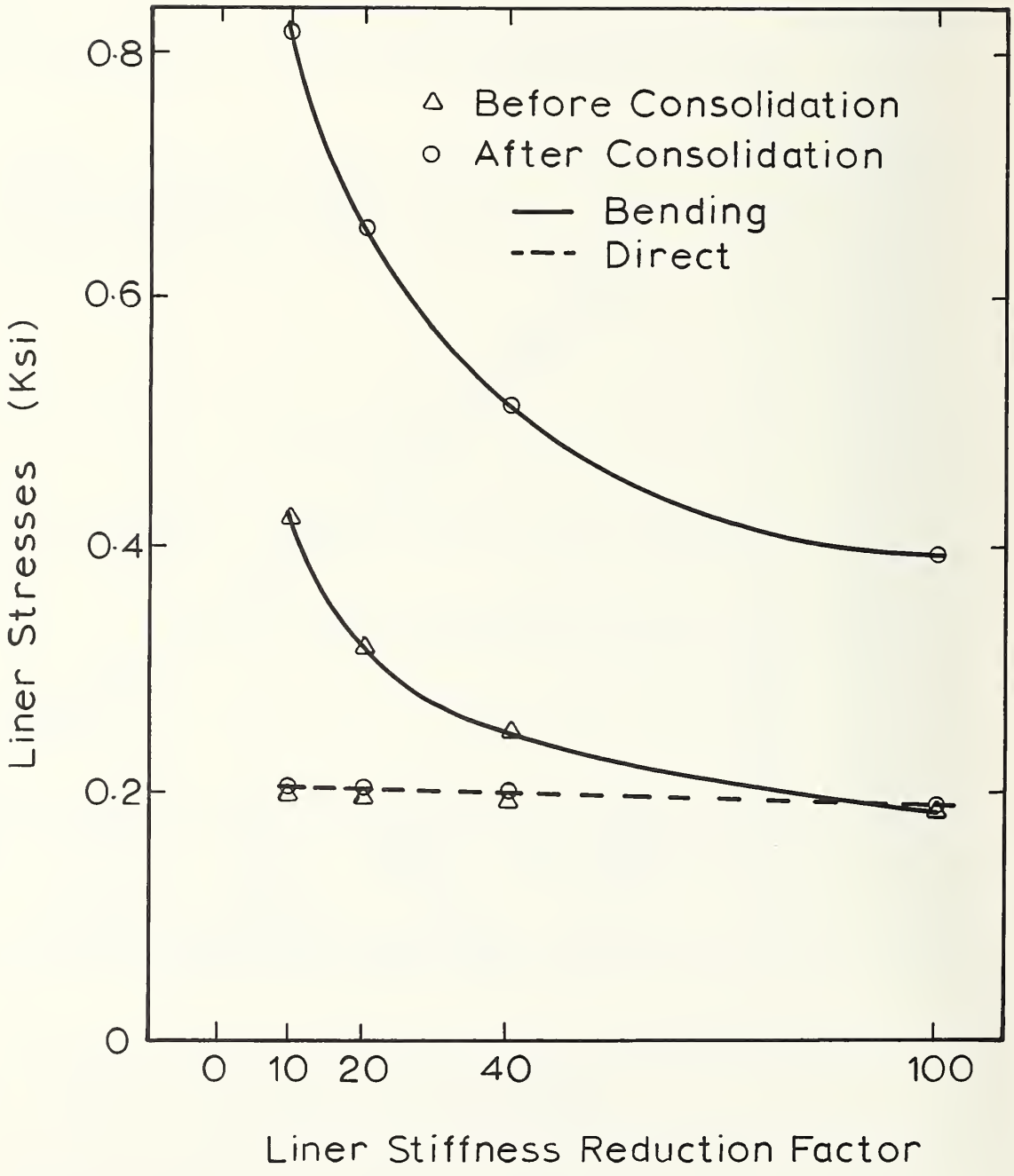

Figure 6.16: Effect of Liner Stiffness on Liner Stresses

Excess pore pressure contours for the most flexible and most stiff cases are shown in Figure 6.17. The greater extent of excess pore pressures is clearly shown for the more flexible liner.

TABLE 6.8

Effect of Liner Stiffness on Maximum Excess Pore Pressure

Reduction Factor	Pore Pressure (psf)
10	388
20	424
40	457
100	482

The corresponding contour plots for percentage of critical state are shown in Figure 6.18. Again, the most flexible liner produces the greatest yield zone.

6.4.4 Summary

The use of a stiff liner will reduce movements close to the liner. Thus, the buildup of excess pore pressures will be minimized, ultimately reducing surface settlements.

The use of a flexible liner will greatly reduce the bending stresses in the liner.

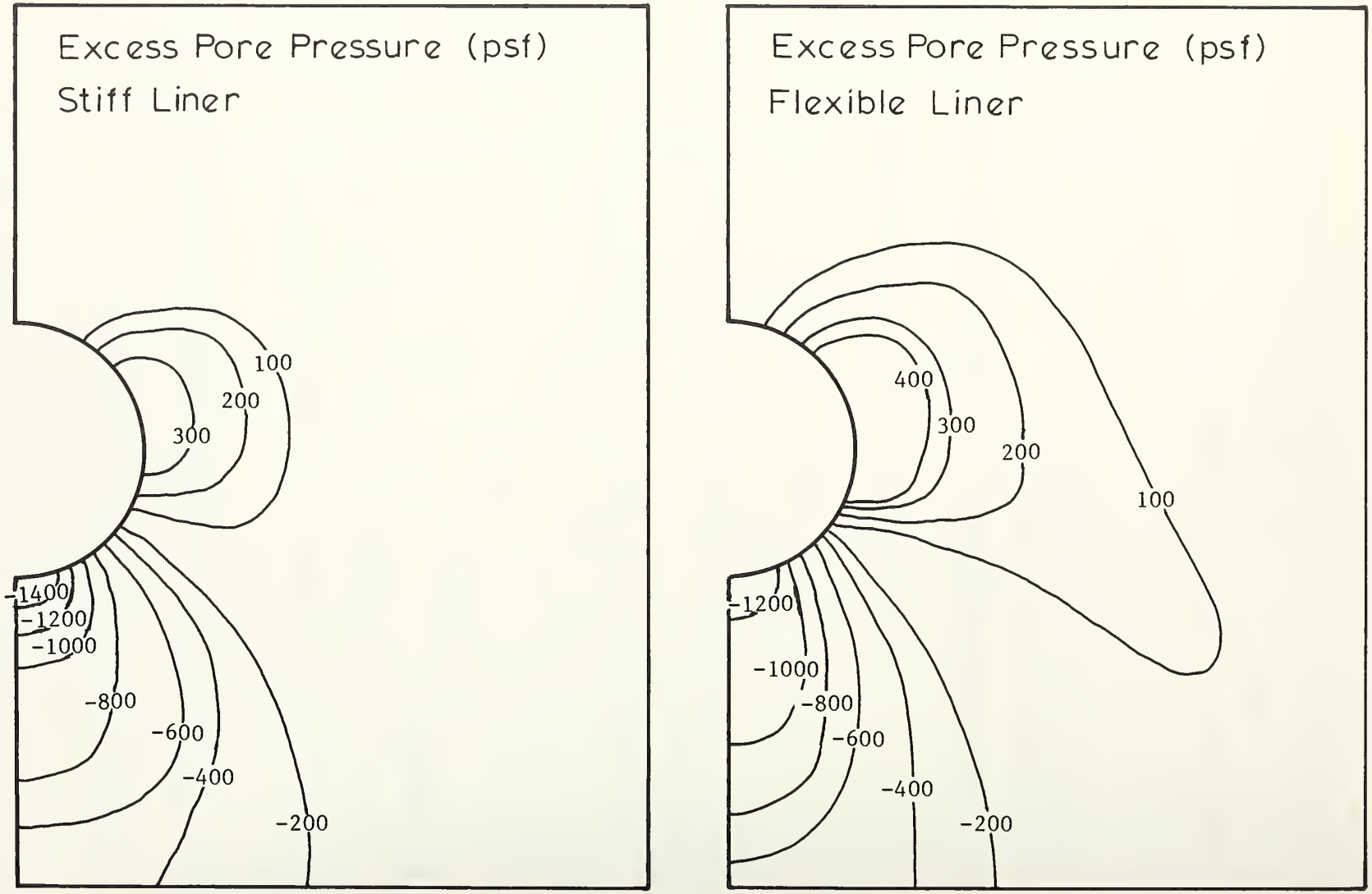

Figure 6.17: Effect of Liner Stiffness on Excess Pore Pressures

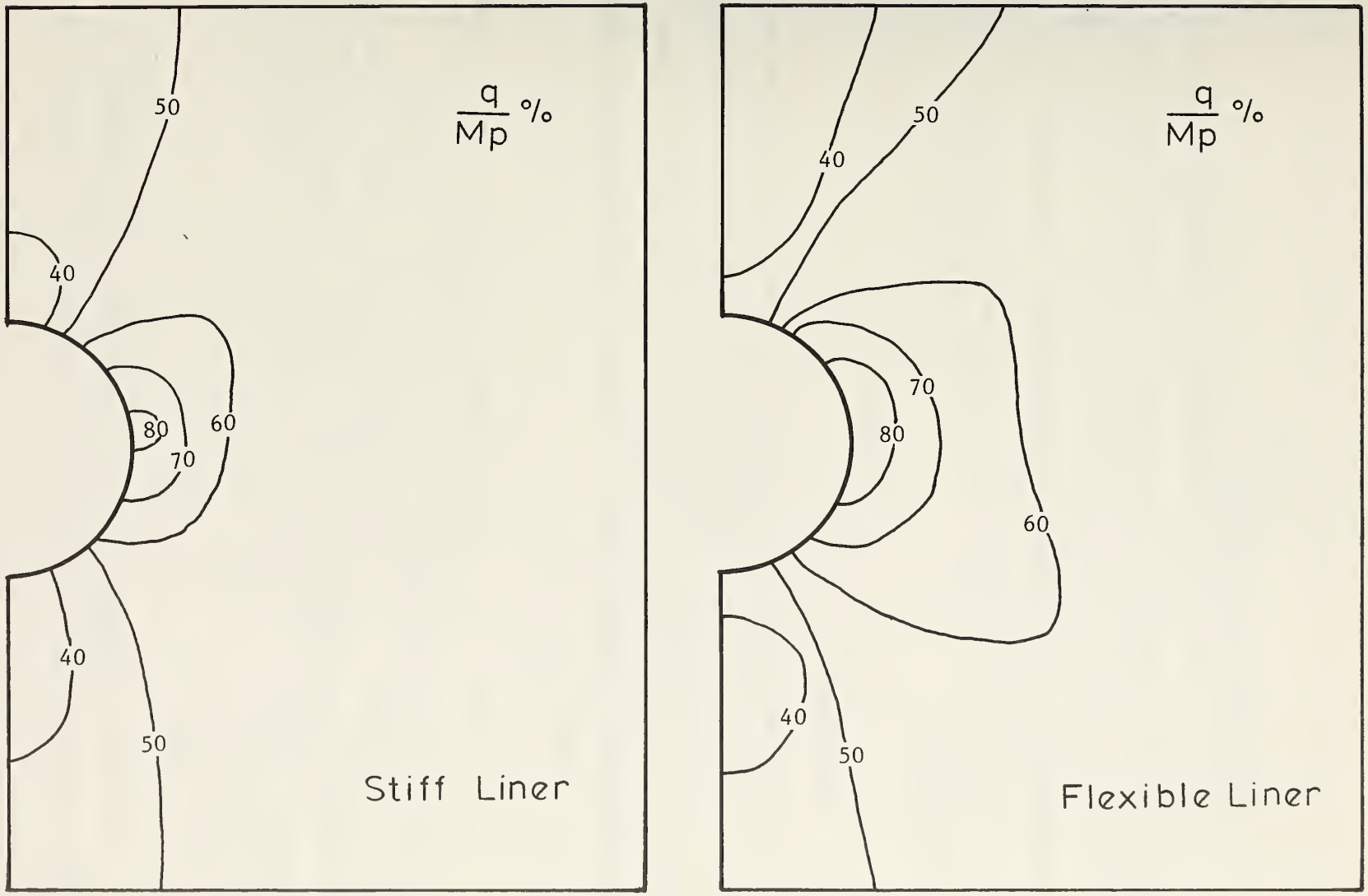

Figure 6.18: Effect of Liner Stiffness on Percent of Critical State

6.5 EFFECT OF THE TAIL VOID SIZE

The effect of construction performance is modelled by varying the size of the tail void gap. Two values of this parameter were used; 2.0 inches (50 mm) and 3.6 inches (90 mm). The 2.0 inch value corresponds to good control of the alignment of the shield, whereas the 3.6 inch value may often be experienced in practice when less than ideal conditions exist.

6.5.1 Settlements

A comparison of maximum surface settlements at three stages of construction is given in Table 6.9. The settlements are considerably larger when construction performance is poor. The increase in settlement due to consolidation is much more significant when larger initial movements are allowed.

For the Thunder Bay tunnel discussed in Chapter II, settlements increases due to consolidation ranged from 15 to 100 percent of the initial settlements. One factor contributing to the larger increase was the difficulty experienced in properly aligning the shield which led to a larger tail void. This effect is observed in the finite element parametric study.

The surface settlement profile before and after consolidation is shown in Figure 6.19. By comparing this to Figure 6.3 it can be clearly seen that the size of the tail void has a big influence on the

TABLE 6.9

Effect of Tail Void on Maximum Surface Settlements

	Maximum Surface Settlements (inches)	
	Tail Void 2.0 inches	Tail Void 3.6 inches
At Tail Void Closure	0.90	1.91
Before Consolidation	1.06	2.08
After Consolidation	1.24	2.74

time-dependent component of settlement. The corresponding error function plots are shown in Figure 6.20. The volume of the trough is reduced from 4.3 percent to 1.9 percent as the tail void gap is reduced from 3.6 inches to 2.0 inches. The width of the trough remains almost unchanged.

6.5.2 Soil Pressures Acting on the Liner

An increase in soil movement prior to liner installation causes a reduction in the average liner pressure both before and after consolidation. The pressure term that produces bending stresses is initially slightly smaller, but after consolidation it becomes slightly larger for the case of the larger tail void. The liner pressure terms are shown in Table 6.10.

TABLE 6.10

Effect of Tail Void on Liner Pressures

Tail Void (inches)	Pressures as a Percentage of the Vertical Insitu Stress at the Springline			
	Before Consolidation		After Consolidation	
	P_o	P_2	P_o	P_2
2.0	70.0	5.5	71.0	11.5
3.6	66.4	5.2	68.5	11.9

6.5.3 Excess Pore Pressures and Soil Stresses

When greater movement is allowed before the liner comes into contact much larger excess pore pressures are mobilized, (see Figure 6.21). Figure 6.22 shows the larger zone of yielding clay close to the springline of the tunnel for the case of the larger tail void. These percentage of critical state contours were plotted at the time when the tail void had just closed.

6.6 EFFECT OF SOIL STRENGTH

The effect of soil strength on the tunnel behavior was investigated by comparing the response for two different values of the overconsolidation ratio. The values of OCR used were one and two. Other basic parameters for the finite element computer runs were kept constant. The liner stiffness reduction factor was 40 and the tail void gap was 2.0 inches (50 mm).

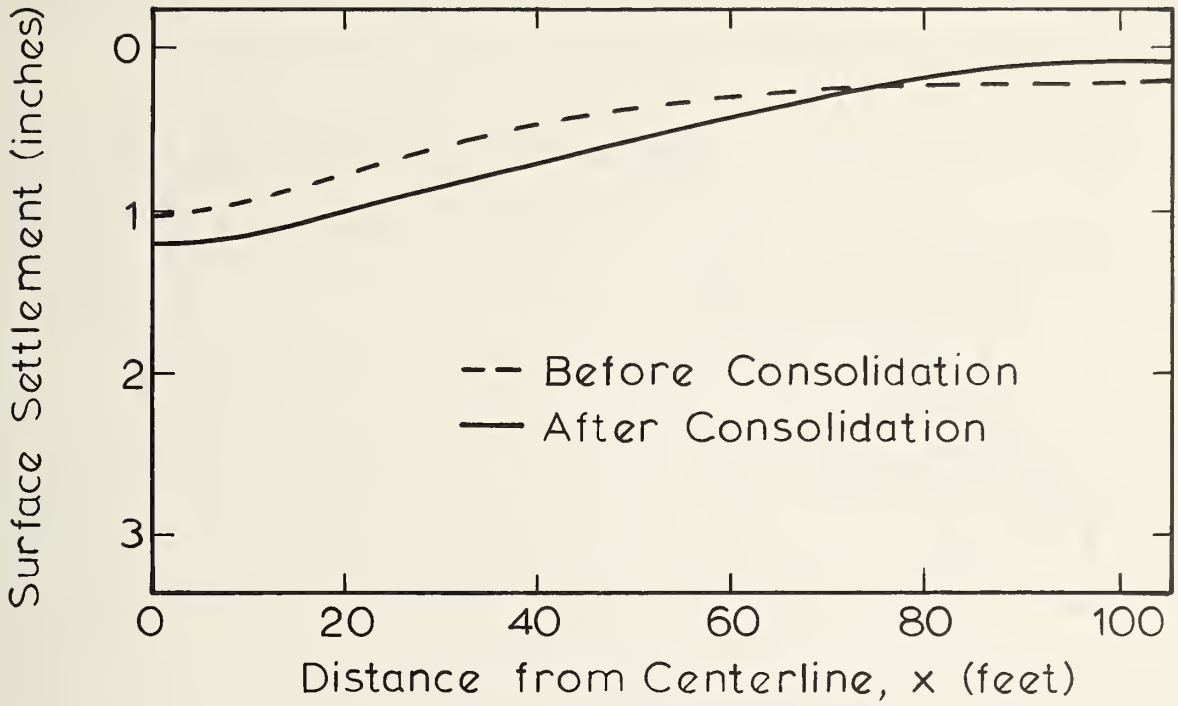

Figure 6.19: Surface Settlement Profiles for a Tail Void of 2 inches

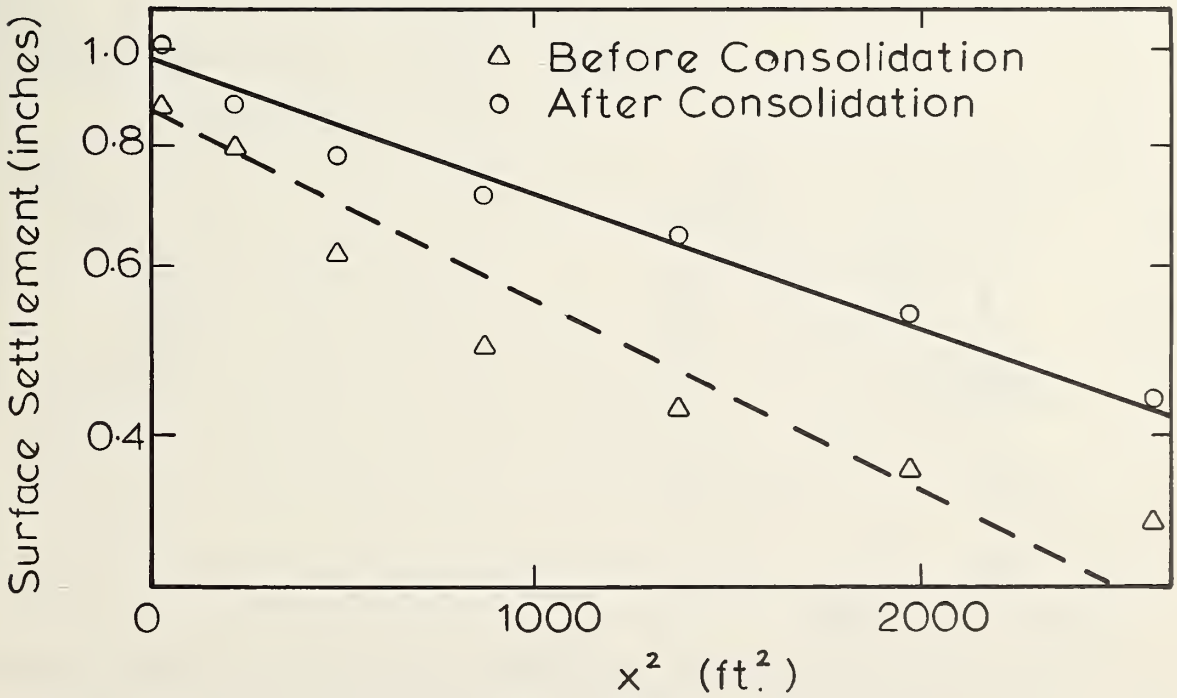

Figure 6.20: Error Function Plot for a Tail Void of 2 inches

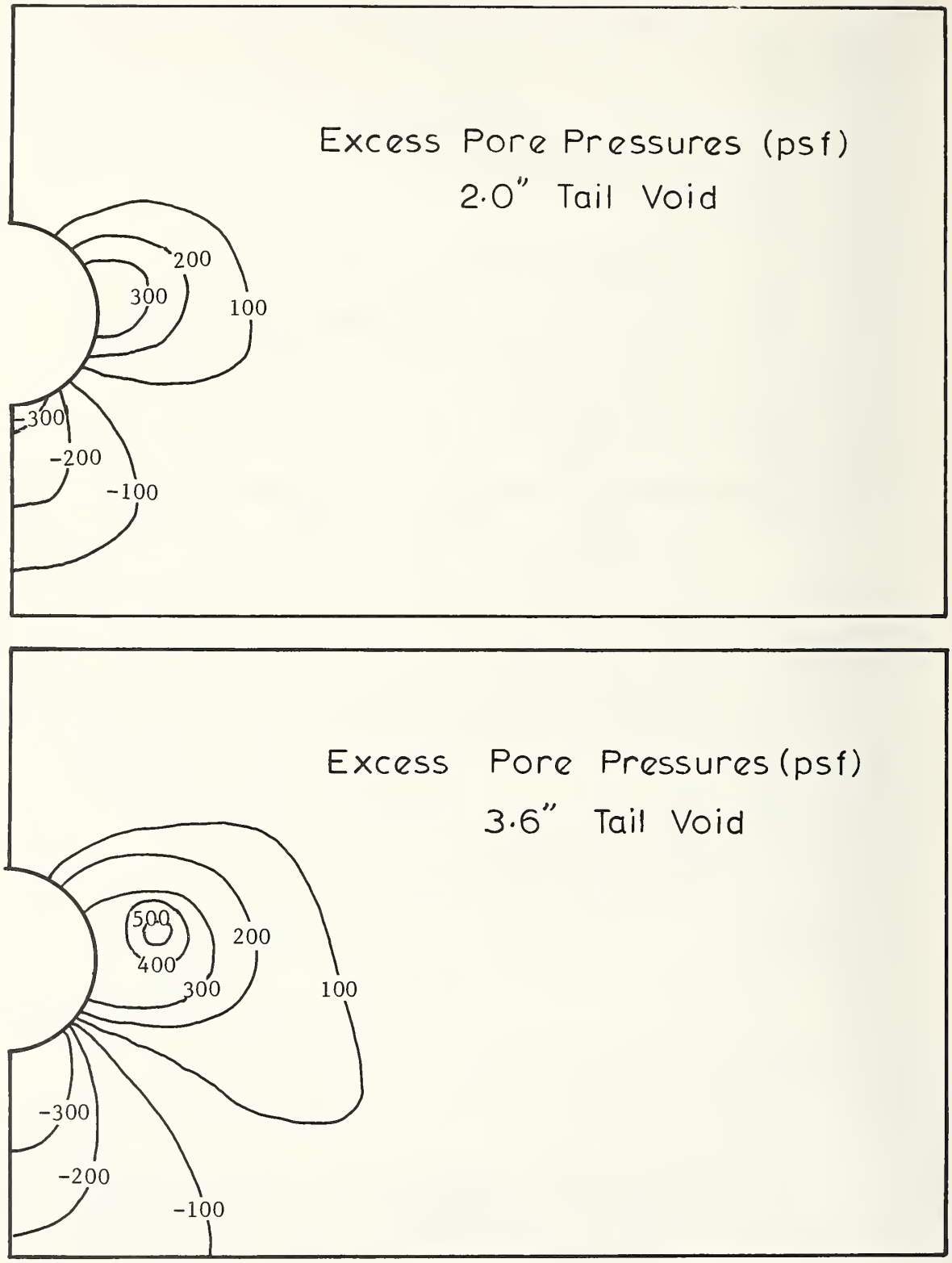

Figure 6.21: Effect of Tail Void Size on Excess Pore Pressures

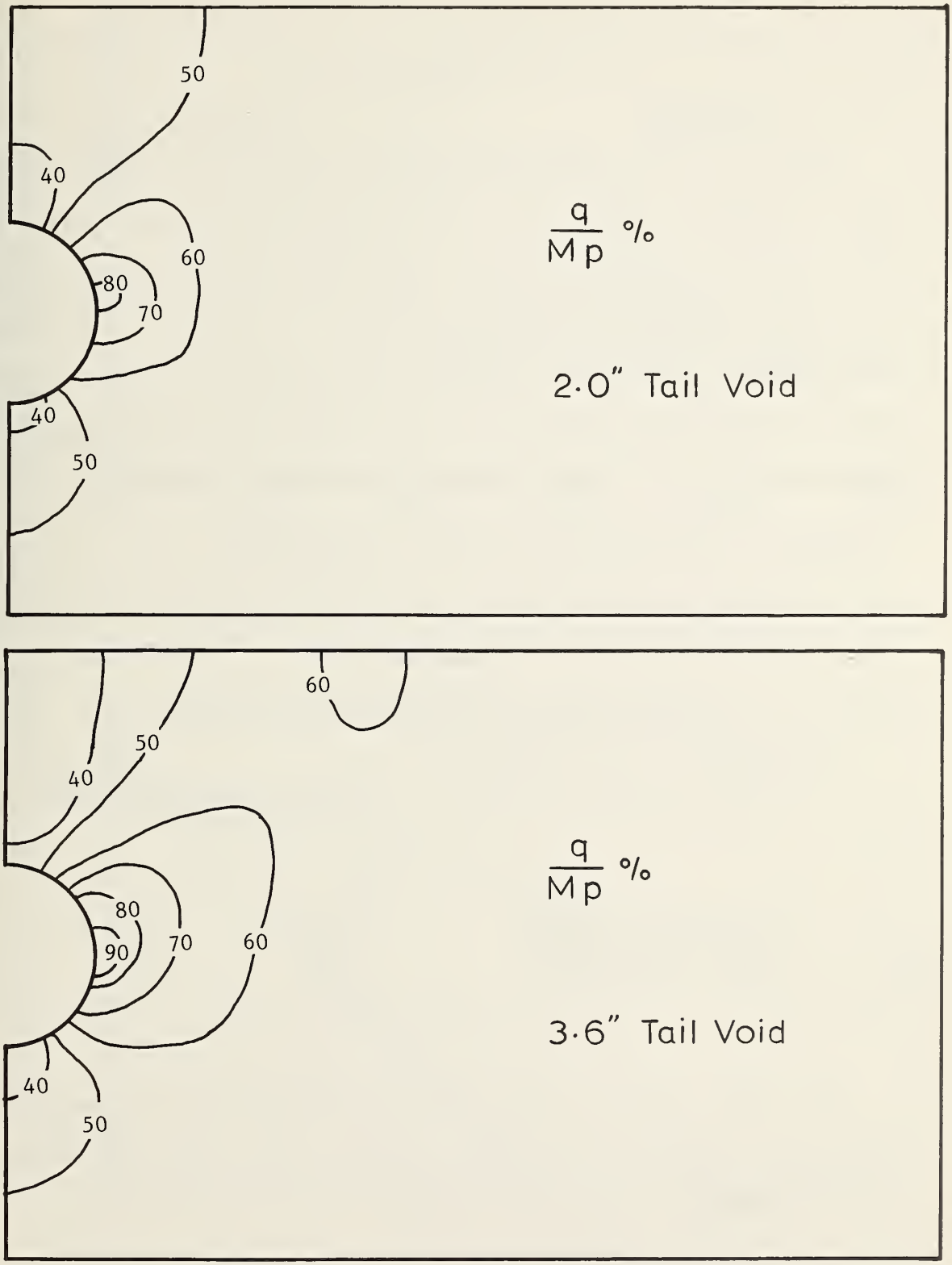

Figure 6.22: Effect of Tail Void Size on Remolded Zone

6.6.1 Settlements

Smaller surface settlements would be expected for higher strength soil. Since the excess pore pressures generated are also considerably less, smaller settlements due to consolidation would also be expected. The values of maximum settlement are shown in Table 6.11. The surface settlement profiles before and after consolidation are shown in Figure 6.23. The maximum settlement increases slightly, but further away from the tunnel centerline some decrease in settlement is observed.

TABLE 6.11

Effect of OCR on Maximum Surface Settlement

	Maximum Surface Settlements (inches)	
	OCR = 1	OCR = 2
At Tail Void Closure	0.90	0.77
Before Consolidation	1.06	0.77
After Consolidation	1.24	0.83

The error function are plotted in Figure 6.24 to obtain the settlement trough properties shown in Table 6.12, where z is the depth to the springline.

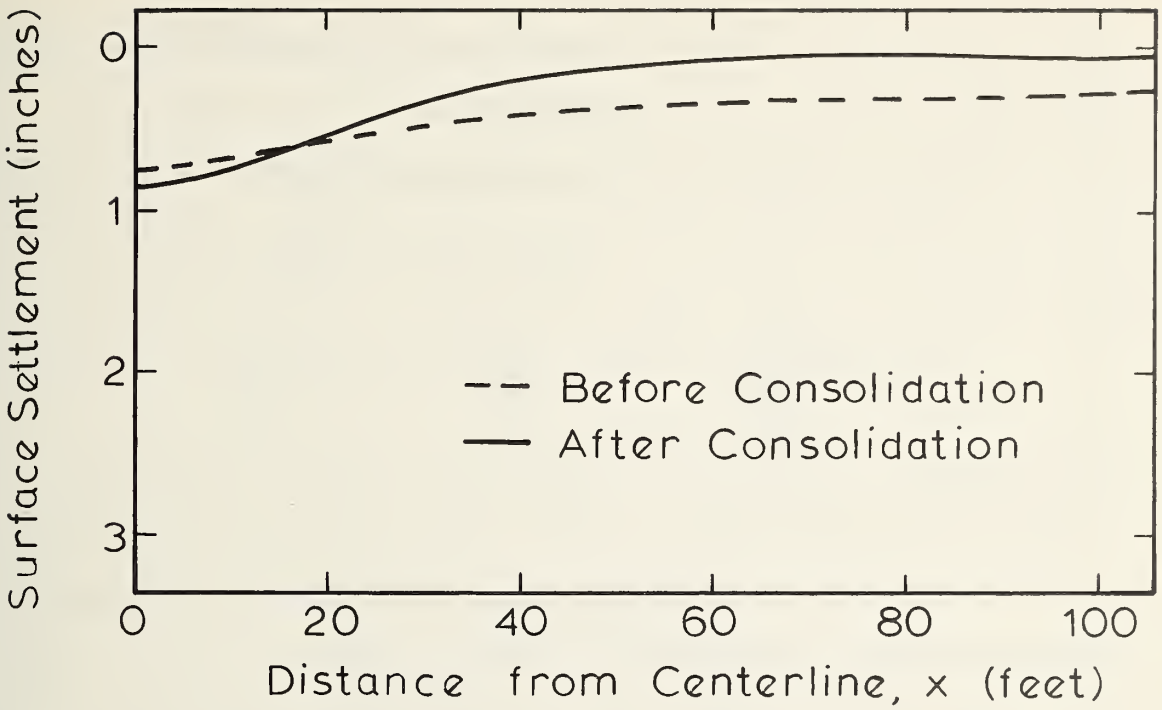

Figure 6.23: Surface Settlement Profiles for OCR = 2

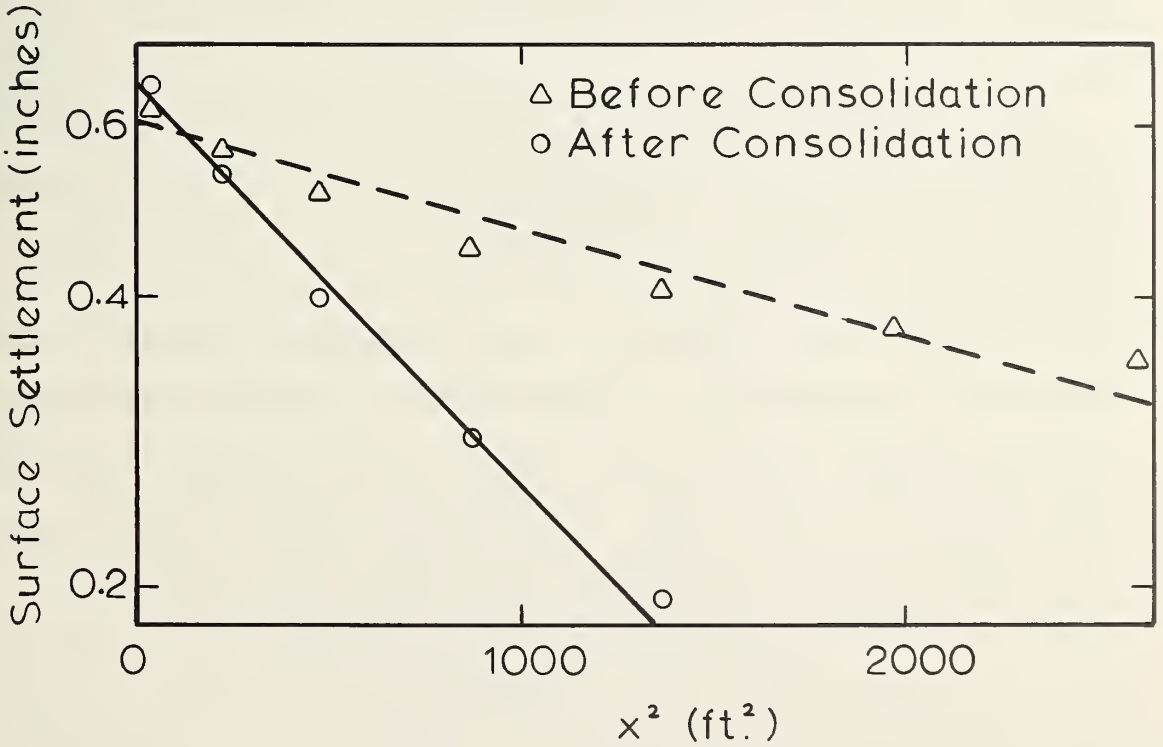

Figure 6.24: Error Function Plot for OCR = 2

TABLE 6.12

Effect of OCR on Settlement Trough

	OCR = 1	OCR = 2
OFS	7.3	4.9
v_s%	1.9	0.8
i/a	3.0	1.8
z/2a	1.7	1.7

The volume of lost ground in the finite element studies may be compared to field data reported by Schmidt (1969). For both values of OFS, the finite element studies produced ground loss close to the smallest ground loss observed in the field for the corresponding values of OFS.

This indicates good agreement, since the tail void gap of 2.0 inches represents good control of the shield, and since ground loss due to face movement is not considered in this study.

The width of the settlement trough for the case of OCR=1 is large compared with data reported by Schmidt (1969). The one field case with a wider settlement trough was for a deeper tunnel in Ottawa, where some consolidation also took place. This confirms that settlements may be more widespread when consolidation takes place, Peck (1969).

6.6.2 Soil Stresses Acting on Liner

The average liner pressure did not change during the consolidation period and was found to be 63 percent of the vertical insitu stress at the springline. This is smaller than the average liner pressure of 71 percent observed for the weaker soil case. Thus, the soil is more capable of providing support when it has a higher strength.

The bending stresses are reduced by a factor of almost five by increasing the strength of the soil. This effect may be expected because of the axisymmetric behavior of the tunnel in the stronger soil.

6.6.3 Excess Pore Pressures and Soil Stresses

Excess pore pressure contours are shown in Figure 6.25. The excess pore pressures generated were considerably smaller than those for OCR=1. The maximum positive excess pore pressure of 207 psf, halfway between the springline and the crown, is small compared to 437 psf obtained near the springline for OCR=1. The shape of the excess pore pressure contours is considerably different for the two cases. Positive excess pore pressures occur at the crown for OCR=2, while small negative excess pore pressures were obtained at this location for OCR=1.

Using OCR=2 the insitu stresses were calculated with k_0=0.8. Thus, the initial conditions correspond to q/Mp=0.19. Axisymmetric conditions are more closely approximated around the tunnel opening. Percentage of critical state contours are shown at tail void closure and before consolidation in Figure 6.26. The contours show considerable changes from those previously shown in Figure 6.13 for OCR=1.

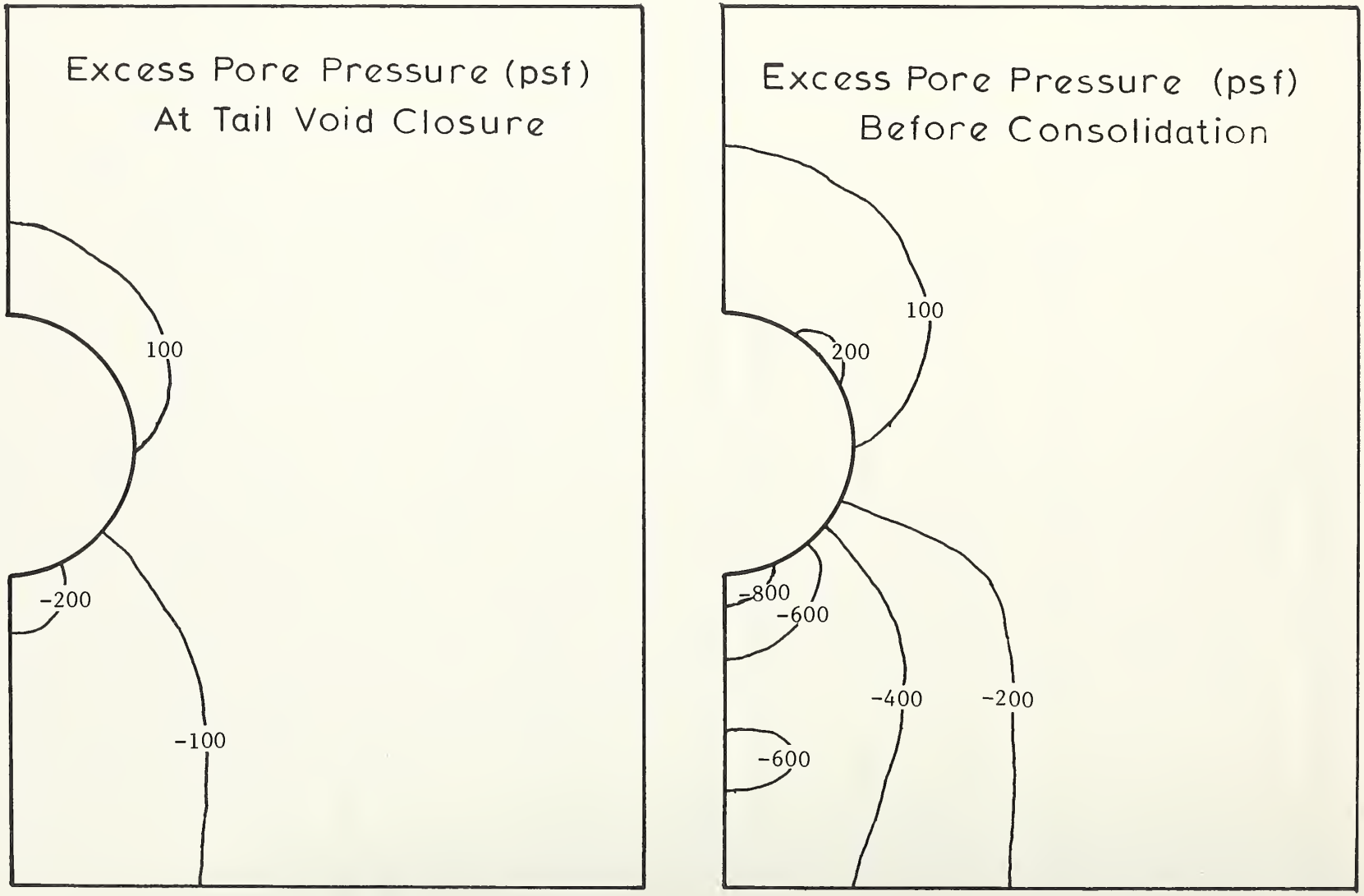

Figure 6.25: Excess Pore Pressure Contours for OCR = 2

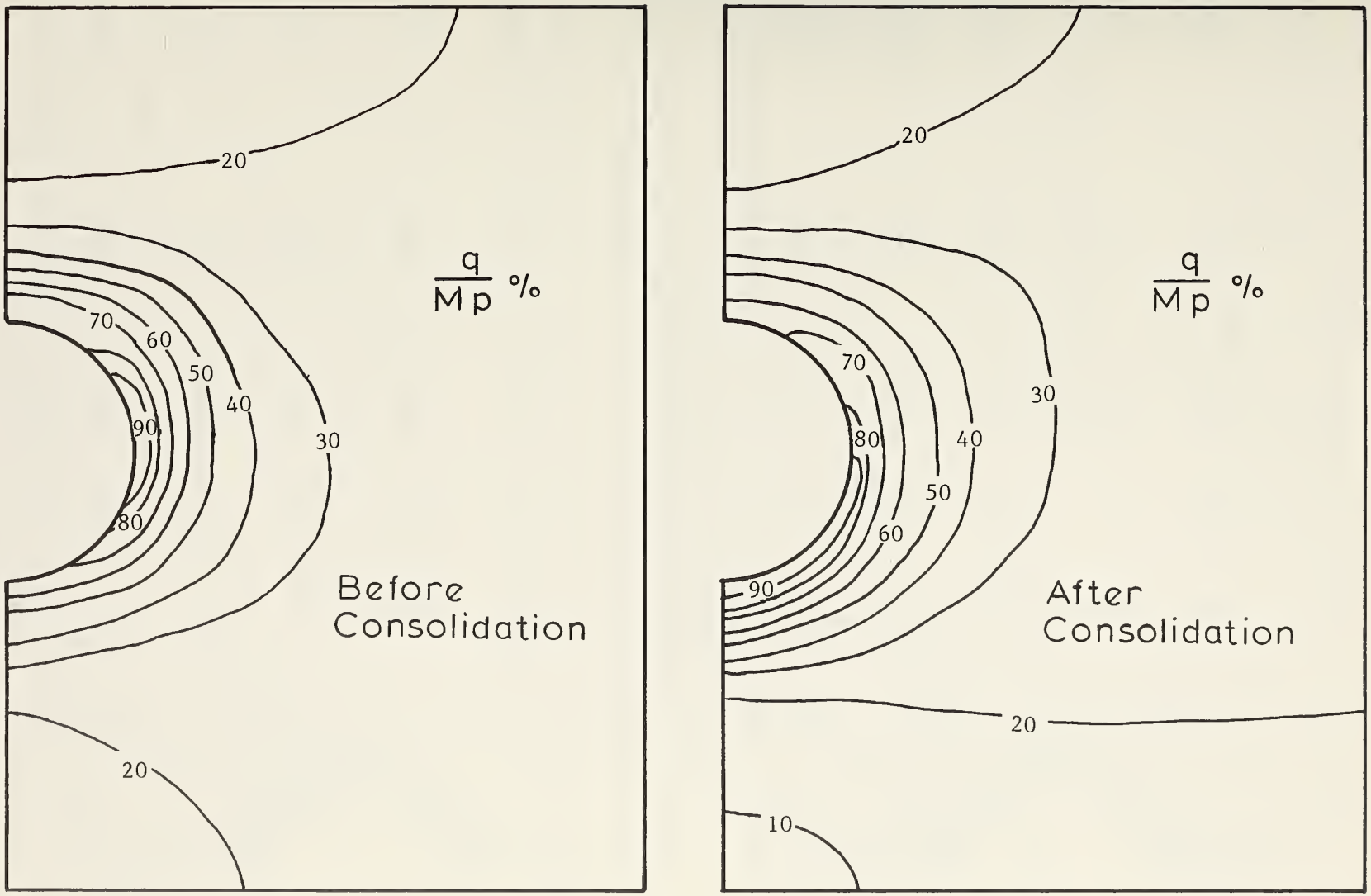

Figure 6.26: Remolded Zone for OCR = 2

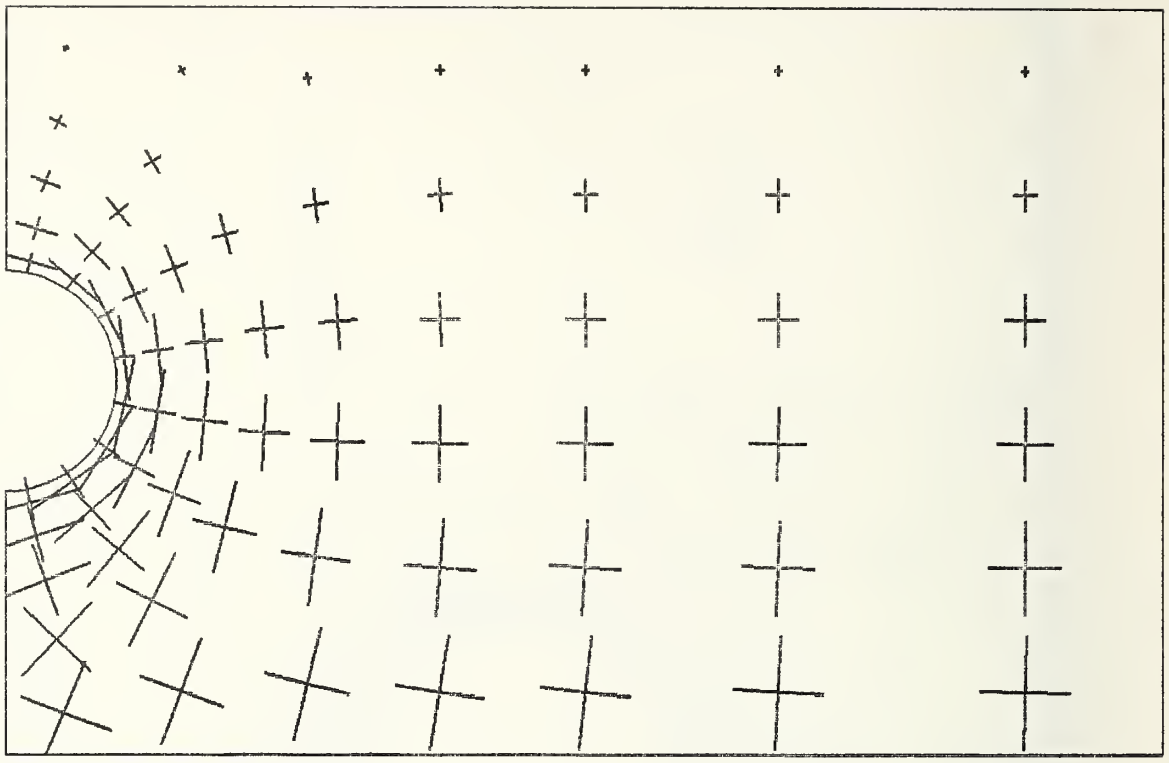

Before Consolidation

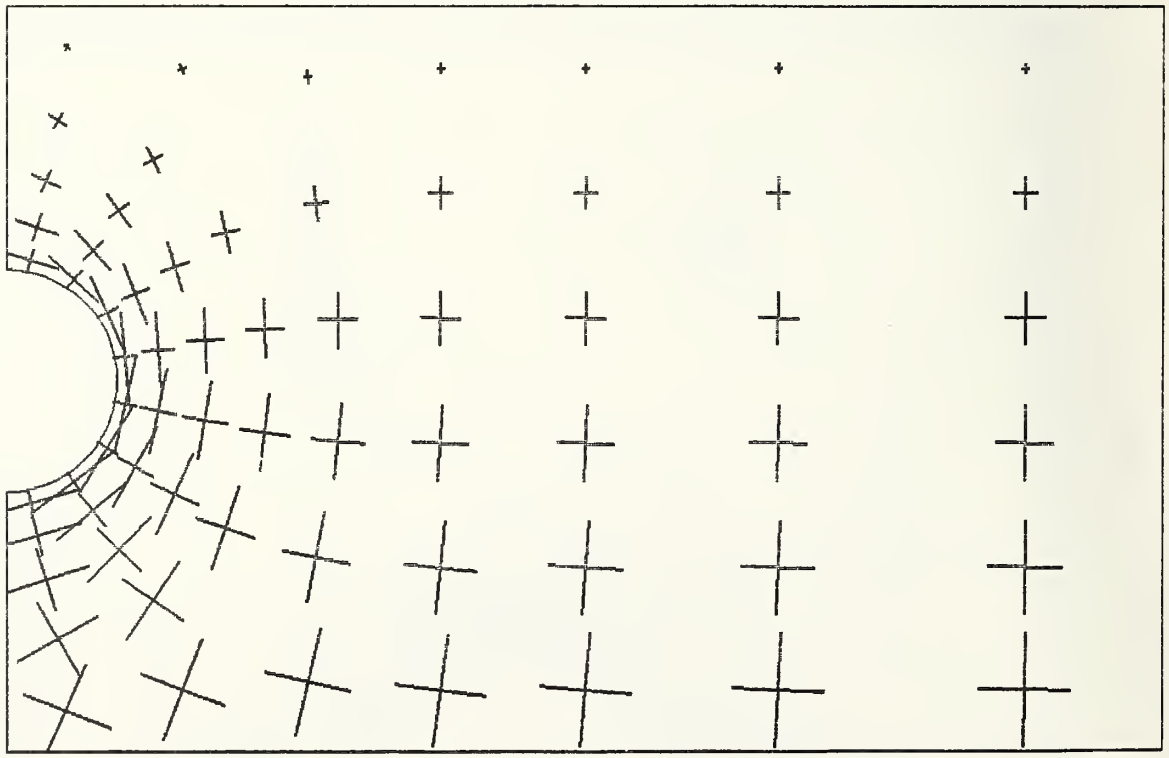

After Consolidation

Figure 6.27: Principal Stresses for OCR = 2

The principal stresses shown in Figure 6.27 reflect this axisymmetric behavior. The principal stresses have rotated much more completely at the crown and invert than those obtained for the OCR=1 case.

6.7 EFFECT OF SOIL PERMEABILITY

The permeability of the soil has a purely non-dimensional effect on the results. All results that are a function of time include the permeability parameter. Thus, the value of the permeability does not alter any of the stresses or displacements reported. This is based, however, on the assumption that the permeability is small enough that an insignificant dissipation of excess pore pressures takes place before the liner is installed and the heading sufficiently advanced.

Two representative soil permeabilities are chosen and the time-dependent effects of settlement and liner spreading are plotted against real time in Figures 6.28 and 6.29 respectively.

6.8 EFFECT OF INITIAL EXCESS PORE PRESSURES

As noted, this case was analyzed to develop an understanding of what effects in time dependent response might be created by initial pore pressures set up around the tunnel due to the use of a pressurized face shield machine. This situation can easily develop with a slurry or earth pressure balance shield as illustrated in Chapter II. It was also pointed out earlier that the present analytical approach utilizing plane strain assumption is only approximate in this case since the initial excess pore pressures are assumed to be developed by in-plane movement,

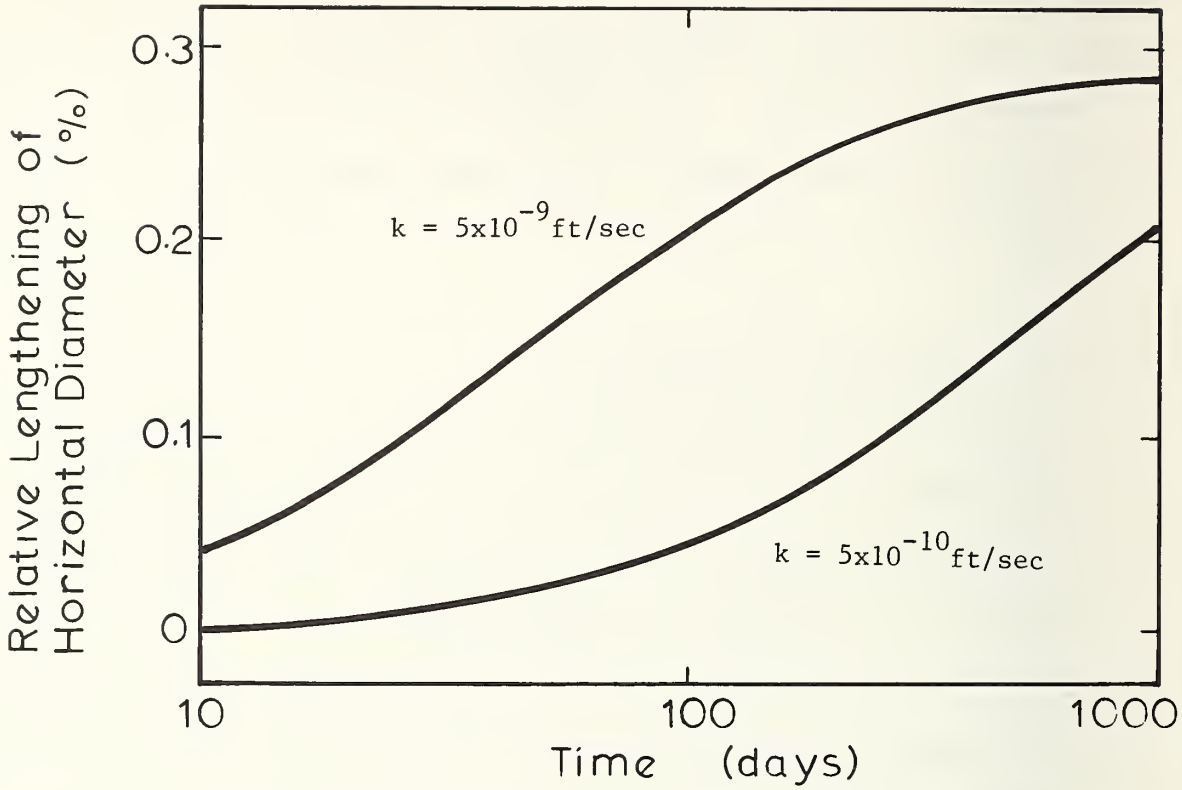

Figure 6.28: Settlement Versus Time for Different Soil Permeabilities

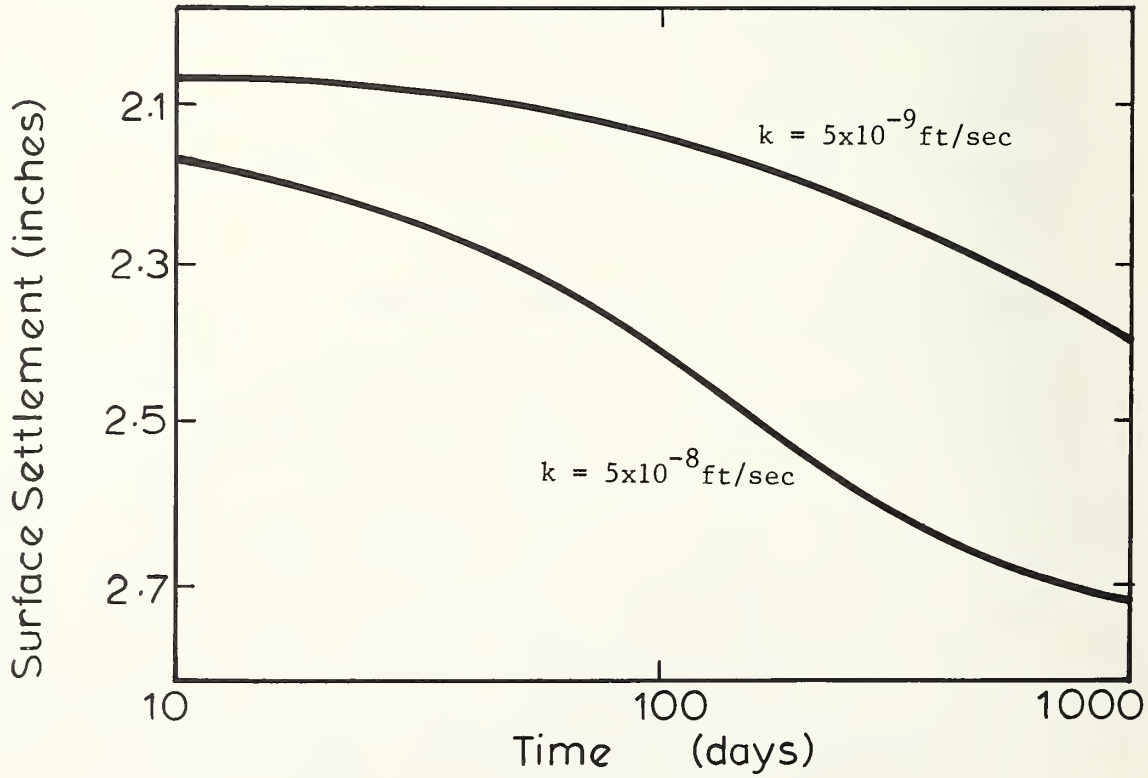

Figure 6.29: Liner Spreading Versus Time for Different Permeabilities

whereas they are actually developed by out-of-plane movements in front of the shield. Additional studies will be undertaken at a later date using the axisymmetric program option to explore these effects further. However, the present approach allows for a reasonable assessment of the general importance of these conditions.

The process of creating the initial excess pore pressures involves expanding the circular tunnel under undrained plane strain conditions using a trapezoidal pressure distribution with the highest pressure at the tunnel invert and the lowest at the crown. The nonuniform pressure distribution is used to reflect the fact that the soil is assumed to have an increasing stiffness with depth, and the stiffer soil is more likely to allow a higher pressure to be developed during the shove of the shield. The pressures used are chosen to produce a set of outward peripheral movements around the tunnel which are in line with those observed recently at the site of an earth balance shield project in San Francisco (Clough, et al., 1982). The resulting movements are depicted in Figure 6.30. As would be the case in the field, the movements are nonuniform - 3.6 in. (9.1 cm), 1.2 in. (3.1 cm) and 1.0 in. (2.5 cm) at the crown, springline and invert respectively.

The procedures for modeling the remainder of the tunnel loading are the same as those used previously. It is assumed that the soil is displaced inwards to fill the tail void, whereupon the liner is installed. A tail void gap of 3.2 in. (8.1 cm) is used at the crown. Note that the soil is not assumed to have to recover the entire initial heave before displacing inward. The reason for this is that during the

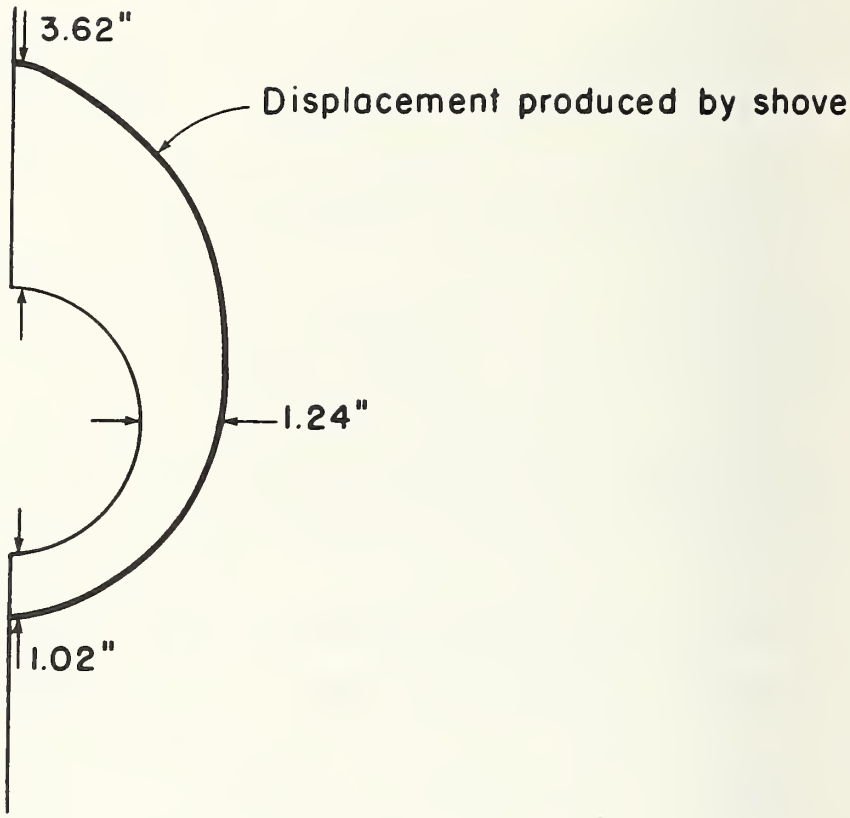

Figure 6.30: Outward Tunnel Displacements Designed to Induce Initial Pore Pressure

actual out-of-plane movements in front of the shield when the soil at the perimeter of the shield moves away, new soil takes its place by moving from in front of the shield. Thus, soil is always in contact with the shield and can only move inwards the amount of the tail void gap.

The excess pore pressures developed after expansion of the tunnel periphery are shown in Figure 6.31. High positive values developed in the areas around the crown and the invert. At the springline negative pore pressures are predicted. These different behaviors reflect the fact that in the crown and invert areas the shear stress levels are increased over their original at-rest values, while at the springline area, stress levels are decreased. Also in Figure 6.31 the excess pore pressures after closure of the tail void are depicted. The primary effect of this movement is to eliminate the negative pore pressures at the springline, while the positive pore pressures are largely unaffected. Importantly, the excess pore pressure distribution at this stage prior to consolidation is quite different than that for simple tail void closure (see Figure 6.21).

The contours of percent development of critical state for the initially outwardly displaced tunnel after tail void closure (Figure 6.32), show that less of the soil strength is mobilized as compared to the case of simple tail void closure (see Figure 6.22). The largest difference occurs at the springline where only a maximum of 60% of critical state is mobilized in Figure 6.32, while upwards of 80-90% is mobilized in Figure 6.22.

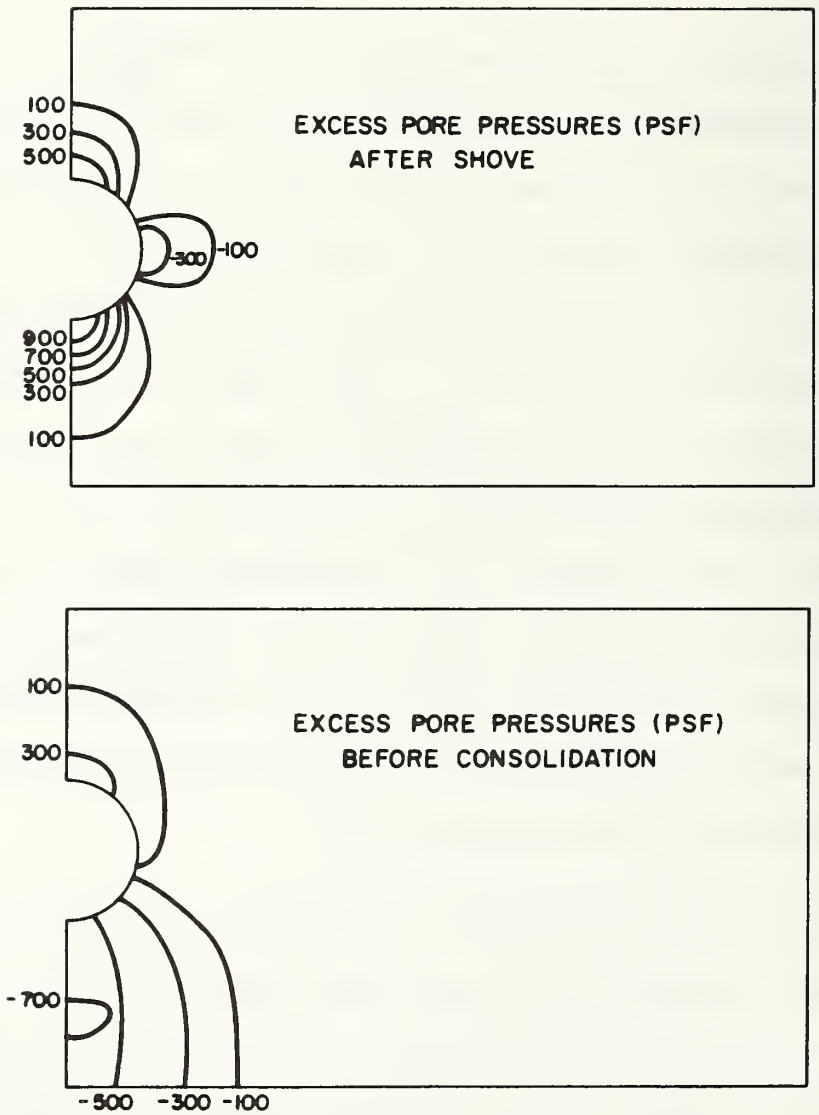

Figure 6.31: Excess Pore Pressures for Case of Initial Outward Movements

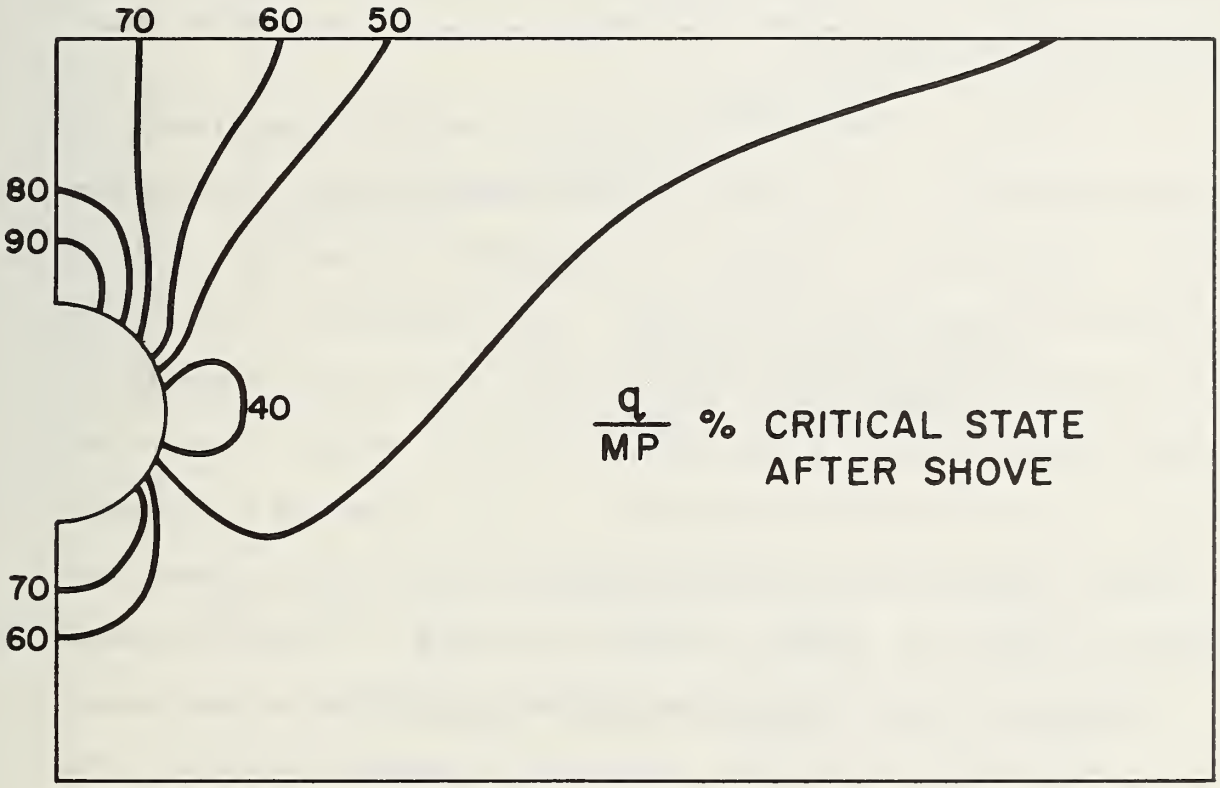

Figure 6.32: Contours of Percent Critical State Mobilized

Surface settlement profiles after tail void closure and consolidation are given in Figure 6.33. These profiles are drawn assuming that the ground surface is initially level, since the amount of initial heave predicted by the plain strain analysis is not considered representative of the actual case. Initially the settlement trough is much flatter than those observed for simple tail void closure. Subsequently, after consolidation, the settlement trough takes on a more conventional form.

The effects of the initial heave on settlement magnitudes is generally positive. In Table 6.13 the maximum movements at the surface on the centerline of the tunnel are tabulated and compared to those predicted for simple tail void closure. Even assuming no initial heave of the ground surface the settlements of the present case are smaller in every instance than those for simple tail void closure. Since the ground surface would be heaved upwards to some degree by out-of-plane movements, the resulting settlements would be even smaller. Thus, for the assumptions made in these analyses and levels of movement assumed, it appears that the effects of the initial outward displacement caused by a pressurized face shield are effective in reducing movements. The data suggests that the initial heave process tends to "precompress" the soil. Actually shear stress levels in the springline are initially reduced, and shear stress increases thereafter cause less development of excess pore pressures during subsequent inward movement. Further study of this problem is clearly warranted however, to determine if this finding holds for a wide range of conditions. Very large initial outward heaves may actually be detrimental since large remolded zones of soil could be created.

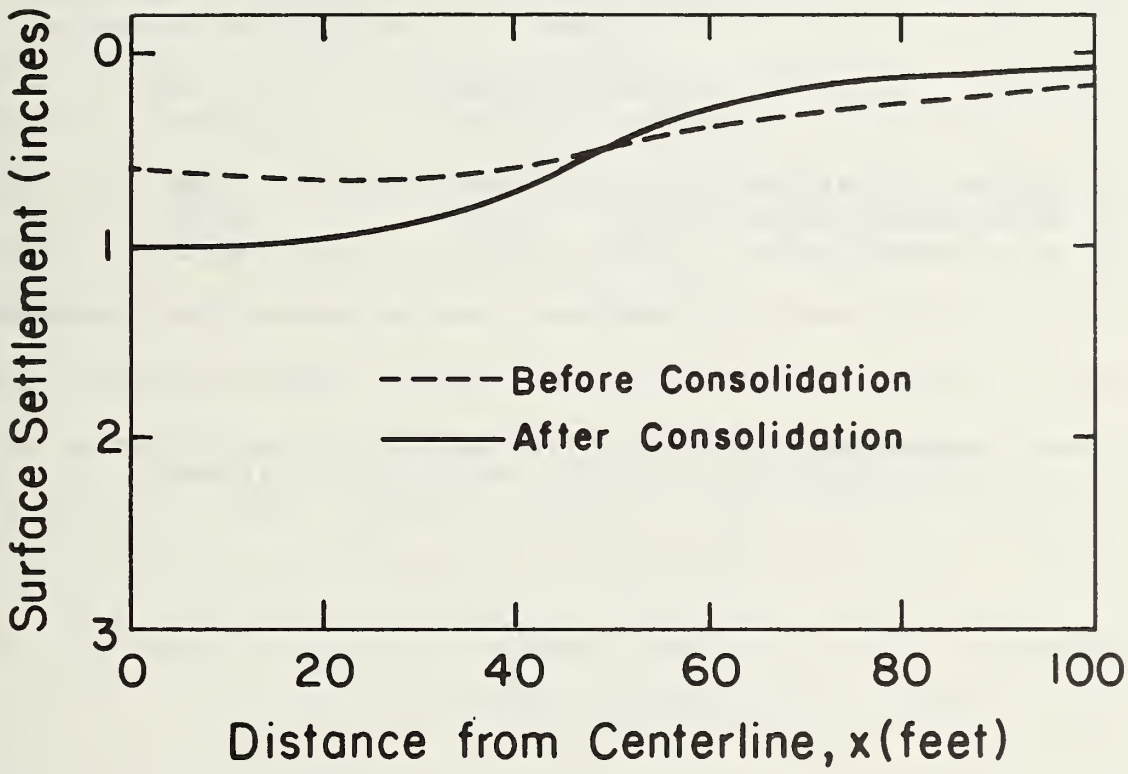

Figure 6.33: Surface Settlement Profiles for Case of Initial Outward Movements

TABLE 6.13

Effect of Initial Outward Displacement Caused By Pressurized Face Shield

	Maximum Surface Settlement (inches)		
	Simple Tail Void Closure		Initial Heave Followed* by Tail Void Closure of
	2.0 Inch Closure	3.6 Inch Closure	3.2 Inch Closure
At Tail Void Closure	0.9	1.91	0.62
Before Consolidation	1.06	2.08	0.72
After Consolidation	1.24	2.74	0.98

*Note: Assumes Ground Surface Horizontal After Shove. Any Heave Which Might Occur at Surface Would Reduce Settlements.

Chapter 7

SUMMARY AND CONCLUSIONS

Control of ground movements during tunneling is one of the major issues related to construction in the urban environment. New shield tunneling techniques have been developed to address this problem along with improvements in conventional methods. However, these improvements have not been paralleled by development of our understanding of the reasons for the behavior of the ground during soil tunneling. In the past, movements around tunnels have largely been studied by field observations, a particularly effective technique where the data can be extrapolated to other projects. However, these procedures cannot be readily used to predict performance for new tunneling machines. Also, since measurements are often discontinued with the construction completion, little is learned about long term effects, which in some cases can be very important.

This report describes a research program devoted to the study of time-dependent behavior of shallow tunnels in clay due to the effects of mobilization and dissipation of excess pore pressure. To the knowledge of the authors it is the first of its kind. The problem is investigated by:

1. Reviewing available field data

2. Developing a finite element code to model shield tunneling effects while explicitly taking into account excess pore pressure effects in the soil.

3. Performing a series of parametric studies on the time-dependent behavior of tunnels.

The finite element program which is developed is fully described and should be useful in future studies of a range of advanced tunneling problems.

As expected, the review of existing field data revealed that few cases of tunnel behavior have been monitored long enough to define long term time effects. Interestingly, about half of those available are very recently reported and concern advanced shield tunnel projects. All of the data available shows that in cohesive soils surface settlements increase with time following tunnel passage. Most authors agree that this effect can largely be explained as due to dissipation of excess pore pressures set up in the soil during tunneling. Also, there is strong evidence that the greater the degree of disturbance of ground during tunneling, the greater are the resulting time-dependent movements. In addition to the ground movements, liner loads and deformation of the liner continue with time. Thus, although the data are somewhat limited, there is strong evidence for significant time effects, particularly in the case of the newer shield types.

In order to study the time dependent behavior, a finite element code was developed to model construction of a shield tunnel from the initial

condition to excavation to liner installation, and finally until all excess pore pressures have dissipated. In particular, the finite element code was designed to

1. Simulate the construction procedure.
2. Use an elasto-plastic soil model.
3. Include the effect of consolidation.
4. Maintain accuracy for large strains.

The construction procedure was simulated in plane strain since the tail void is the most significant cause of settlements. During excavation the soil closes in on the opening

by an amount equal to the size of the tail void gap, at which point the liner elements are activated. The liner was modelled using a ring of 16 eight-noded isoparametric elements which give a good response in bending. Undrained conditions were assumed during the construction sequence. The excess pore pressures were then allowed to dissipate and the resulting consolidation behavior was observed.

An elasto-plastic soil model was used to model the soil yielding accurately near the tail void. The Cam clay soil model was chosen and developed to a form suitable for coding in a finite element program. This part of the finite element code was verified by comparing computed and experimental results for drained triaxial tests.

An eight-noded isoparametric element with pore pressure degrees of freedom at the corner nodes, Q8P4, was used to model the soil.

Verification of the consolidation routines was performed by comparing computed results for one- and two-dimensional flow and consolidation problems with appropriate closed form solutions.

The Q8P4 element was chosen over other elements, Q8P8 and Q4P4, because it gave more accurate results for the above problems. The time integration parameter, β, was set equal to 0.5 as the result of a stability analysis study.

Large strains may exist in the soil near the tail void. It is important that accurate solutions be obtained in this area. It was found that sufficient accuracy could be obtained by updating the mesh geometry after each time increment since many time increments are used.

Typical tunnel response was examined using the finite element code for a large diameter shallow tunnel in Boston Blue Clay. The results obtained are in agreement with reported behavior for a tunnel in soft clay. In particular,

1. The maximum surface settlement was found to increase significantly during consolidation. The width of the settlement trough also increased.
2. The bending stresses in the liner were found to increase significantly with time although the average stress remained almost constant.
3. Liner spreading was observed during consolidation; the spreading stopped once the excess pore pressures had dissipated.

Parametric studies were performed to determine the effects on the behavior of tunnels due to:

1. The stiffness of the liner.

2. The tail void size.

3. The overconsolidation ratio.

4. The permeability of the soil.

5. Initial excess pore pressure set up by outward pressures at the face of a pressurized face shield.

The following is a list of some of the more important results of the parametric studies:

1. A flexible liner allows soil movement, which leads to greater disturbance and thus higher excess pore pressures. The maximum surface settlement increases more during consolidation for this case than for a stiff liner.

2. Bending stresses in the liner are reduced as the liner becomes more flexible. The average soil pressure acting on the liner, however, is reduced only by a small amount.

3. Bending stresses in the liner always approximately double during consolidation without regard to liner stiffness.

4. The surface settlement increase due to consolidation becomes greater as the tail void is increased.

5. The average soil pressure acting on the liner decreases slightly both before and after consolidation with an increase in the size of the tail void.

6. The behavior of a tunnel located in overconsolidated clay is different from the behavior of one in normally consolidated clay. In normally consolidated clay, the maximum excess pore pressures exist near the springline of the tunnel. They are several times greater than the maximum excess pore pressures which occur near the crown of a tunnel for an overconsolidated soil.

7. The maximum surface settlement remains almost unchanged for a soil with OCR = 2.

8. The average soil pressure acting on the liner is reduced by about 12 percent as the value of OCR is increased from one to two.

9. The permeability of the soil is contained in a non-dimensional time parameter. Thus results are valid for a wide range of soil permeabilities.

10. Small levels of initial outward displacements around the tunnel periphery due to pressure at the face produce beneficial effects in reducing time-dependent movements and loadings.

Appendix A

PEPCO USER'S MANUAL

A.1 INTRODUCTION

PEPCO is an acronym for Program for Elasto-Plastic COnsolidation. It was developed at Stanford University as a research tool for analysing the consolidation behavior of soil using the finite element method. The program has been used primarily for consolidation analyses of tunnel behavior in clay. Details pertaining to the theory behind the program are given in the Ph.D. report entitled 'Finite Element Consolidation Analyses of Tunnel Behavior in Clay' by Paul R. Johnston.

The program is coded in FORTRAN IV and has been in use on an IBM 3033 computer at Stanford's Center for Information Technology.

A.2 PROGRAM CAPABILITIES

The capabilities of this finite element program are controlled by the variety of element and material types in its respective libraries. In its current state the following features are available:

1. Plane strain or axisymmetric analysis
2. One-dimensional analysis
3. Elastic analysis
4. Elasto-plastic analysis using the Cam clay soil model
5. Fully drained or undrained analysis

6. Fluid flow analysis
7. Consolidation analysis
8. Large strain analysis
9. Initial stress generation
10. Installation of structural members
11. Construction of embankments
12. Incremental loading
13. Restart capability
14. Expandable element library
15. Expandable material library
16. Output control
17. Keyword controlled input

It is relatively easy to add new features to the program by making additions to the element and material type libraries. For example, the program may be converted to include three-dimensional problems simply by adding a three-dimensional element, since the input, solution and output routines do not need to be altered.

A.3 PROGRAM OVERVIEW

The program consists of a main program and approximately 40 subroutines, see Figure A.1. The program can be executed using a REGION of 512K for small problems. Double precision is used for all REAL variables. The array storage is controlled by the dimension of the vector A in the main program.

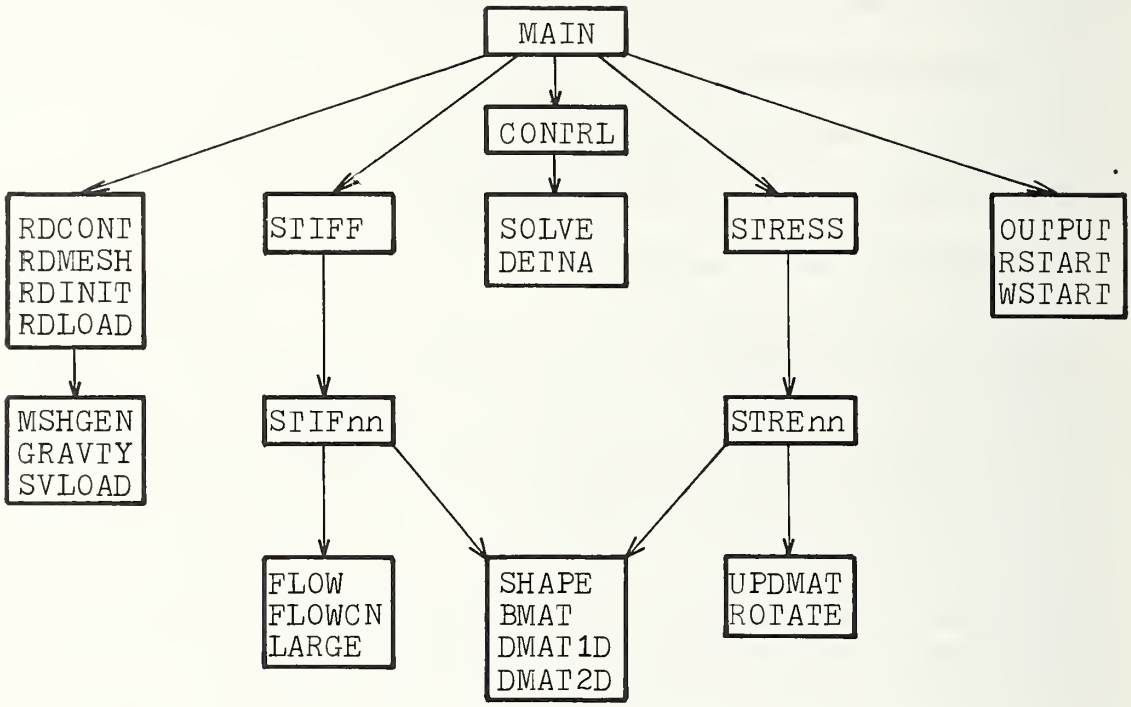

Figure A.1: Program Structure

The main program calls the subroutine CONTRL. This subroutine allocates the array space dynamically by mapping the smaller arrays, both INTEGER and REAL, into the space allocated for A. CONTRL then calls the other main subroutines in order.

The subroutines RDCONT, RDMESH, RDINIT and RDLOAD are used to read the input data. MSHGEN is a mesh generation routine and SVLOAD calculates equivalent nodal loads for body forces.

The subroutine STIFF assembles the structure stiffness matrix. The subroutine calls the appropriate STIFnn to calculate the element stiffness matrices. The element stiffness subroutines call other subroutines, for example, to calculate the shape functions or stress-strain matrix.

The subroutine SOLVE solves the finite element equations using a skyline solution algorithm, Mondkar and Powell (1974). The bookkeeping for the stiffness vector is performed by the subroutine DETNA.

The stresses are updated using the subroutine STRESS. This subroutine calls the appropriate STREnn for each element to calculate the updated element stresses. The element stress recovery routines call other routines, for example, to calculate the incremental stress contribution due to rotations.

Results are printed using subroutine OUTPUT. They may also be saved on a restart file using WSTART. A future run may start where this run left off using RSTART.

A.4 ELEMENT LIBRARY

The program currently has eight element types. New elements may be added to the program by including two new subroutines per element.

1. STIFnn, where nn is the element type number, is a subroutine that calculates an element stiffness matrix.
2. STREnn is a subroutine that computes the incremental element stresses and updates the total stresses.

The subroutine CONTRL must be modified to include the following information regarding the new element type:

1. Number of coordinates per node.
2. Maximum number of degrees of freedom per node.
3. Number of integration points per element.
4. Number of nodal points per element.

A figure is given for each element type showing the degrees of freedom at each node, the node numbering order for the element connectivity list, and the local and global coordinate systems.

The element types are:

1. A four-noded isoparametric quadrilateral element, Q4. The stiffness matrix is evaluated at four integration points. The element uses the following shape functions:

$$f_1 = (1-\xi)(1-\eta)/4 \tag{A.1}$$

$$f_2 = (1+\xi)(1-\eta)/4 \tag{A.2}$$

$$f_3 = (1+\xi)(1+\eta)/4 \tag{A.3}$$

$$f_4 = (1-\xi)(1+\eta)/4 \tag{A.4}$$

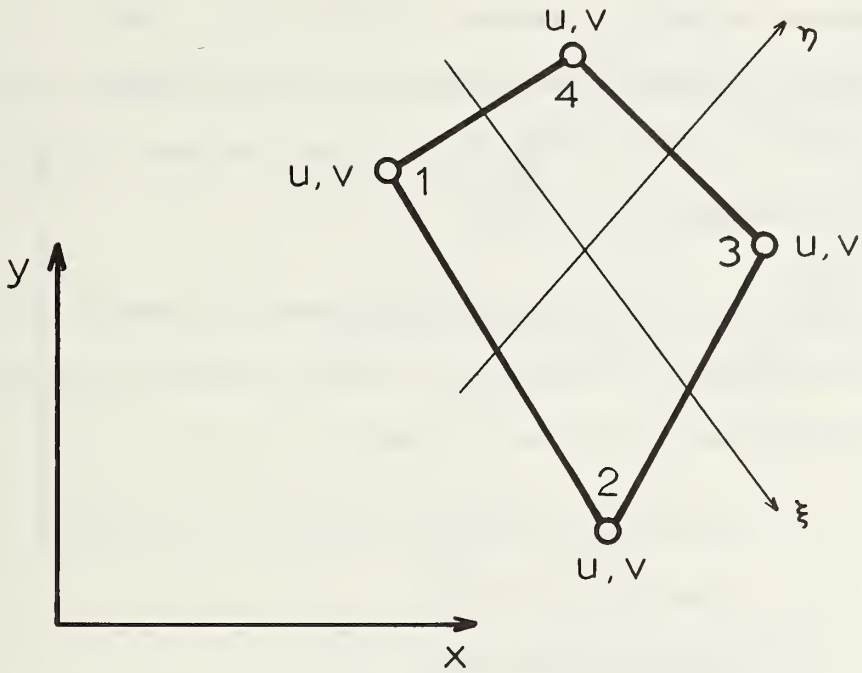

Figure A.2: Q4 Element Type 1

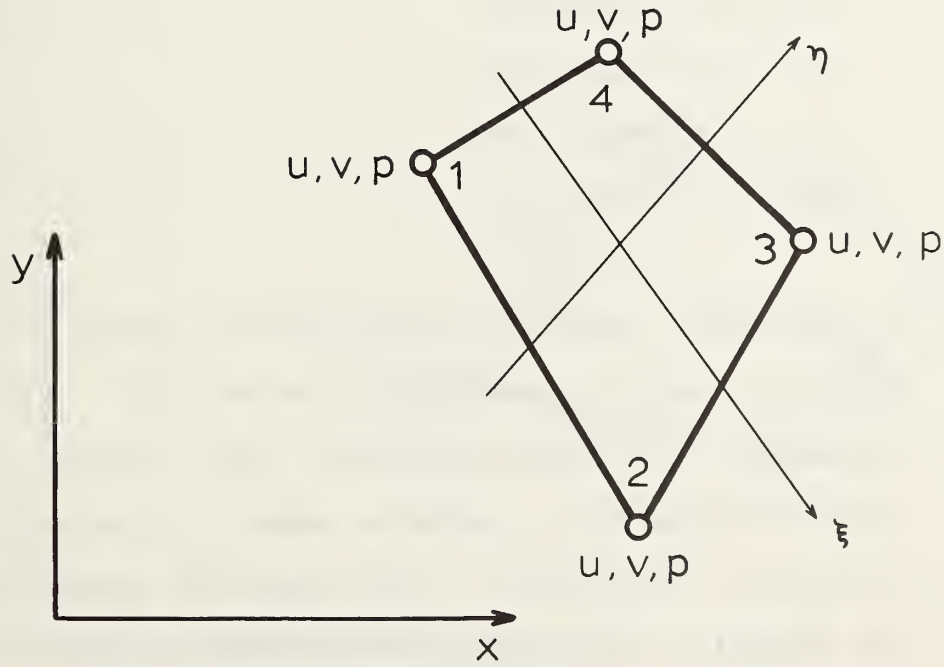

Figure A.3: Q4P4 Element Type 2

2. A four-noded isoparametric quadrilateral element with a pore pressure degree of freedom at each node, Q4P4. The shape functions for both pore pressure and displacement degrees of freedom are identical to those of the previous element. Four integration points are used.

3. An eight-noded isoparametric quadrilateral element, Q8. The stiffness matrix is evaluated at nine integration points, and the following shape functions are used:

$$f_1 = -(1-\xi)(1-\eta)(1+\xi+\eta)/4 \tag{A.5}$$

$$f_2 = -(1+\xi)(1-\eta)(1-\xi+\eta)/4 \tag{A.6}$$

$$f_3 = -(1+\xi)(1+\eta)(1-\xi-\eta)/4 \tag{A.7}$$

$$f_4 = -(1-\xi)(1+\eta)(1+\xi-\eta)/4 \tag{A.8}$$

$$f_5 = (1-\xi)(1-\eta)(1+\xi)/2 \tag{A.9}$$

$$f_6 = (1+\xi)(1-\eta)(1+\eta)/2 \tag{A.10}$$

$$f_7 = (1+\xi)(1+\eta)(1-\xi)/2 \tag{A.11}$$

$$f_8 = (1-\xi)(1+\eta)(1-\eta)/2 \tag{A.12}$$

4. An eight-noded isoparametric quadrilateral element with pore pressure degrees of freedom at the corner nodes, Q8P4. The displacement shape functions are the same as those used in element 3, while the pore pressure shape functions are the same as those used in element 1. Four integration points are used. This element is recommended for two-dimensional consolidation analyses.

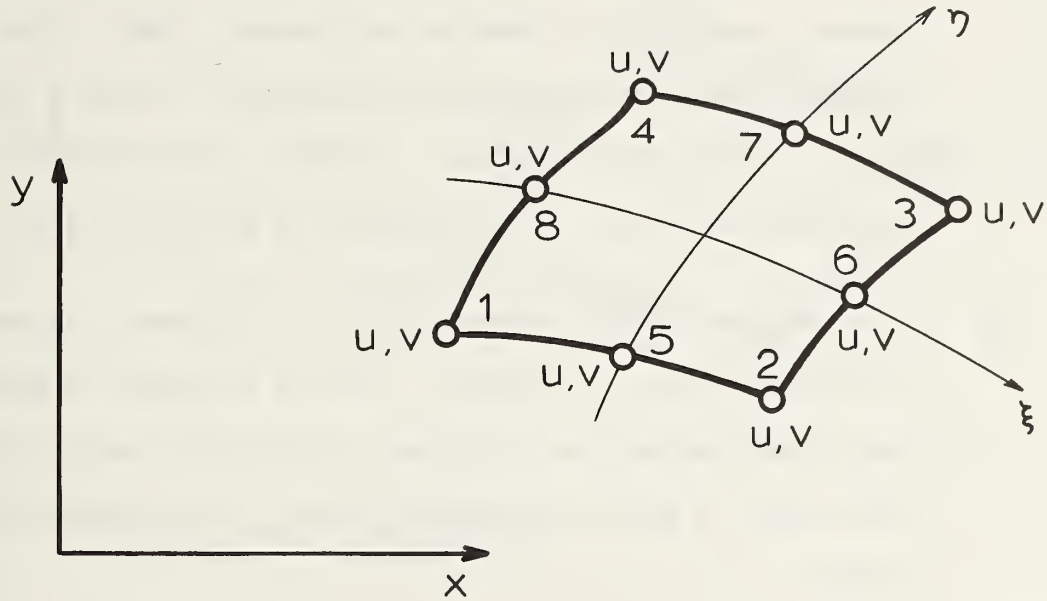

Figure A.4: Q8 Element Type 3

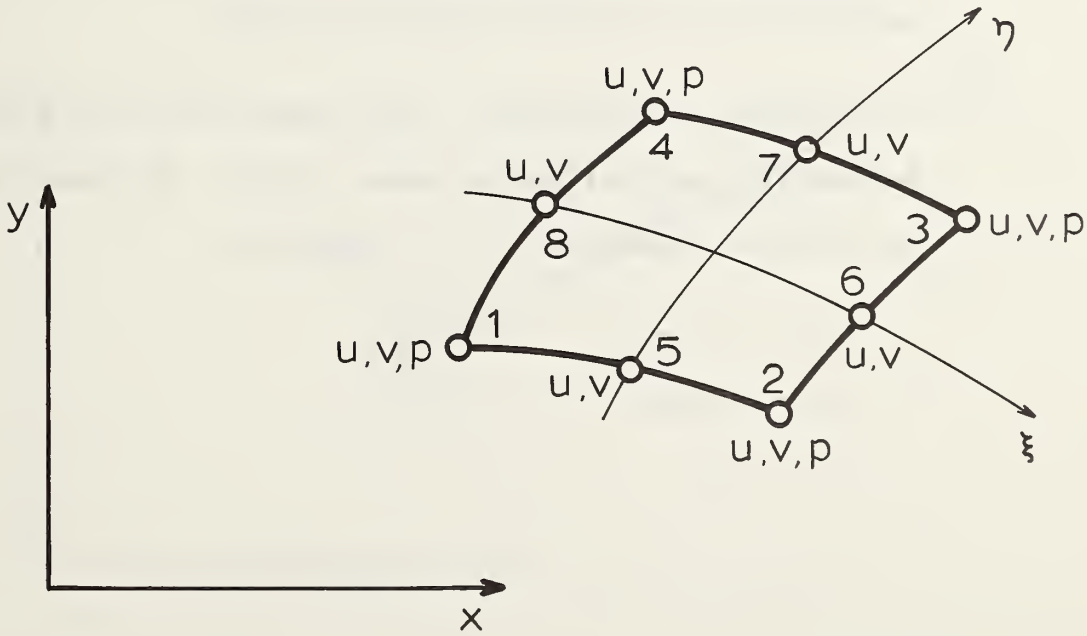

Figure A.5: Q8P4 Element Type 4

5. An eight-noded isoparametric quadrilateral element with pore pressure degrees of freedom at all nodes, Q8P8. The shape functions used for both the displacement and pore pressure degrees of freedom are the same, and they are identical to those used in element type 3. Four integration points are used.

6. A two-dimensional beam element, BM2D. This element is useful for a plane frame type of analysis, or as a structural member in a plane strain geotechnical problem. The stiffness matrix for this elastic beam is written in closed form. The displaced shape is given by

$$\eta = a_0 + a_1\xi + a_2\xi^2 + a_3\xi^3 \tag{A.13}$$

A beam element must not share a node with an element possessing a pore pressure degree of freedom.

7. A three-noded isoparametric link element with pore pressure degrees of freedom at the end nodes, L3P2. The shape functions for the displacement degrees of freedom are

$$f_1 = -\xi(1-\xi)/2 \tag{A.14}$$

$$f_2 = \xi(1+\xi)/2 \tag{A.15}$$

$$f_3 = 1-\xi^2 \tag{A.16}$$

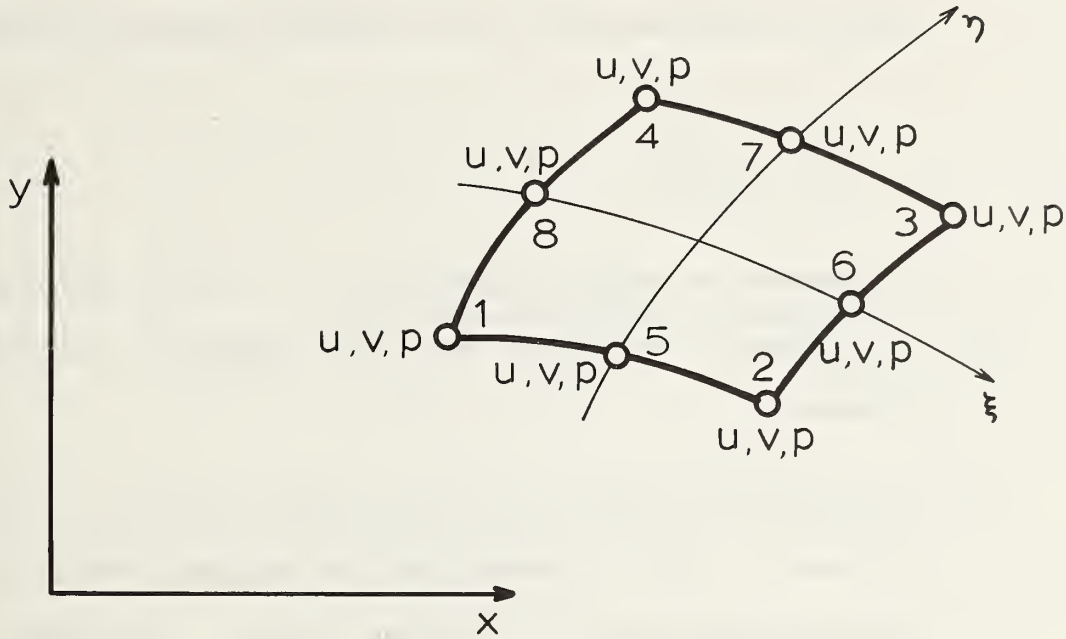

Figure A.6: Q8P8 Element Type 5

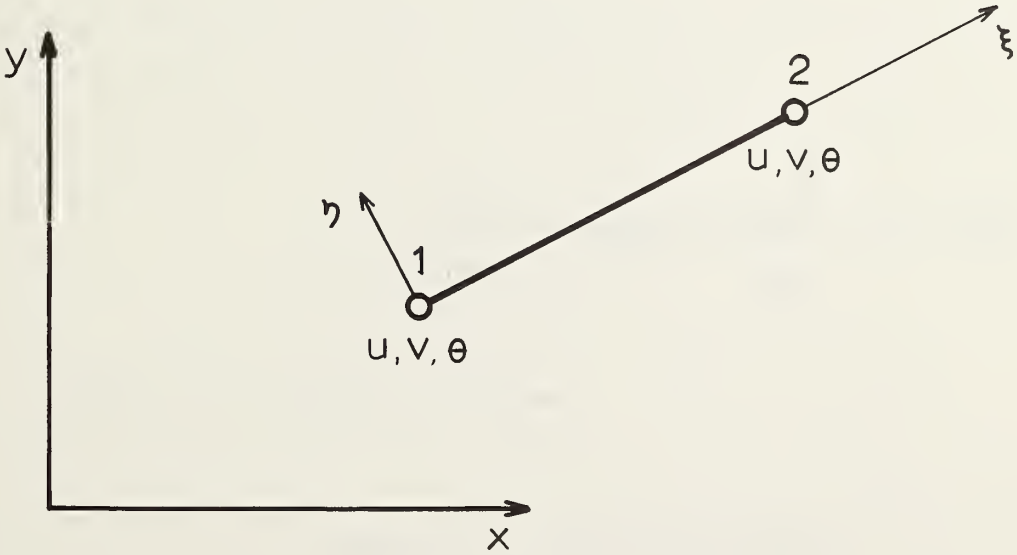

Figure A.7: BM2D Element Type 6

The shape functions for the pore pressure degrees of freedom are

$$f_1 = (1-\xi)/2 \tag{A.17}$$

$$f_2 = (1+\xi)/2 \tag{A.18}$$

The element has two integration points. It has limited uses but is extremely efficient for one-dimensional consolidation problems.

8. A two-noded link element with pore pressure degrees of freedom at both nodes, L2P2. This element was developed for problems of combined axial symmetry and plane strain; for example, the expansion of a cylindrical cavity. Two integration points are used and the displaced shape is given by

$$u = c_1 r + c_2/r \tag{A.19}$$

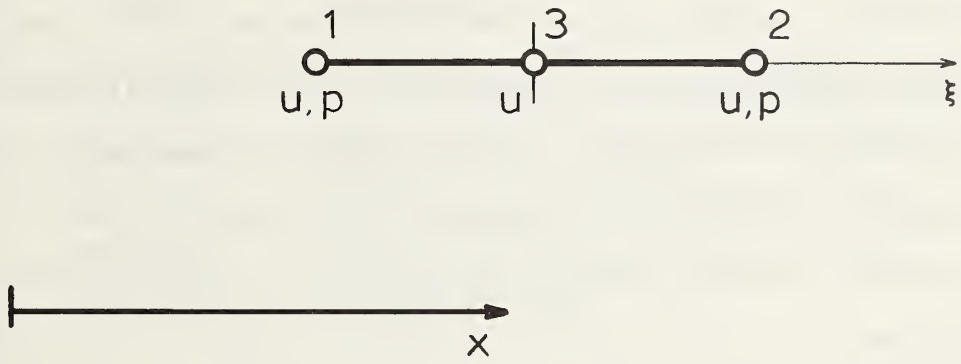

Figure A.8: L3P2 Element Type 7

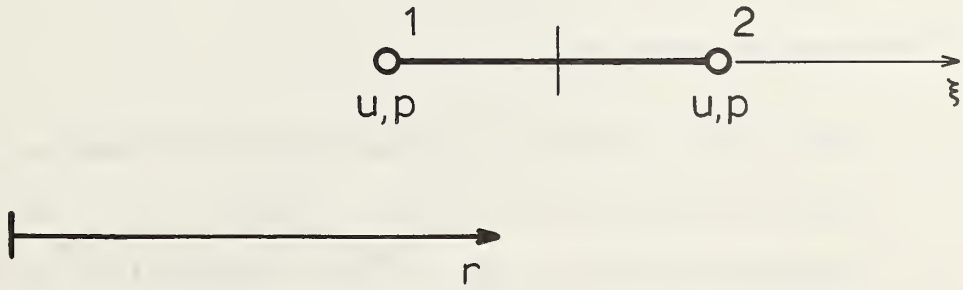

Figure A.9: L2P2 Element Type 8

A.5 MATERIAL LIBRARY

Materials may be defined as elastic or elasto-plastic. The elasto-plastic material is defined using the Cam clay model developed at Cambridge University. However, because it is necessary to make a distinction between one- and two-dimensional materials, and because the beam element has its own material type, five material types exist. As many material numbers may be used as needed to descibe the problem; for example, five kinds of Cam clay could be used along with two elastic materials and nine different beam sections for a total of 16 material numbers.

New material types may be added to the program by expanding subroutines DMAT1D, DMAT2D and UPDMAT. The subroutine CONTRL must be modified to include the following information regarding the new material type:

1. Number of material properties needed to define the material.
2. Number of stress and strain variables to be stored at each integration point.

The material types are:

1. Linear elastic material for two-dimensional elements, EL2D. The material properties are given in Table A.1. The first seven parameters may be set to zero when elements that do not possess pore pressure degrees of freedom are being used.

   The input for the first three parameters may be explained using an example: if the hydrostatic head increases in the negative y direction then i_{gx}=0.0, i_{gy}=-1.0, and i_{gz}=0.0.

TABLE A.1

Parameters for Material Type 1, EL2D

Variable	Explanation
PR(1,NMAT)	i_{gx} x component of the hydrostatic head
PR(2,NMAT)	i_{gy} y component of the hydrostatic head
PR(3,NMAT)	i_{gz} z component of the hydrostatic head
PR(4,NMAT)	γ_w the density of water
PR(5,NMAT)	k_x the permeability in the x direction
PR(6,NMAT)	k_y the permeability in the y direction
PR(7,NMAT)	k_z the permeability in the z direction
PR(8,NMAT)	E Young's modulus
PR(9,NMAT)	ν Poisson's ratio

The output of stress and strain variables at each integration point is as follows:

1. ϵ_x, the strain in the x direction
2. ϵ_y, the strain in the y direction
3. ϵ_z, the strain in the z direction
4. γ_{xy}, the shear strain
5. σ_x', the effective stress in the x direction
6. σ_y', the effective stress in the y direction
7. σ_z', the effective stress in the z direction
8. τ_{xy}, the shear stress
9. u, the pore pressure

2. Cam clay material for two-dimensional elements, CC2D. This material may be specified with a shear strength that varies with depth. The first seven properties are identical to those for material type 1. The remainder of the parameters are given in Table A.2.

TABLE A.2

Parameters for Material Type 2, CC2D

Variable	Explanation
PR(8,NMAT)	κ slope of the rebound isotropic consolidation curve
PR(9,NMAT)	λ slope of the virgin isotropic consolidation curve
PR(10,NMAT)	e_{cs} the voids ratio for unit p' on the critical state line
PR(11,NMAT)	M the slope of the failure line in p'-q space
PR(12,NMAT)	m where the shear modulus $G = ms_u$ if the value is less than one half the value is assumed to be Poisson's ratio ν
PR(13,NMAT)	s_0 where the shear strength is given by $s_u = s_0 + s_1 d$ where d is the depth
PR(14,NMAT)	s_1 given above

Stresses are output in the same order as those for the previous material In addition, the following variables are output at each integration point:

10. p_c', the effective preconsolidation stress
11. p', the effective mean stress
12. q, the octahedral shear stress
13. e, the voids ratio

3. Material properties and cross-sectional geometry for a beam element, BM2D. The first seven fields are left blank. The parameters are given in Table A.3. The six member end actions are printed for each element.

TABLE A.3

Parameters for Material Type 3, BM2D

Variable	Explanation
PR(8,NMAT)	E Young's modulus
PR(9,NMAT)	A the cross-sectional area
PR(10,NMAT)	I the second moment of area

4. Linear elastic material for one-dimensional elements, EL1D. The input is identical to that for material type 1. However, since there is no shear, only seven of the variables are printed at each integration point.

5. Cam clay material for one-dimensional elements, CC1D. The input is identical to that for material type 2. However, since γ_{xy} and τ_{xy} are zero, only eleven of the variables are printed at each integration point.

A.6 INPUT

The input for PEPCO is separated into four blocks, as shown in Figure A.10, and read from unit 5. Each block is terminated by an appropriate END card.

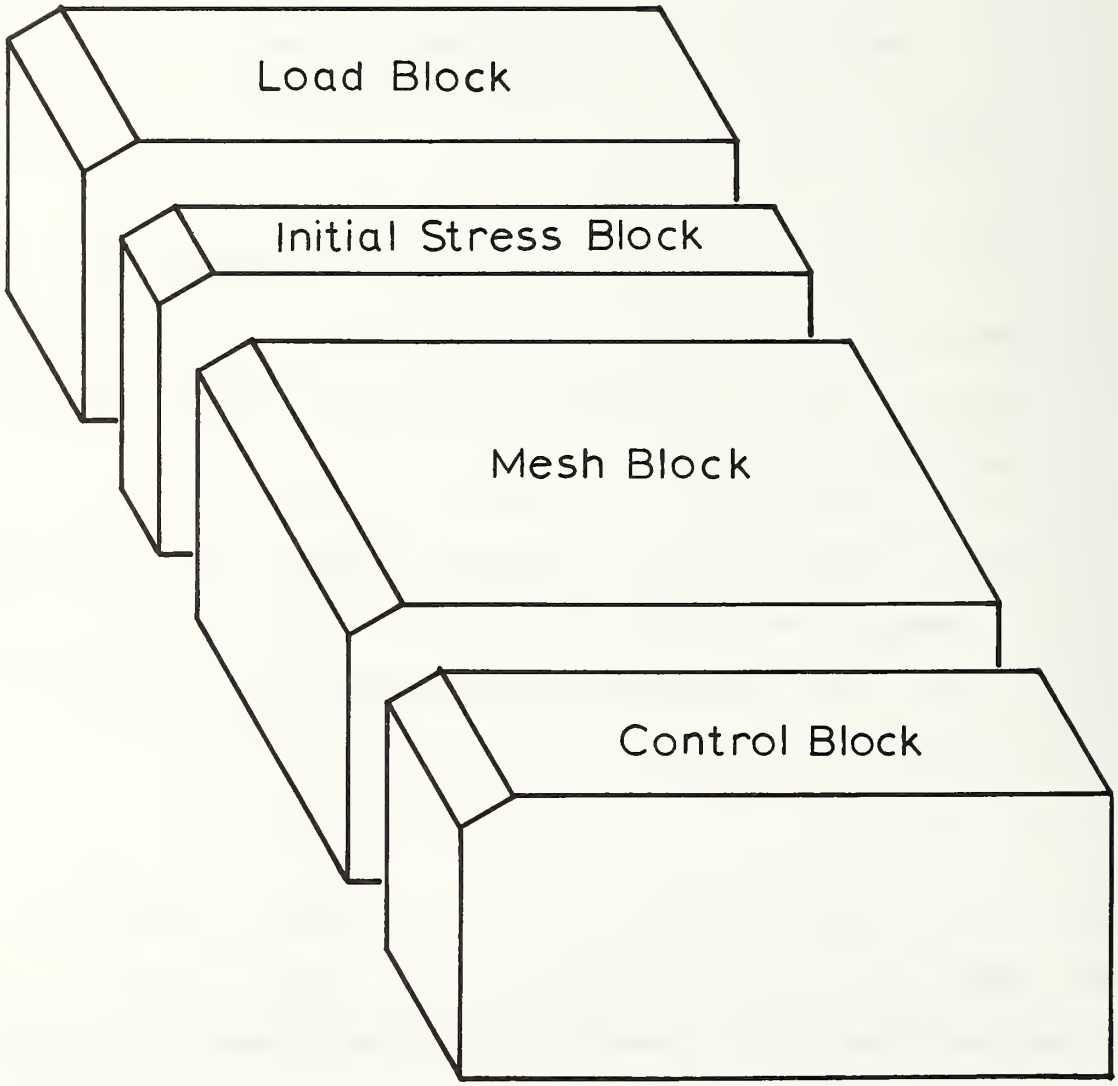

Figure A.10: Input Data Blocks

Within each block there may be a number of groups of cards. Each group of cards has a descriptive keyword on its first card. For example, the first card in the material properties group has the keyword MATERIAL in the first eight columns, and the cards following the keyword card contain the material properties. The groups of cards may be arranged in any order, within any given block. Only those groups pertinent to the problem being analysed need be included. For example, if one does not wish to use a restart file, the RESTART group need not be used.

A.6.1 Control Block

This block contains information regarding the type of analysis, the size of the problem and the number of load increments desired. The information provided in this block is used to allocate the array space.

a) Title group

This group of cards is used to input a descriptive title for the problem. The group may be repeated if more than one title line is desired.

Title

Card	Columns	Variable	Format	Explanation
1	1 - 8	WORD	A8	Enter the word TITLE
2	1 - 80	TITLE	10A8	Enter a title for the problem

b) Size group

This group of cards is used for the purpose of internally dimensioning the arrays.

Problem size

Card	Columns	Variable	Format	Explanation
1	1 - 8	WORD	A8	Enter the word SIZE
2	1 - 5	NN	I5	Number of nodes
	6 - 10	NE	I5	Number of elements
	11 - 15	NM	I5	Number of materials
	16 - 20	NBC	I5	Number of boundary conditions

c) Large displacement option

This card is used if a large displacement analysis is to be performed. When this option is invoked, the initial stress stiffness matrix is added, and rotations are considered when updating the stresses. The nodal coordinates are updated regardless of whether this option is used.

Large displacements

Card	Columns	Variable	Format	Explanation
1	1 - 8	WORD	A8	Enter the words LARGE DI

d) Residual load correction

This option may be used with or without the large displacement option. However, if the large displacement option is being used, this option is recommended in order to maintain equilibrium. By using this option, the out-of-balance forces are calculated at the end of each increment and applied as nodal loads during the next increment.

Residual load correction

Card	Columns	Variable	Format	Explanation
1	1 - 8	WORD	A8	Enter the word RESIDUAL

e) Print group

This group may be used to suppress output or define the number of load increments between printings. This group may be placed in any of the four blocks. Hence, it is possible to turn printing on and off as desired. Users are warned that if the default printing is used, large amounts of output are produced. Output is written on unit 6.

Print

Card	Columns	Variable	Format	Explanation
1	1 - 8	WORD	A8	Enter the word PRINT
2	1 - 5	IPRT	I5	Results will be printed every IPRT increments. IPRT=1 is the default. Set IPRT=0 to suppress output.

f) Restart group

This group is used to save the results of a run on a restart file. The option may then be used subsequently to read this file and continue an analysis. If the read option in this group is used, then the mesh block and initial stress block should be omitted, since this information was provided in a previous run and saved on the restart file. This option is particularly useful in consolidation analyses when the time taken for the pore pressures to dissipate is unknown. It is also useful in elasto-plastic runs in order to break up a large run into a number of smaller runs and reduce the chances of wasting a great deal of money on one bad run. Restart files are written without format statements to unit 8, and they are similarly read from unit 9.

Restart

Card	Columns	Variable	Format	Explanation
1	1 - 8	WORD	A8	Enter the word RESTART
2	1 - 5	IRST	I5	Increment IRST will be read from the restart file. Set IRST=-1 if this option is not required.
	5 - 10	IWST	I5	Results will be saved on a restart file beginning at increment IWST. Set IWST=-1 if this option is not required.

g) Number of increments group

This group should be used if more than one increment is desired.

Increments

Card	Columns	Variable	Format	Explanation
1	1 - 8	WORD	A8	Enter the word INCREMEN
2	1 - 5	NFLI	I5	Number of the first load increment
	6 - 10	NLLI	I5	Number of the last load increment

h) Pore pressure degree of freedom group

This group must be used to define the time integration parameter when pore pressure degrees of freedom are used for consolidation or fluid flow problems.

Pore pressure

Card	Columns	Variable	Format	Explanation
1	1 - 8	WORD	A8	Enter the words PORE PRE
2	1 - 10	BETA	F10.0	Time integration parameter, the recommended value is BETA=0.5

i) Undrained analysis option

This option is used when an undrained analysis is being performed without the use of elements possessing pore pressure degrees of freedom.

Undrained analysis

Card	Columns	Variable	Format	Explanation
1	1 - 8	WORD	A8	Enter the word UNDRAINE

j) Axisymmetric analysis option

This option is used to obtain an axisymmetric analysis. The beam element formulation is not affected by use of this option. Integration is performed over one radian; loads should be calculated accordingly.

Axisymmetric analysis

Card	Columns	Variable	Format	Explanation
1	1 - 8	WORD	A8	Enter the word AXISYMME

k) Plane strain analysis option

This option is used to obtain a plane strain analysis. The beam element formulation is not affected by use of this option, since it assumes a plane stress analysis.

Plane strain analysis

Card	Columns	Variable	Format	Explanation
1	1 - 8	WORD	A8	Enter the words PL STRAI

l) Type of materials group

This group specifies the material types used in the analysis. For details of the available material types, users should consult the material library section.

Type of materials

Card	Columns	Variable	Format	Explanation
1	1 - 8	WORD	A8	Enter the words TYPE MAT
2	1 - 5	N	I5	Number of different material types
	6 -	NTYPE(I)	5I5	List of material type numbers used
		•		

m) Type of elements group

This group specifies the element types used in the analysis. For details of the available element types users should consult the element library section.

Type of elements

Card	Columns	Variable	Format	Explanation
1	1 - 8	WORD	A8	Enter the words TYPE ELE
2	1 - 5	N	I5	Number of different element types
	6 -	NTYPE(I)	8I5	List of element type numbers used

n) End of control block card

This card is required to define the end of the control block input.

End of control block

Card	Columns	Variable	Format	Explanation
1	1 - 8	WORD	A8	Enter the words END CONT

A.6.2 Mesh Block

This block contains the detailed information describing the mesh geometry, its materials and boundary conditions. This entire block should be omitted if a continuation run is being made using the RESTART option.

a) Nodal coordinate group

The coordinates are input for each node. They may be placed in any order.

Nodes

Card	Columns	Variable	Format	Explanation
1	1 - 8	WORD	A8	Enter the word NODES
2	1 - 5	N	I5	Number of nodes in this group
	6 - 10	NCN	I5	Number of coordinates per node
3	1 - 5	NNOD	I5	Node number
	6 -	X(I,NNOD)	6F10.0	Nodal coordinates I=1,NCN

3rd card repeated for a total of N times

b) Element connectivity group

The connectivity is input for each element. The elements may be placed in any order. The numbering sequence for a given element may be found in the element library section. This group will have to be used more than once if more than one element type or more than one material is used.

Elements

Card	Columns	Variable	Format	Explanation
1	1 - 8	WORD	A8	Enter the word ELEMENT
2	1 - 5	N	I5	Number of elements in this group
	6 - 10	NETY	I5	Element type number
	11 - 15	NMAT	I5	Material number
3	1 - 5	NELE	I5	Element number
	6 -	LC(I,NELE)	20I5	Element connectivity I=1,NNE NNE = number of nodes in element

3rd card repeated for a total of N times

c) Material properties group

The material properties are input for each material. The materials may be placed in any order. The type of parameter to be specified for each material property is shown in the material library section. If more than one material type is used, it will be necessary to use this group more than once.

Material properties

Card	Columns	Variable	Format	Explanation
1	1 - 8	WORD	A8	Enter the word MATERIAL
2	1 - 5	N	I5	Number of materials in this group
	6 - 10	NMTY	I5	Material type number
3	1 - 5	NMAT	I5	Material number
	6 - 75	PR(I,NMAT)	7F10.0	Material properties for I=1,7
4	1 -	PR(I,NMAT)	8F10.0	Material properties for I=8,NPRM NPRM = number of properties for this material type

3rd and 4th cards are repeated in pairs for a total of N times

d) Boundary conditions group

The boundary conditions are input in this group. The total number of constraints should equal the value of NBC specified in the control block.

Boundary conditions

Card	Columns	Variable	Format	Explanation
1	1 - 8	WORD	A8	Enter the word BOUNDARY
2	1 - 5	NSETS	I5	Number of sets of constraints
3	1 - 5	N	I5	Number of nodes in this set
	6 - 10	NDOF	I5	Degree of freedom number being constrained in this set
	11 - 20	ADIS	F10.0	Applied displacement for this set
4	1 -	NNBC(I)	16I5	Node number I=1,N

3rd and 4th cards are repeated in pairs for a total of NSETS times

e) Mesh generation group

This group may be used to generate both nodal coordinates and element connectivity for four- and eight-noded quadrilateral elements. The mesh so generated may be rectangular or radial. The first node has the smallest values of x and y as coordinates. The node numbers then increase first along a line of constant y. The elements are similarly numbered. This group may be used to generate all or part of the mesh, and may be used more than once.

Mesh generator

Card	Columns	Variable	Format	Explanation
1	1 - 8	WORD	A8	Enter the words MESH GEN
2	1 - 5	MGTY	I5	Mesh generator type number MGTY=1 for a rectangular mesh MGTY=2 for a radial mesh
	6 - 10	NETY	I5	Element type number
	11 - 15	NMAT	I5	Material number
3	1 - 5	NN1	I5	First node number generated
	6 - 10	NE1	I5	First element number generated
	11 - 15	NEX	I5	Number of elements in the x or r direction
	16 - 20	NEY	I5	Number of elements in the y or θ direction
4	1 -	CX(I)	8F10.0	Corner nodal coordinates in the x or r direction for I=1,NEX+1
5	1 -	CY(I)	8F10.0	Corner nodal coordinates in the y or θ direction for I=1,NEY+1

f) End of mesh block card

This card is required to define the end of the mesh block input.

End of mesh block

Card	Columns	Variable	Format	Explanation
1	1 - 8	WORD	A8	Enter the words END MESH

A.6.3 Initial Stress Block

This block sets up the initial stress conditions in the soil. If zero stresses are desired then only the end of initial stress block card is needed. The entire block should be omitted if a continuation run is being made using the RESTART option.

a) Initial stress variable group

Element stress and strain variables may be explicitly set by using this group. The order of the stress input depends on the material type. This order is the same as the stress output order and may be found in the material library section.

Initial stresses

Card	Columns	Variable	Format	Explanation
1	1 - 8	WORD	A8	Enter the word STRESS
2	1 - 5	NSETS	I5	Number of initial condition sets
3	1 - 5	NE1	I5	First element number
	6 - 10	NE2	I5	Last element number
	11 - 15	NI1	I5	First integration point number
	16 - 20	NI2	I5	Last integration point number
	21 - 25	NSV	I5	Number of stress variables to be set at each integration point
4	1 -	SIG(I)	8F10.0	Initial stress values for I=1,NSV

3rd and 4th cards are repeated in pairs for a total of NSETS times

b) Initial pore pressure group

This group is used to set the pore pressure at nodal points. Pore pressures may be set at the integration points by using the previous group.

Initial pore pressures

Card	Columns	Variable	Format	Explanation
1	1 - 8	WORD	A8	Enter the words PORE PRE
2	1 - 5	N	I5	Number of nodes in this group
3	1 - 5	NNOD	I5	Node number
	6 - 15	U	F10.0	Pore pressure

3rd card repeated for a total of N times

c) Initial time group

The total and incremental times may be set in this group.

Initial time

Card	Columns	Variable	Format	Explanation
1	1 - 8	WORD	A8	Enter the word TIME
2	1 - 5	TIMEI	F10.0	Incremental time
	6 - 10	TIMET	F10.0	Total time

d) Gravity group

This group is used to simulate gravity turn-on for material type 2, Cam clay. This material has no strength at zero initial stress. Hence, it is not possible to use the normal procedure of gravity turn on. The stresses are calculated at each integration point as shown below, where the depth, d, is taken to be the negative of the y coordinate at that point. The pore pressure, u, is given by

$$u = d\gamma_w + q_w \tag{A.20}$$

The effective stresses are given by

$$\sigma_y' = d\gamma_t + q_t - u \tag{A.21}$$

$$\sigma_x' = k_0\sigma_y' \tag{A.22}$$

$$\sigma_z' = k_0\sigma_y' \tag{A.23}$$

where the constants q_w and q_t may be used to simulate a linear change of stress with depth for any water table and overburden pressure. The preconsolidation pressure is given by

$$p_c' = OCR\left[p' + \frac{q^2}{p'M^2}\right] \tag{A.24}$$

Gravity

Card	Columns	Variable	Format	Explanation
1	1 - 8	WORD	A8	Enter the word GRAVITY
2	1 - 5	NSETS	I5	Number of sets of elements for which gravity properties are input
3	1 - 5	NE1	I5	First element number
	6 - 10	NE2	I5	Last element number
	11 - 20	PRG(1)	F10.0	γ_t unit weight of soil
	21 - 30	PRG(2)	F10.0	γ_w unit weight of water
	31 - 40	PRG(3)	F10.0	k_0 the coefficient of earth pressure at rest
	41 - 50	PRG(4)	F10.0	OCR the overconsolidation ratio
	51 - 60	PRG(5)	F10.0	q_t the overburden constant
	61 - 70	PRG(6)	F10.0	q_w the water table constant

3rd card repeated for a total of NSETS times

e) End of initial stress block card

This card is required to define the end of the initial stress input.

End of initial stress block

Card	Columns	Variable	Format	Explanation
1	1 - 8	WORD	A8	Enter the words END INIT

A.6.4 Load Block

This block is used to apply loads. The entire block may be repeated so that incremental load problems may be solved. The maximum number of load increments applied in one run is controlled by the value of NLLI,

which is input in the control block. Execution will stop before NLLI increments if insufficient load increment data is provided.

The incremental load vector is initially set to zero, but it is not reset to zero between increments. Thus, nodal loads applied in one increment will be applied again in the next increment unless PINC is set to zero in the proportional increment group.

a) Nodal load group

This group may be used to apply nodal loads. These incremental loads are added to the existing values in the incremental load vector.

Nodal loads

Card	Columns	Variable	Format	Explanation
1	1 - 8	WORD	A8	Enter the words NODAL LO
2	1 - 5	N	I5	Number of nodes in this group
	6 - 10	NDFN	I5	Number of degrees of freedom at this node
3	1 - 5	NNOD	I5	Node number
	6 -	A(I)	7F10.0	Nodal loads I=1,NDFN

3rd card repeated for a total of N times

b) Body force group

This group is used to input body forces. These forces are converted into equivalent nodal loads which are then added to the existing incremental load vector.

Body forces

Card	Columns	Variable	Format	Explanation
1	1 - 8	WORD	A8	Enter the words BODY FOR
2	1 - 5	NSETS	I5	Number of sets of elements for which body forces are input
3	1 - 5	NE1	I5	First element number
	6 - 10	NE2	I5	Last element number
	11 - 20	FX	F10.0	x force per unit volume
	21 - 30	FY	F10.0	y force per unit volume
	31 - 40	FZ	F10.0	z force per unit volume

3rd card repeated for a total of NSETS times

c) Proportional increment group

This group may be used for two purposes; to scale the existing incremental load vector, and secondly, to apply repeated load increments without repeating the entire load block. The incremental load vector may be reset to zero by using this group with PINC=0.0.

Proportional increment

Card	Columns	Variable	Format	Explanation
1	1 - 8	WORD	A8	Enter the word PROPORTI
2	1 - 5	NPINC	I5	The number of load increments for which PINC is to be applied
	6 - 15	PINC	F10.0	The incremental load vector is scaled by this factor

d) Time increment group

This group is used to control the time increment for problems which have pore pressure degrees of freedom. After each increment the total time is incremented by adding the incremental time; however, the incremental time is not reset to zero. Thus, if the incremental time is set in the initial stress block and this group is not used the time increment will remain constant. For most consolidation problems this is undesirable, since simulating conditions from undrained to drained usually requires about a 1000 to 10000 fold increase in time. The following two schemes are provided for altering this time step

1. The manual method is implemented by explicitly setting the time increment for each step. This is done by setting NTINC=0 and using this group in each repeated load block.

2. The automatic method is to specify how many increments are desired to achieve a tenfold increase in time. For example, TINC=5.0 allows the time to increase by a factor of ten every five increments. The time increments will appear evenly spaced when plotted on a logarithmic scale. The incremental time is computed using the following formula:

$$t_i = t_0 \left(10^{1/TINC} - 1 \right) \tag{A.25}$$

where t_0 is the total time at the start of the current increment. Note that the value of t_0 must not be zero.

Time increment

Card	Columns	Variable	Format	Explanation
1	1 - 8	WORD	A8	Enter the words TIME INC
2	1 - 5	NTINC	I5	Number of time increments NTINC=0 for absolute increment
	6 - 15	TINC	F10.0	Number of increments for a tenfold increment in total time If NTINC=0 absolute increment

e) Change material group

This group is used to change the material properties of an existing material. With careful choice of properties it may be used to simulate the construction of embankments or an excavation.

Change material

Card	Columns	Variable	Format	Explanation
1	1 - 8	WORD	A8	Enter the words CHANGE M
2	1 - 5	NMAT	I5	Material number
	6 - 10	NPRM	I5	Number of properties for this material
3	1 -	PR(I,NMAT)	8F10.0	New properties I=1,NPRM

f) End of load block card

This card is required to define the end of the load block. This block should be repeated if more than one load increment is desired, unless NPINC or NTINC is greater than one.

End of load block

Card	Columns	Variable	Format	Explanation
1	1 - 8	WORD	A8	Enter the words END LOAD

A.7 SAMPLE INPUT

The input for the simple problem of one-dimensional consolidation of an elastic layer is given below. A mesh consisting of five L3P2 elements is used. The displacement at node eleven is fixed, and the pore pressure at node one is fixed. A uniform load is applied at node one during the first increment. A total of fourteen time increments are used.

```
TITLE
ONE DIMENSIONAL CONSOLIDATION OF AN ELASTIC LAYER
SIZE
   11    5    1    2
PORE PRESSURE
       0.5
TYPE ELEMENT
    1    7
TYPE MATERIAL
    1    4
INCREMENTS
    1   14
END CONTROL
NODES
   11    1
    1       0.0
    2     -10.0
    3     -20.0
    4     -30.0
    5     -40.0
    6     -50.0
    7     -60.0
    8     -70.0
    9     -80.0
```

```
   10      -90.0
   11     -100.0
ELEMENTS
    5    7    1
    1    3    1    2
    2    5    3    4
    3    7    5    6
    4    9    7    8
    5   11    9   10
MATERIALS
    1    4
    1       0.0       0.0       0.0      62.4    0.0433
  144000.0       0.0
BOUNDARY CONDITIONS
    2
    1    1
   11
    1    2
    1
END MESH
END INITIAL
NODAL LOADS
    1    1
    1      -1.0
TIME INCREMENT
    0      0.63
END LOAD
PROPORTIONAL INCREMENT
    1       0.0
TIME INCREMENT
   13       0.2
END LOAD
```

Appendix B

SUBROUTINE LISTINGS

This appendix includes listings of FORTRAN subroutines similar to those used in PEPCO. They are

1. DMAT, a subroutine for calculating the stress-strain matrix at an integration point for problems of axial symmetry or plane strain.

2. UPDATE, a subroutine for updating the Cam clay yield surface at an integration point after the incremental stresses have been recovered.

3. FLOW, a subroutine for expanding a Q8 element to a Q8P4 element in order to include the effect of consolidation.

4. LARGE, a subroutine for calculating the initial stress stiffness matrix which is to be added to the element stiffness matrix in order to include the effect of large strains.

5. ROTATE, a subroutine to calculate the true stress increment as a result of rotations.

```
      SUBROUTINE DMAT(D,SVT,PR,DEPTH)
C
C SUBROUTINE CALCULATES THE STRESS-STRAIN MATRIX FOR CAM CLAY
C
      IMPLICIT REAL*8(A-H,O-Z)
      DIMENSION SVT(1),PR(1),D(4,4),A1(4),A2(4)
      PC=SVT(10)
      P=SVT(11)
      Q=SVT(12)
      E=SVT(13)
C
C CALCULATE THE ELASTIC STRESS-STRAIN MATRIX
C
      BMOD=(1.+E)*P/PR(1)
      SU=PR(6)+PR(7)*DEPTH
      SMOD=PR(5)*SU
      D1=(3.*BMOD+4.*SMOD)/3.
      D2=(3.*BMOD-2.*SMOD)/3.
      D(1,1)=D1
      D(1,2)=D2
      D(1,3)=D2
      D(1,4)=0.
      D(2,1)=D2
      D(2,2)=D1
      D(2,3)=D2
      D(2,4)=0.
      D(3,1)=D2
      D(3,2)=D2
      D(3,3)=D1
      D(3,4)=0.
      D(4,1)=0.
      D(4,2)=0.
      D(4,3)=0.
      D(4,4)=SMOD
C
C CHECK TO SEE IF THIS POINT LIES ON THE YIELD SURFACE
C
      AM=PR(4)
      PO=P+Q*Q/(P*AM*AM)
      IF (PO.LT.0.999*PC) RETURN
C
C CALCULATE THE ELASTO-PLASTIC STRESS-STRAIN MATRIX
C
      D1=(2.*P-PC)/3.
      D2=3./(AM*AM)
      A1(1)=D1+(SVT(5)-P)*D2
      A1(2)=D1+(SVT(6)-P)*D2
      A1(3)=D1+(SVT(7)-P)*D2
      A1(4)=2.*SVT(8)*D2
      DO 22 I=1,3
      TEMP=0.
      DO 21 J=1,3
   21 TEMP=TEMP+D(I,J)*A1(J)
   22 A2(I)=TEMP
```

```
      A2(4)=SMOD*A1(4)
      TEMP=0.
      DO 23 I=1,4
   23 TEMP=TEMP+A1(I)*A2(I)
      TEMP=TEMP+P*PC*(1.+E)*(2.*P-PC)/(PR(2)-PR(1))
      DO 24 I=1,4
      DO 24 J=1,4
   24 D(I,J)=D(I,J)-A2(I)*A2(J)/TEMP
      RETURN
      END




      SUBROUTINE UPDATE(SVI,SVT,PR)
C
C SUBROUTINE TO UPDATE CAM CLAY DEPENDENT STRESS QUANTITIES
C
      IMPLICIT REAL*8(A-H,O-Z)
      DIMENSION SVI(1),SVT(1),PR(1)
      AK=PR(1)
      AL=PR(2)
      EO=PR(3)
      AM=PR(4)
      SX=SVT(5)
      SY=SVT(6)
      SZ=SVT(7)
      TXY=SVT(8)
      PC=SVT(10)
      P=(SX+SY+SZ)/3.
      Q=DSQRT(SX*(SX-SY)+SY*(SY-SZ)+SZ*(SZ-SX)+3.*TXY*TXY)
      IF (P.LT.0.01) P=0.01
      PO=P+Q*Q/(P*AM*AM)
      IF (PO.GT.PC) PC=PO
      E=EO-AK*DLOG(P)-(AL-AK)*DLOG(PC/2.)
      SVT(10)=PC
      SVT(11)=P
      SVT(12)=Q
      SVT(13)=E
      RETURN
      END
```

```
      SUBROUTINE FLOW(SE,AE,PP,PR,F4,B4,B8,DETJ4,DETJ8,WGHT,TIMEI,
     2BETA,N,N2)
C
C SUBROUTINE TO EXPAND THE ELEMENT STIFFNESS MATRIX TO INCLUDE A PORE
C PRESSURE DEGREE OF FREEDOM AT THE CORNER NODES, AND ALSO TO
C CALCULATE THE CORRESPONDING RIGHT HAND SIDE VECTOR
C
      IMPLICIT REAL*8(A-H,O-Z)
      DIMENSION SE(1),AE(1),PP(N),PR(7),F4(N),B8(4,N2),E(3,8),PE(3,8),
     2ETPE(8,8),RN(16),B4(4,8)
      GAMMAW=PR(4)
      PERMX=PR(5)/GAMMAW
      PERMY=PR(6)/GAMMAW
      DO 1 I=1,N
      E(1,I)=B4(1,I)
      E(2,I)=B4(2,I+N)
    1 E(3,I)=0.0
      DO 2 I=1,N
      PE(1,I)=PERMX*E(1,I)
      PE(2,I)=PERMY*E(2,I)
    2 PE(3,I)=PERMX*E(3,I)
      DO 3 I=1,N
      DO 3 J=1,N
      TEMP=0.0
      DO 4 K=1,3
    4 TEMP=TEMP+E(K,I)*PE(K,J)
    3 ETPE(I,J)=TEMP*TIMEI*DETJ4*WGHT
      DO 5 I=1,N2
    5 RN(I)=B8(1,I)+B8(2,I)+B8(3,I)
      N2T=(N2+1)*N2/2
      L=N2T
      DO 6 J=1,N
      L=L+J-1
      DO 6 I=1,N2
      L=L+1
    6 SE(L)=SE(L)+RN(I)*F4(J)*DETJ8*WGHT
      L=N2T
      DO 7 J=1,N
      L=L+N2
      DO 7 I=1,J
      L=L+1
    7 SE(L)=SE(L)-ETPE(I,J)*BETA
      DO 8 I=1,N
      K=I+N2
      TEMP=0.0
      DO 9 J=1,N
    9 TEMP=TEMP+ETPE(I,J)*PP(J)
      GIN=0.
      DO 10 J=1,3
   10 GIN=GIN+PR(J)*PE(J,I)
      GIN=GIN*TIMEI*DETJ4*WGHT*PR(4)
    8 AE(K)=AE(K)+TEMP+GIN
      RETURN
      END
```

```
      SUBROUTINE LARGE(SE,SIG,PFS,PFT,DETJ,WGHT,N)
C
C SUBROUTINE TO CALCULATE THE INITIAL STIFFNESS MATRIX FOR A LARGE
C DEFORMATION ANALYSIS FOR A N NODED ISOPARAMETRIC QUADRILATERAL
C ELEMENT IN PLANE STRAIN
C
      IMPLICIT REAL*8(A-H,O-Z)
      DIMENSION SE(1),SIG(4),PFS(N),PFT(N),SSS(8,8),STT(8,8),SST(8,8)
      XXJ=-SIG(1)*DETJ*WGHT
      YYJ=-SIG(2)*DETJ*WGHT
      XYJ=-SIG(4)*DETJ*WGHT
      HDIF=0.5*(YYJ-XXJ)
      HSUM=0.5*(XXJ+YYJ)
      DO 1 I=1,N
      DO 1 J=1,N
      SSS(I,J)=PFS(I)*PFS(J)
      STT(I,J)=PFT(I)*PFT(J)
    1 SST(I,J)=PFT(I)*PFS(J)
      NT=(N+1)*N/2
      L=0
      DO 2 J=1,N
      DO 2 I=1,J
      L=L+1
      SE(L)=SE(L)+HDIF*STT(I,J)-XXJ*SSS(I,J)
      K=L+NT+J*N
    2 SE(K)=SE(K)-HDIF*SSS(I,J)-YYJ*STT(I,J)
      L=NT
      DO 3 J=1,N
      L=L+J-1
      DO 3 I=1,N
      L=L+1
    3 SE(L)=SE(L)-HSUM*SST(I,J)-XYJ*(SSS(I,J)+STT(I,J))
      RETURN
      END
```

```
      SUBROUTINE ROTATE(SIGT,SIGI,EPSI,B,DX,N,N2)
C
C SUBROUTINE TO MAKE A CORRECTION TO THE INCREMENTAL STRESSES DUE TO
C THE EFFECT OF ROTATIONS, FOR A N NODED ISOPARAMETRIC QUADRILATERAL
C
      IMPLICIT REAL*8(A-H,O-Z)
      DIMENSION SIGT(4),SIGI(4),EPSI(4),B(4,N2),DX(N2)
      PUY=0.0
      PVX=0.0
      DO 1 I=1,N
      PUY=PUY+B(4,I)*DX(I)
      J=I+N
    1 PVX=PVX+B(4,J)*DX(J)
      R=0.5*(PVX-PUY)
      E=EPSI(1)+EPSI(2)+EPSI(3)
```

```
SIGI(1)=SIGI(1)+SIGT(1)*E+2.*R*SIGT(4)
SIGI(2)=SIGI(2)+SIGT(2)*E-2.*R*SIGT(4)
SIGI(3)=SIGI(3)+SIGT(3)*E
SIGI(4)=SIGI(4)+SIGT(4)*E-R*(SIGT(1)-SIGT(2))
RETURN
END
```

Appendix C

TUNNEL INPUT DECK FOR PEPCO

This appendix provides a listing of the input deck for a typical tunnel consolidation analysis. The finite element mesh is given in Chapter VI.

```
TITLE
TUNNEL IN BOSTON BLUE CLAY, DIAMETER = 8M, DEPTH TO CROWN = 9.5M
TITLE
LINER ACTIVATED AFTER 3.6 INCHES OF DISPLACEMENT AT THE CROWN
SIZE
  263   74    2   88
PL STRAIN
PORE PRESSURE
       0.5
TYPE ELEMENT
    2    3    4
TYPE MATERIAL
    2    1    2
INCREMENTS
    1   63
END CONTROL
NODES
  263    2
    1    0.0000  -32.8000
    2    2.2396  -33.0207
    3    4.3932  -33.6738
    4    6.3780  -34.7349
    5    8.1177  -36.1623
    6    9.5451  -37.9020
    7   10.6062  -39.8867
    8   11.2593  -42.0404
    9   11.4800  -44.2800
   10   11.2593  -46.5196
   11   10.6062  -48.6732
   12    9.5451  -50.6579
   13    8.1177  -52.3977
   14    6.3780  -53.8251
```

15	4.3932	-54.8862
16	2.2396	-55.5392
17	0.0000	-55.7600
18	0.0000	-31.9800
19	4.7071	-32.9161
20	8.6976	-35.5827
21	11.3636	-39.5729
22	12.3000	-44.2800
23	11.3636	-48.9871
24	8.6976	-52.9772
25	4.7071	-55.6435
26	0.0000	-56.5800
27	0.0000	-31.1600
28	2.5597	-31.4122
29	5.0207	-32.1588
30	7.2891	-33.3710
31	9.2771	-35.0028
32	10.9090	-36.9908
33	12.1212	-39.2593
34	12.8678	-41.7203
35	13.1200	-44.2800
36	12.8678	-46.8397
37	12.1212	-49.3007
38	10.9090	-51.5691
39	9.2771	-53.5571
40	7.2891	-55.1889
41	5.0207	-56.4012
42	2.5597	-57.1477
43	0.0000	-57.4000
44	0.0000	-29.5200
45	5.6485	-30.6434
46	10.4370	-33.8430
47	13.6366	-38.6315
48	14.7600	-44.2800
49	13.6366	-49.9285
50	10.4370	-54.7170
51	5.6485	-57.9162
52	0.0000	-59.0400
53	0.0000	-27.8800
54	3.1996	-28.1952
55	6.2760	-29.1284
56	9.1115	-30.6440
57	11.5964	-32.6835
58	13.6359	-35.1688
59	15.1516	-38.0040
60	16.0848	-41.0804
61	16.4000	-44.2800
62	16.0848	-47.4796
63	15.1516	-50.5559
64	13.6359	-53.3912
65	11.5964	-55.8764
66	9.1115	-57.9159
67	6.2760	-59.4316
68	3.1996	-60.3648

69	0.0000	-60.6800
70	0.0000	-25.4200
71	7.2173	-26.8557
72	13.3362	-30.9438
73	17.4243	-37.0627
74	18.8600	-44.2800
75	17.4243	-51.4973
76	13.3362	-57.6161
77	7.2173	-61.7043
78	0.0000	-63.1400
79	0.0000	-22.9600
80	4.1594	-23.3697
81	8.1587	-24.5829
82	11.8447	-26.5532
83	15.0755	-29.2045
84	17.7271	-32.4353
85	19.6971	-36.1213
86	20.9103	-40.1206
87	21.3200	-44.2800
88	20.9103	-48.4394
89	19.6971	-52.4387
90	17.7271	-56.1247
91	15.0755	-59.3555
92	11.8447	-62.0067
93	8.1587	-63.9771
94	4.1594	-65.1903
95	0.0000	-65.6000
96	0.0000	-19.6800
97	9.4139	-21.5525
98	17.3948	-26.8852
99	22.7274	-34.8661
100	24.6000	-44.2800
101	22.7274	-53.6939
102	17.3948	-61.6748
103	9.4139	-67.0074
104	0.0000	-68.8800
105	0.0000	-16.4000
106	5.4392	-16.9356
107	10.6692	-18.5222
108	15.4895	-21.0986
109	19.7141	-24.5659
110	23.1814	-28.7908
111	25.7578	-33.6108
112	27.3444	-38.8408
113	27.8800	-44.2800
114	27.3444	-49.7192
115	25.7578	-54.9492
116	23.1814	-59.7691
117	19.7141	-63.9941
118	15.4895	-67.4614
119	10.6692	-70.0378
120	5.4392	-71.6244
121	0.0000	-72.1600
122	0.0000	-12.3000

123	12.2383	-14.7344
124	22.6133	-21.6667
125	29.5456	-32.0417
126	31.9800	-44.2800
127	29.5456	-56.5183
128	22.6133	-66.8933
129	12.2383	-73.8256
130	0.0000	-76.2600
131	0.0000	-8.2000
132	7.0389	-8.8934
133	13.8072	-10.9463
134	20.0451	-14.2805
135	25.5125	-18.7675
136	29.9995	-24.2349
137	33.3336	-30.4728
138	35.3866	-37.2411
139	36.0800	-44.2800
140	35.3866	-51.3189
141	33.3336	-58.0872
142	29.9995	-64.3250
143	25.5125	-69.7925
144	20.0451	-74.2792
145	13.8072	-77.6137
146	7.0389	-79.6666
147	0.0000	-80.3600
148	0.0000	-4.1000
149	14.2837	-5.4733
150	27.5162	-9.3838
151	34.8962	-16.7637
152	38.8070	-29.9966
153	40.1800	-44.2800
154	38.8070	-58.5637
155	34.8962	-71.7962
156	27.5162	-79.1762
157	14.2837	-83.0866
158	0.0000	-84.4600
159	0.0000	0.0000
160	7.3800	0.0000
161	14.7600	0.0000
162	22.1400	0.0000
163	29.5200	0.0000
164	36.9000	0.0000
165	44.2800	0.0000
166	44.2800	-7.3800
167	44.2800	-14.7600
168	44.2800	-22.1400
169	44.2800	-29.5200
170	44.2800	-36.9000
171	44.2800	-44.2800
172	44.2800	-51.6600
173	44.2800	-59.0400
174	44.2800	-66.4200
175	44.2800	-73.8000
176	44.2800	-81.1800

177	44.2800	-88.5600
178	36.9000	-88.5600
179	29.5200	-88.5600
180	22.1400	-88.5600
181	14.7600	-88.5600
182	7.3800	-88.5600
183	0.0000	-88.5600
184	51.6600	0.0000
185	51.6600	-14.7600
186	51.6600	-29.5200
187	51.6600	-44.2800
188	51.6600	-59.0400
189	51.6600	-73.8000
190	51.6600	-88.5600
191	59.0400	0.0000
192	59.0400	-7.3800
193	59.0400	-14.7600
194	59.0400	-22.1400
195	59.0400	-29.5200
196	59.0400	-36.9000
197	59.0400	-44.2800
198	59.0400	-51.6600
199	59.0400	-59.0400
200	59.0400	-66.4200
201	59.0400	-73.8000
202	59.0400	-81.1800
203	59.0400	-88.5600
204	68.8800	0.0000
205	68.8800	-14.7600
206	68.8800	-29.5200
207	68.8800	-44.2800
208	68.8800	-59.0400
209	68.8800	-73.8000
210	68.8800	-88.5600
211	78.7200	0.0000
212	78.7200	-7.3800
213	78.7200	-14.7600
214	78.7200	-22.1400
215	78.7200	-29.5200
216	78.7200	-36.9000
217	78.7200	-44.2800
218	78.7200	-51.6600
219	78.7200	-59.0400
220	78.7200	-66.4200
221	78.7200	-73.8000
222	78.7200	-81.1800
223	78.7200	-88.5600
224	91.8400	0.0000
225	91.8400	-14.7600
226	91.8400	-29.5200
227	91.8400	-44.2800
228	91.8400	-59.0400
229	91.8400	-73.8000
230	91.8400	-88.5600

231	104.9600	0.0000
232	104.9600	-7.3800
233	104.9600	-14.7600
234	104.9600	-22.1400
235	104.9600	-29.5200
236	104.9600	-36.9000
237	104.9600	-44.2800
238	104.9600	-51.6600
239	104.9600	-59.0400
240	104.9600	-66.4200
241	104.9600	-73.8000
242	104.9600	-81.1800
243	104.9600	-88.5600
244	121.3600	0.0000
245	121.3600	-14.7600
246	121.3600	-29.5200
247	121.3600	-44.2800
248	121.3600	-59.0400
249	121.3600	-73.8000
250	121.3600	-88.5600
251	137.7600	0.0000
252	137.7600	-7.3800
253	137.7600	-14.7600
254	137.7600	-22.1400
255	137.7600	-29.5200
256	137.7600	-36.9000
257	137.7600	-44.2800
258	137.7600	-51.6600
259	137.7600	-59.0400
260	137.7600	-66.4200
261	137.7600	-73.8000
262	137.7600	-81.1800
263	137.7600	-88.5600

ELEMENTS

8	3	1						
1	3	29	27	1	19	28	18	2
2	5	31	29	3	20	30	19	4
3	7	33	31	5	21	32	20	6
4	9	35	33	7	22	34	21	8
5	11	37	35	9	23	36	22	10
6	13	39	37	11	24	38	23	12
7	15	41	39	13	25	40	24	14
8	17	43	41	15	26	42	25	16

ELEMENTS

66	4	2						
9	29	55	53	27	45	54	44	28
10	31	57	55	29	46	56	45	30
11	33	59	57	31	47	58	46	32
12	35	61	59	33	48	60	47	34
13	37	63	61	35	49	62	48	36
14	39	65	63	37	50	64	49	38
15	41	67	65	39	51	66	50	40
16	43	69	67	41	52	68	51	42
17	55	81	79	53	71	80	70	54

18	57	83	81	55	72	82	71	56
19	59	85	83	57	73	84	72	58
20	61	87	85	59	74	86	73	60
21	63	89	87	61	75	88	74	62
22	65	91	89	63	76	90	75	64
23	67	93	91	65	77	92	76	66
24	69	95	93	67	78	94	77	68
25	81	107	105	79	97	106	96	80
26	83	109	107	81	98	108	97	82
27	85	111	109	83	99	110	98	84
28	87	113	111	85	100	112	99	86
29	89	115	113	87	101	114	100	88
30	91	117	115	89	102	116	101	90
31	93	119	117	91	103	118	102	92
32	95	121	119	93	104	120	103	94
33	107	133	131	105	123	132	122	106
34	109	135	133	107	124	134	123	108
35	111	137	135	109	125	136	124	110
36	113	139	137	111	126	138	125	112
37	115	141	139	113	127	140	126	114
38	117	143	141	115	128	142	127	116
39	119	145	143	117	129	144	128	118
40	121	147	145	119	130	146	129	120
41	131	133	161	159	132	149	160	148
42	133	135	163	161	134	150	162	149
43	135	167	165	163	151	166	164	150
44	135	137	169	167	136	152	168	151
45	137	139	171	169	138	153	170	152
46	139	141	173	171	140	154	172	153
47	141	143	175	173	142	155	174	154
48	143	179	177	175	156	178	176	155
49	143	145	181	179	144	157	180	156
50	145	147	183	181	146	158	182	157
51	167	193	191	165	185	192	184	166
52	169	195	193	167	186	194	185	168
53	171	197	195	169	187	196	186	170
54	173	199	197	171	188	198	187	172
55	175	201	199	173	189	200	188	174
56	177	203	201	175	190	202	189	176
57	193	213	211	191	205	212	204	192
58	195	215	213	193	206	214	205	194
59	197	217	215	195	207	216	206	196
60	199	219	217	197	208	218	207	198
61	201	221	219	199	209	220	208	200
62	203	223	221	201	210	222	209	202
63	213	233	231	211	225	232	224	212
64	215	235	233	213	226	234	225	214
65	217	237	235	215	227	236	226	216
66	219	239	237	217	228	238	227	218
67	221	241	239	219	229	240	228	220
68	223	243	241	221	230	242	229	222
69	233	253	251	231	245	252	244	232
70	235	255	253	233	246	254	245	234
71	237	257	255	235	247	256	246	236

```
   72  239  259  257  237  248  258  247  238
   73  241  261  259  239  249  260  248  240
   74  243  263  261  241  250  262  249  242
BOUNDARY CONDITIONS
    3
   52    1
    1   18   27   44   53   70   79   96  105  122  131  148  159   17   26   43
   52   69   78   95  104  121  130  147  158  183  182  181  180  179  178  177
  190  203  210  223  230  243  250  263  251  252  253  254  255  256  257  258
  259  260  261  262
   15    2
  183  182  181  180  179  178  177  190  203  210  223  230  243  250  263
   21    3
  159  161  163  165  191  211  231  251  253  255  257  259  261  263  243  223
  203  177  179  181  183
MATERIALS
    1    1
    1
       1.0       0.3
MATERIALS
    1    2
    2       0.0      -1.0       0.0      62.4    0.0433    0.0433    0.0433
      0.03      0.15      1.74      1.20     74.00      0.00     15.78
END MESH
GRAVITY
    1
    9   74     115.0      62.4      0.55       1.0       0.0       0.0
END INITIAL
NODAL LOADS
   17    2
   27       0.0   -3293.7
   28   -1935.8  -11466.0
   29   -1928.0   -6310.9
   30   -5840.2  -10222.0
   31   -3894.2   -5353.6
   32   -9648.4   -7337.7
   33   -5734.9   -3441.5
   34  -12779.0   -2424.1
   35   -7034.2    -451.7
   36  -14293.0    4357.4
   37   -7260.9    3335.0
   38  -13303.0   11973.0
   39   -6052.6    7171.6
   40   -9495.3   18677.0
   41   -3453.8   10053.0
   42   -3449.9   22623.0
   43       0.0    5563.5
PROPORTIONAL INCREMENT
    1      0.01
PRINT
   15
TIME INCREMENT
    0   0.00005
END LOAD
```

```
PROPORTIONAL INCREMENT
   14       1.00
TIME INCREMENT
   14       1.00
END LOAD
CHANGE MATERIAL
    1     9
       0.0        0.0        0.0        0.0        0.0        0.0        0.0 10800000.
       0.3
PRINT
    5
PROPORTIONAL INCREMENT
    1       3.40
TIME INCREMENT
    0  0.000170
BODY FORCES
    1
    1     8       0.00      -7.39
END LOAD
PROPORTIONAL INCREMENT
   24        1.0
TIME INCREMENT
   24        1.0
END LOAD
PRINT
    1
PROPORTIONAL INCREMENT
    0       0.00
TIME INCREMENT
    0      0.005
END LOAD
TIME INCREMENT
    0      0.006
END LOAD
TIME INCREMENT
    0      0.009
END LOAD
TIME INCREMENT
    0      0.015
END LOAD
TIME INCREMENT
    0      0.023
END LOAD
TIME INCREMENT
    0      0.037
END LOAD
TIME INCREMENT
    0      0.060
END LOAD
TIME INCREMENT
    0      0.090
END LOAD
TIME INCREMENT
    0      0.150
```

```
END LOAD
TIME INCREMENT
    0      0.230
END LOAD
TIME INCREMENT
    0      0.370
END LOAD
TIME INCREMENT
    0      0.600
END LOAD
TIME INCREMENT
    0      0.900
END LOAD
TIME INCREMENT
    0      1.500
END LOAD
TIME INCREMENT
    0      2.300
END LOAD
TIME INCREMENT
    0      3.700
END LOAD
TIME INCREMENT
    0      6.000
END LOAD
TIME INCREMENT
    0      9.000
END LOAD
TIME INCREMENT
    0     15.000
END LOAD
TIME INCREMENT
    0     23.000
END LOAD
TIME INCREMENT
    0     37.000
END LOAD
TIME INCREMENT
    0     60.000
END LOAD
TIME INCREMENT
    0     90.000
END LOAD
```

Appendix D
REPORT OF NEW TECHNOLOGY

The work performed under this contract has lead to no new technological inventions. Conclusions and recommendations regarding various types of equipment and procedures, design parameters, and soil/structure interaction are intended to expand and improve the state-of-the-art of tunnel design and construction on soft ground.

REFERENCES

Banerjee, P.K. and Stipho, A.S., "Associated and Non-associated Constitutive Relations for Undrained Behaviour of Isotropic Soft Clays" Int. J. for Numerical and Analytical Methods in Geomechanics, Vol. 2, pp. 35-56, 1978

Belshaw, D.J., and Palmer, J.H.L., "Results of a Program of Instrumentation Involving a Precast Segmented Concrete-lined Tunnel in Clay" Canadian Geotechnical Journal, Vol. 15, pp. 573-583, 1978

Biot, Maurice A., "General Theory of Three-Dimensional Consolidation" J. of Applied Physics, Vol. 12, pp. 135-164, February, 1941

Bishop, A.W. and Henkel, D.J., The Measurement of Soil Properties in the Triaxial Test, London, Edward Arnold, 1971

Booker, J.R., "A Numerical Method for the Solution of Biot's Consolidation Theory" Q. J. Mech. Appl. Math., Vol. XXVI, Part 4, 1973

Booker, J.R. and Small, J.C., "An Investigation of the Stability of Numerical Solutions of Biot's Equations of Consolidation" Int. J. Solids Structures, Vol. II, pp. 907-917, 1975

Broms, B.B. and Bennermark, H., "Stability of Clay of Vertical Openings" ASCE JSMFD, Vol. 93, No. SM1, pp. 71-94, 1967

Carter, J.P., Booker, J.R. and Davis, E.H., "Finite Deformation of an Elasto-plastic Soil" I.J. for Numerical and Analytical Methods in Geomechanics, Vol. 1, pp. 25-43, 1977

Carter, J.P., Booker, J.R. and Small, J.C., "The Analysis of Finite Elasto-plastic Consolidation" I.J. for Numerical and Analytical Methods in Geomechanics, Vol. 3, pp. 107-129, 1979

Carter, J.P., Randolph, M.F., and Wroth, C.P., "Stress and Pore Pressure Changes in Clay During and After the Expansion of a Cylindrical Cavity" I.J. for Numerical and Analytical Methods in Geomechanics, Vol. 3, pp. 305-322, 1979

Carter, J.P., Small, J.C. , and Booker, J.R., "A Theory of Finite Elastic Consolidation" Int. J. Solids Structures, Vol. 13, pp. 467-478, 1977

Chang, C.S. and Duncan, J.M., "Analysis of Consolidation of Earth and Rock Fill Dams" Report No. TE77-3 C.E. Dept., Berkeley, 1977

Christian, John T., Boehmer, Jan Willem, and Martin, Philippe P., "Consolidation of a Layer Under a Strip Load" ASCE JSMFD, ASCE, pp. 693-707, July, 1972

Clough, G.W., "Advanced Soil and Soft Rock Tunneling Technology in Japan" Technical Report No. CE252, Stanford University, 1980

Clough, G.W. and Schmidt, Birger, "Design and Performance of Excavations and Tunnels in Soft Clay" Technical Report No. CE235, Stanford University, 1977

Clough, G.W., "Innovations in Tunnel Construction and Support Techniques," Bulletin of the Association of Engineering Geologists, Vol. 18, No. 2, May, 1981, pp. 151-167.

Clough, G.W., Sweeney, B.P, Finno, R.J., and Kavazanjian, E., "Observed Performance of an Earth Pressure Balance Shield in San Francisco Bay Mud," Report to be published, Stanford University, 1982.

Cook, Robert D., Concepts and Applications of Finite Element Analysis, John Wiley, 1974

Deere, D.U., Peck, R.B., Monsees, J.E. and Schmidt, B., "Design of Tunnel Liners and Support Systems" U.S. Department of Commerce, PB-183 799, February, 1969

Denby, Gordon M., "Self-Boring Pressuremeter Study of the San Francisco Bay Mud" Ph.D. Thesis, Stanford University, 1978

Derbalian, K.A., "Eulerian Finite Element Plasticity Analysis" Ph.D. Thesis, Stanford University, 1978

Dimaggio, F.L. and Sandler, I.S., "Material Model for Granular Soils" ASCE JEMD, Vol. 97, No. EM3, pp. 935-950, 1971

Drucker, D.C., Gibson, R.E. and Henkel, D., "Soil Mechanics and Work-Hardening Theories of Plasticity" ASCE Transactions, Vol. 122, 1957

Eisenstein, R. and Thomson, S., "Geotechnical Performance of a Tunnel in Till" Canadian Geotechnical Journal, Vol. 15, pp. 332-345, 1978

Fitzpatrick, Lynne, "Lining Leakage and Consolidation Around Soft-ground Tunnels" Masters' Thesis, Cornell University, 1980

Fitzpatrick, L., Kulhawy, F.H. and O'Rourke, T.D., "Flow Patterns Around Tunnels and Their Use in Evaluating Construction Problems," Soft Ground Tunneling, Ed. D. Resendiz and M.P. Romo, A.A. Balkema, Rotterdam, Netherlands, 1981, pp. 95-103.

Ghaboussi, Jamshid and Gioda, Giancarlo, "On the Time-dependent Effects in Advancing Tunnels" I.J. for Numerical and Analytical Methods in Geomechanics, Vol. 1, pp. 249-269, 1977

Gibson, R.E., England, G.L. and Hussey, M.J.L., "The Theory of One-dimensional Consolidation of Saturated Clays" Geotechnique, Vol. 17, pp. 261-273, 1967

Gibson, R.E., Schiffman, R.L. and Pu, S.L., "Plane Strain and Axially Symmetric Consolidation of a Clay Layer on a Smooth Impervious Base" Q.J. Mech. and Applied Math., Vol. XXIII, Pt. 4, 1970

Graf, Edward D., "Compaction Grouting Technique and Observations" ASCE JSMFD, Vol. 95, SM5, pp. 1151-1158, September, 1969

Gunn, M.J., "The Use of the Finite Element Method for the Design of Tunnels in Soft Ground" Supplementary Report to Director of the Transport and Road Research Lab, Cambridge University, 1977

Henkel, D.J., "The Shear Strength of Saturated Remolded Clays" ASCE Conference on Shear Strength of Cohesive Soils, Boulder, Colorado, pp. 533-560, 1960

Hibbit, H.D., Marcal, P.V. and Rice, J.R., "A Finite Element Formulation for Problems of Large Strain and Large Displacement" Int. J. Solids Structures, Vol. 6, pp. 1069-1086, 1970

Hill, R., The Mathematical Theory of Plasticity, Oxford University Press, 1950

Kasali, G., Ph.D. Thesis to be published, Stanford University, 1981

Kasali, G. and Clough, G.W., "Analysis of the Behavior of Advanced Shields by Three Dimensional Finite Element Techniques," Report to be Published by U.S. Department of Transportation, 1982.

Kawamoto, T. and Okuzono, K., "Analysis of Ground Surface Settlement Due to Shallow Shield Tunnels" I.J. for Numericcal and Analytical Methods in Geomechanics, Vol. 1, pp. 271-281, 1977

Kitamura, M., Ito, S. and Fugiwara, T., Shield Tunneling Performance and Behavior of Soft Ground,". Proceedings, Rapid Excavation and Tunneling Conference, Vol. I, Mayo 1981, Eds. R.L. Bullock, H.J. Jacoby, pp. 201-220.

Ladd, C.C., Foott, R., Ishihara, K., Schlosser, F. and Poulos, H.G., "Stress Deformation and Strength Characteristics" 9th ICSMFE, Tokyo, Japan, pp. 421-494, 1977

Lambe, T. William and Marr, W. Allen, "Stress Path Method: Second Edition" Journal of the Geotechnical Engineering Division, ASCE, Vol. 105, No. GT6, pp. 727-738, June 1979

Lambe, T. William and Whitman, Robert V., Soil Mechanics, Wiley, 1969

Lewin, P.I. and Burland, J.B., "Stress-probe Experiments on Saturated Normally Consolidated Clay" Geotechnique, Vol. 20, No. 1, pp. 38-56, 1970

Malvern, Lawrence E., Introduction to the Mechanics of a Continuous Medium, Prentice-Hall, 1969

Mana, A.I., "Finite Element Analyses of Deep Excavation Behavior in Soft Clay" Ph.D. Thesis, CE Dept. Stanford University, 1978

Marcal, Pedro V., "Finite Element Analysis of Combined Problems of Non-linear Material and Geometric Behavior" ASME Conference on Computational Approaches in Applied Mechanics, pp. 133-149, June 1969

McMeeking, R.M. and Rice, J.R., "Finite Element Formulations for Problems of Large Elastic-plastic Deformation" Int. J. Solids Structures, Vol. II, pp. 601-616, 1975

Mesri, Gholamroza and Rokhsar, Anoushiravan, "Theory of Consolidation for Clays" ASCE Geotechnical Journal, Vol. 8, pp. 889-904, August, 1974

Mondkar, D.P., and Powell, G.H., "Towards Optimal In-core Equation Solving" Computers and Structures, Vol. 4, pp. 531-548, 1974

Olson, Roy E. and Ladd, Charles C., "One-dimensional Consolidation Problems" ASCE JGED, Vol. 105, No. GT1, pp. 11-30, January, 1979

Orr, T.L.L., "The Behaviour of Lined and Unlined Tunnels in Stiff Clay" Ph.D. Thesis, Cambridge University, 1976

Osaimi, A.E., "Finite Element Analysis of Time-dependent Deformations and Pore Pressures in Excavations and Embankments" Ph.D. Thesis, CE Dept., Stanford University, 1977

Palmer, J.H.L., and Belshaw, D.J., "Deformations and Pore Pressures in the Vicinity of a Precast, Segmented, Concrete-lined Tunnel in Clay" Canadian Geotechnical Journal, Vol. 17, pp. 174-184, 1980

Peck, Ralph B., "Deep Excavations and Tunneling in Soft Ground" 7th International Conference on Soil Mechanics and Foundation Engineering, Mexico, pp. 225-290, 1969

Pender, Michael J., Discussion of "Stress Path Method: Second Edition" ASCE JGED, Vol. 106, No. G79, pp. 1068-1071, September, 1980

Prevost, J.H. and Hoeg, K., "Effective Stress-strain-strength Model for Soils" ASCE JGED, Vol. 101, No. G73, March 1975

Richardson, Harold W., and Mayoo, Robert S., Practical Tunnel Driving, McGraw-Hill, 1941

Roscoe, K.H. and Burland, J.B., "On the Generalized Stress-strain Behaviour of 'Wet' Clay" Engineering Plasticity, pp. 535-609, Cambridge University Press, 1968

Roscoe, K.H. and Schofield, A.N., "Mechanical Behaviour of an Idealized 'Wet' Clay" Proceedings of the Second European Conference on Soil Mechanics, 1963

Roscoe, K.H., Schofield, A.W., and Thurairajah, A., "Yielding of Clays in States Wetter than Critical" Geotechnique, Vol. 13, No. 3, pp. 211-240, 1963

Sakurai, Shunsure, "Approximate Time-Dependent Analysis of Tunnel Support Structure Considering Progress of Tunnel Face" Int. J. for Numerical and Analytical Methods in Geomechanics, Vol. 2, pp. 159-175, 1978

Sandhu, Ranbir S., Howho, Liu, and Singh, Kamar, J., "Numerical Performance of Some Finite Element Schemes for Analysis of Seepage in Porous Elastic Media" Int. J. for Numerical and Analytical Mechods in Geomechanics, Vol. 1, pp. 177-194, 1977

Sandhu, Ranbir S. and Wilson, Edward L., "Finite-Element Analysis of Seepage in Elastic Media" ASCE J. Engineering Mechanics, pp. 641-652, June 1969

Schiffmann, R.L., Chen, A.T.F., and Jordan, J.C., "An Analysis of Consolidation Theories" ASCE JSMFD, Vol. 95, pp. 285-312, 1969

Schmidt, Birger, "Settlements and Ground Movements Associated with Tunneling in Soil" Ph.D. Thesis, University of Illinois, Urbana, 1969

Schmidt, Birger, "Slurry Shield Technology" Symposium: Ground Movement Control for Soft Ground Tunneling, October 1978

Schofield, Andrew and Wroth, Peter, Critical State Soil Mechanics, McGraw-Hill, 1968

Seneviratne, Tunnel Model Test Results, Cambridge University, 1977

Simpson, B. and Wroth, C.P., "Finite Element Computations for a Model Retaining Wall in Sand" Conference on European Soil Mechanics, pp. 85-93, 1972

Small, J.L., Booker, J.R., and Davis, E.H., "Elasto-plastic Consolidation of Soil" Int. J. Solids Structures, Vol. 12, pp. 431-448, 1976

Tan, D.Y., "Finite Element Analysis and Design of Chemically Stablilized Tunnels" Ph.D. Thesis, Stanford University, 1977

Taylor, D.W., Fundamentals of Soil Mechanics, Wiley, 1948

Terzaghi, K., Erdbaumechanik, Franz Deuticke, Vienna, 1925

Terzaghi, Karl, "Shield Tunnels of the Chicago Subway" Journal of the Boston Society of Civil Engineers, Vol. XXIX, No. 3, pp. 67-113, July 1942

Terzaghi, K., "Liner-plate tunnels on the Chicago (Ill.) Subway" ASCE Transactions, Vol 108, pp. 970-1007, 1943

Timoshenko, S.P. and Goodier, J.N., Theory of Elasticity, McGraw-Hill, 3rd Edition, 1970

Vesic, A.S., "Expansion of Cavities in Infinite Soil Mass" ASCE JSMFD, pp. 265-290, March 1972

Ward, W.H. and Thomas, H.S.H., "The Development of Earth Loading and Deformation in Tunnel Linings in London Clay" Proceedings, 6th Int. Conference on Soil Mechanics and Foundation Engineering, Montreal, Vol. 2, pp. 432-436

Wroth, C.P. and Zytynski, M., "Applications of the Finite Element Method to the Solution of Geotechnical Field Problems" Report submitted to the Head of the Highway Engineering Computer Branch, D.O.T., Cambridge University, 1977

Yamada, Yoshiaki and Wifi, Abdalla S., "Large Strain Analysis of Some Geomechanics Problems by the Finite Element Method" Int. J. for Numerical and Analytical Methods in Geomechanics, Vol. 1, pp. 299-318, 1977

Zienkiewicz, O.C., The Finite Element Method, McGraw-Hill, 3rd Edition, 1977

352 copies

☆ U. S. GOVERNMENT PRINTING OFFICE: 1983--600-902--366

HE 18.5 .A37
UMTA- 82-

Development
technology

Form DOT F 17
FORMERLY FORM D

partment
sportation

rch and
l Programs
istration

uare
, Massachusetts 02142

DOT LIBRARY
00010214

Postage and Fees Paid
Research and Special
Programs Administration
DOT 513

U.S. MAIL

Official Business
Penalty for Private Use $300